

Design and Development of Sodium Submersible Electromagnetic Pump for High Temperature Application

By

B.K. NASHINE

(ENGG02200804010)

**Indira Gandhi Centre for Atomic Research
Kalpakkam**

*A thesis submitted to the
Board of Studies in Engineering Sciences
In partial fulfillment of requirements
for the Degree of*

DOCTOR OF PHILOSOPHY
of
Homi Bhabha National Institute



April, 2015

Homi Bhabha National Institute

Recommendations of the Viva Voce Board

As members of the Viva Voce Board, we certify that we have read the dissertation prepared by **Mr. B. K. Nashine** entitled “**Design and Development of Sodium Submersible Electromagnetic Pump for High Temperature Application**” and recommend that it may be accepted as fulfilling the dissertation requirement for the Degree of Doctor of Philosophy.

 Date: 29/2/2016

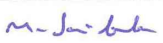
Chairman – **Dr. K. Velusamy**

 Date: 29/2/2016

Supervisor / Convener – **Dr. B. Purna Chandra Rao**

 Date: 29/2/2016

External Examiner – **Krishna Vaanderson**

 Date: 29-2-16

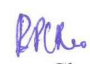
Member 1 – **Dr. M. Sai Baba**

 Date: 29/2/16

Member 2 – **Dr. B. K. Panigrahi**

Final approval and acceptance of this dissertation is contingent upon the candidate's submission of the final copies of the dissertation to HBNI.

I hereby certify that I have read this dissertation prepared under my direction and recommend that it may be accepted as fulfilling the dissertation requirement.


Supervisor/Convener – **Dr. B. Purna Chandra Rao**

Date : 29/2/2016

Place : Kalpakkam (T.N.)

STATEMENT BY AUTHOR

This dissertation has been submitted in partial fulfillment of requirements for an advanced degree at Homi Bhabha National Institute (HBNI) and is deposited in the Library to be made available to borrowers under rules of the HBNI.


Brief quotations from this dissertation are allowable without special permission, provided that accurate acknowledgement of source is made. Requests for permission for extended quotation from or reproduction of this manuscript in whole or in part may be granted by the Competent Authority of HBNI when in his or her judgment the proposed use of the material is in the interests of scholarship. In all other instances, however, permission must be obtained from the author.



(B.K. Nashine)

DECLARATION

I, hereby declare that the investigation presented in this thesis entitled “**Design and Development of Sodium Submersible Electromagnetic Pump for High Temperature Application**” submitted to **Homi Bhabha National Institute (HBNI)**, Mumbai, India for the award of **Doctor of Philosophy in Engineering Sciences** is the record of work which has been carried out by me under the guidance of **Dr. B. Purna Chandra Rao**. The work is original and has not been submitted earlier as a whole or in part for a degree / diploma at this or any other Institution/ University.


(B.K. Nashine)

*Dedicated to my parents,
wife and children*

ACKNOWLEDGEMENT

I wish to express my sincere gratitude to my guide **Dr. B. Purna Chandra Rao** for his invaluable guidance, keen interest, motivation, continuous support and valuable suggestions during my research work. His patience, enthusiasm, and immense knowledge helped me throughout the time of my research and writing thesis.

I am very much grateful to my mentors **Dr. Baldev Raj, Mr. R.D. Kale, Dr. G. Vaidyanathan, Dr. P. Kalyansundaram and Dr. P. Chellapandi** for motivation and encouragement.

I convey my sincere thanks to my Division colleagues **Mr. Prashant Sharma, Mr. Vijay Sharma, Mr. Sarat Kumar Dash, Mr. S. Chandramouli, Mr. G. Vijayakumar, Dr. D. Ponraju, Mr. R. Rajendra Prasad, Mr. R. Iyappan, Mr. R. Parandaman, Mr. S. Krishnakumar, Mr. N. Venkatesan, Mr. B. Babu, Mrs. J.I. Sylvia, Mr. P. Vijaya Mohana Rao, Mr. V. Ramakrishnan, Mr. D. Laxman, Mr. S.K. Das, Mr. T. Lokesh and Mr. E. Hemanth** for their kind help and wholehearted support.

It is my great privilege to acknowledge members of the doctoral committee: **Dr. K. Velusamy** (Chairman), **Dr. M. Sai Baba** (Member) and **Dr. B.K. Panigrahi** (Member) for their critical review and valuable comments.

I take this opportunity to sincerely acknowledge **Mr. K. K. Rajan**, Director FRTG and **Dr. P.R. Vasudeva Rao**, Director IGCAR for allowing testing of Electromagnetic Pump in FRTG, IGCAR and for FRTG colleagues in helping in conduction of test.

Words would be inadequate to express my sincere gratitude to my wife **Dr. Sushma Nashine**, my sons **Mr. Rishabh Nashine & Mr. Spandan Nashine** and my **parents** and other family members for encouragement to complete the research work.

Finally, I thank one and all who have helped me during the research work.

April 2015

B.K. Nashine

CONTENTS

	Page No.
Synopsis	i
List of Figures	iii
List of Tables	vi
Glossary	vii
List of Symbols	viii

CHAPTER 1

INTRODUCTION & REVIEW OF LITERATURE

1.1 Indian Nuclear Power Program	1
1.2 Description of Prototype Fast Breeder Reactor (PFBR)	4
1.3 Research Objective	6
1.4 Motivation for the Present Study	7
1.5 Brief Description of Electromagnetic Pumps	8
1.6 Status of EM Pumps - a review	13
1.7 Knowledge Gained from the Literature Survey	25
1.8 Organization of Thesis	26

CHAPTER 2

DEVELOPMENT OF MATHEMATICAL MODEL FOR ANNULAR LINEAR INDUCTION PUMP (ALIP)

2.1 Introduction	27
2.2 Design Methodology of Annular Linear Induction Pump	27
2.3 Working Principle and Equivalent Circuit of ALIP	27
2.4 Estimation of Equivalent Circuit Parameters – A First Principle Approach	32
2.5 Summary	41

CHAPTER 3

SUBMERSIBLE ANNULAR LINEAR INDUCTION PUMP DESIGN AND ANALYSIS

3.1 Design Requirement	42
------------------------	----

3.2	Design of Submersible Annular Linear Induction Pump	42
3.3	Dimensions of Designed ALIP	43
3.4	Simulation of Submersible ALIP	45
3.5	Effect of Stainless Steel Sheath of Winding and Winding Retainer Plate on ALIP and Derivation of Modified Equivalent Circuit for MI Cable Wound ALIP	57
3.6	Theoretical Characteristics of Developed Submersible ALIP	62
3.7	Calculation of Magnetic Reynolds Number for the developed Submersible ALIP	63
3.8	Summary	64

CHAPTER 4

ANNULAR LINEAR INDUCTION PUMP DEVELOPMENT & MANUFACTURING

4.1	Development of Induction Motor with MI Cable Winding (Stage-1)	65
4.2	Design of Induction Motor with class H insulation	65
4.3	Design of High Temperature Induction Motor with Mineral Insulated Cable Winding	70
4.4.	Demonstration of Use of MI Cable for Rewinding of conventional Induction Motor	80
4.5	Development and Testing of Mineral Insulated Stainless Steel Sheathed Cable for ALIP (Stage II)	81
4.6	Manufacture of Submersible Annular Linear Induction Pump (Stage III)	82
4.7	Summary	84

CHAPTER 5

PERFORMANCE EVALUATION OF SODIUM SUBMERSIBLE ALIP

5.1	Introduction	85
5.2	Description of Sodium Test Facility	85
5.3	Cover Gas System	86
5.4	Sodium Pressure Measurement Methodology	86
5.5	Power Supply Scheme for Testing of Submersible ALIP	87
5.6	Preheating System	87
5.7	Instrumentation and Control	88
5.8	Control Logics	89

5.9 Performance Evaluation of Sodium Submersible ALIP	90
5.10 Testing Procedure	91
5.11 Test Results	92
5.12 Discussion on Test Results	93
5.13 Summary	95

CHAPTER 6

SUMMARY AND FUTURE PROSPECTS

6.1 Summary	110
6.2 Future Research Prospects	113

APPENDIX-A	115
-------------------	-----

APPENDIX-B	126
-------------------	-----

REFERENCES	130
-------------------	-----

PUBLICATIONS	134
---------------------	-----

Synopsis

Sodium is the coolant used in fast reactors due to its excellent heat transfer and favourable neutronic properties but it is highly chemically reactive metal which needs careful handling. This research work focuses on design & development of sodium submersible EM pump for primary sodium draining below sub-assembly head level for visual inspection in the main vessel of Proto Type Fast Breeder Reactor (PFBR) and for complete draining of primary sodium from main vessel during decommissioning stage. The pump shall be capable of operating at sodium submergence condition of 200 °C without any cooling. It has to be insertable in reactor main vessel through an existing inspection canal of 450.0 mm diameter in the roof slab and must be able to withstand radiation present in the reactor. After detailed literature survey and study of PFBR system, it is understood that world wide no device is developed dedicated towards draining of primary sodium from main vessel of pool type sodium cooled fast reactor. Hence, stainless steel encapsulated annular linear induction pump (ALIP), first of its kind, having its stator winding made from mineral insulated (MgO) stainless steel sheathed cable which can withstand temperature up to 550 °C has been designed and developed. The concept of mineral insulated stainless steel based winding was proved in prototype induction motor which was developed during the research work. Subsequently, sodium submersible stainless steel encapsulated ALIP with stator winding made from mineral insulated stainless steel sheathed cable was designed and manufactured. The developed ALIP has capacity of 2.0 m³/h flow rate at 4.0 kg/cm² head and it can operate in sodium submerged condition at 200 °C. The developed pump was tested in sodium loop to validate the design and the concept. The characteristic of the pump namely Pressure Vs Flow, Input Power Vs Flow and Efficiency Vs Flow has been obtained through sodium testing. Endurance test for 1000 h operation in sodium test loop was completed

successfully. The ALIP has worked without cavitation at 0.3 kg/cm² (abs) pressure at inlet. The overstress test at 300 °C successfully also confirmed the robustness of the new design. The pump has not shown any flow instability. The pump was tested sodium submerged condition at temperature of 250 °C to 500 °C for 2000 h. The outcome of research is mainly technology demonstration of new concept and design for sodium submersible annular linear induction pump. The research work has also brought out evolution of new equivalent circuit for the developed annular linear induction pump to take care of effect of eddy current in the mineral insulated SS sheathed cable winding of the pump, which has not been reported in open literature. The research work has also opened up new avenues for further research in ALIP area such as research for accurate analysis of eddy current loss in mineral insulated stainless steel cable used in ALIP and its effect on performance of ALIP, optimization of design, study towards flow instability and use of VFD for ALIP operation. The concept has also opened up path for development of fire survival induction motor which can be used in high temperature application as well as fire fighting domain. Research to develop model to take account of stainless steel sheath in winding is also one of the potential area.

List of Figures

Figure No.	Caption	Page No.
Fig.1.1	PFBR Reactor assembly	4
Fig.1.2	PFBR Flow Sheet	5
Fig.1.3	Broad classification of the electromagnetic pumps	9
Fig 1.4	Schematic of a DC conduction pump	10
Fig.1.5	Schematic of FLIP	12
Fig.1.6	General assembly and principle of an ALIP	13
Fig.2.1	Schematic construction and working principle of ALIP	28
Fig.2.2	Equivalent circuit of ALIP	29
Fig.2.3	Definition of parameters related to coils and slots	30
Fig.2.4	Cross-section view of ALIP along with definition of various parameters	30
Fig.2.5	Different leakage fluxes of primary winding	33
Fig.2.6	Non-magnetic jacket over central core	37
Fig.2.7	Schematic of annular gap D_1	38
Fig.3.1	Flow chart for ALIP design calculations	43
Fig.3.2	General assembly of submersible ALIP	44
Fig.3.3	Simulation model in COMSOL	46
Fig.3.4	Simulation model of ALIP	49
Fig.3.5	Mesh used in simulation	50
Fig.3.6	Flux density at $2.0 \text{ m}^3/\text{h}$ flow	50
Fig.3.7	Magnitude of magnetic flux density in sodium duct at $2.0 \text{ m}^3/\text{h}$	51
Fig.3.8	Variation of radial component of magnetic flux density in duct	51
Fig.3.9	Contour plot of radial component of magnetic flux density	52
Fig.3.10	Arrow plot depicting the magnetic flux density lines	53
Fig.3.11	Model predicted current density in sodium duct	53
Fig.3.12	Volume force in sodium duct at $2.0 \text{ m}^3/\text{h}$	54
Fig.3.13	Pressure development in sodium duct at $2.0 \text{ m}^3/\text{h}$	55
Fig.3.14	Variation in developed pressure with flow	55

Fig. 3.15	Comparison of theoretical developed pressure by COMSOL and equivalent circuit model	57
Fig. 3.16	Winding arrangement in the slot	61
Fig. 3.17	Modified equivalent circuit of ALIP for taking into account the losses taking place in SS sheath of MI cable and in SS retainer plates	61
Fig. 3.18	Theoretical Head Vs Flow curve at 200 ° C	62
Fig. 3.19	Theoretical Input Electrical Power Vs Flow at 200 °C	62
Fig. 3.20	Theoretical Efficiency Vs Flow at 200 °C	63
Fig.4.1	Cross sectional view of stator	66
Fig.4.2	Cross sectional view of rotor	69
Fig.4.3	Cross sectional view of rotor slot	69
Fig.4.4	Low power induction motor	70
Fig. 4.5	Test set up for induction motor	70
Fig. 4.6	Schematic of test set-up for MI cable	71
Fig. 4.7	MI Cable in wound condition over a pipe and slot arrangement	72
Fig. 4.8	Test set up without wound condition.	72
Fig. 4.9	Thermocouple reading at 10 A	72
Fig. 4.10	Current carrying capacity of MI cable	73
Fig. 4.11	Low power induction motor with MI cable	76
Fig. 4.12	Stator of low power motor with MI cable	76
Fig. 4.13	Motor in open condition	76
Fig. 4.14	Two dimensional model of induction motor	78
Fig. 4.15	External current density in stator slot (A/mm^2)	79
Fig. 4.16	Magnetic flux density plot in stator (T)	79
Fig. 4.17	Magnetic flux density plot in rotor (T)	79
Fig. 4.18	Torque - slip characteristics	80
Fig. 4.19	Surface temperature Vs time	80
Fig. 4.20	Conventional motor winding replaced with MI cable winding	81
Fig. 4.21	Cross-section of MI Cable	81
Fig.4.22	View of developed MI cable	81
Fig.4.23	MI cable winding of submersible ALIP along with fixtures	83

	and support	
Fig. 4.24	Submersible ALIP with MI Cable winding and CRGO laminations	83
Fig. 4.25	Manufactured submersible ALIP with outer stainless steel enclosure	84
Fig. 4.26	Photograph of manufactured submersible ALIP other view	84
Fig. 5.1	Flow sheet of BIM loop with submersible ALIP	97
Fig. 5.2	Piping for submersible ALIP testing	98
Fig. 5.3	Pressure pot with level probe details	99
Fig. 5.4	Argon cover gas header for pressure pots of ALIP testing facility	100
Fig. 5.5	Power supply wiring diagram for submersible ALIP	101
Fig. 5.6	Control circuit wiring diagram for submersible ALIP	102
Fig. 5.7	Photograph of pump erected in BIM loop	103
Fig. 5.8	Photograph of control and instrument panel and other electrical systems	103
Fig. 5.9	Experimental Pressure Head Vs Flow Characteristics at 200 °C	104
Fig. 5.10	Comparison of Experimental and Theoretical Pressure Head Vs Flow Characteristics at 200 °C	104
Fig. 5.11	Experimental Input Electrical Power Vs Flow at 200 °C	105
Fig. 5.12	Comparison of Experimental and Theoretical Input Electrical Power Vs Flow at 200 °C	105
Fig. 5.13	Experimental Efficiency Vs Flow at 200 °C	106
Fig. 5.14	Comparison of Experimental and Theoretical Efficiency Vs Flow at 200 °C	106
Fig. 5.15	Experimental Pressure Vs Flow at 300 °C (Overstress Test)	107
Fig. 5.16	Pressure Vs Flow characteristics after endurance test of 1000 h	107
Fig. 5.17	Schematic of submersible ALIP in ICT	108
Fig. 5.18	Erection of submersible ALIP for testing in ICT	109

List of Tables

Table No.	Caption	Page No.
Table 1.1	Technical details of pumps from NII-EFA	14
Table 1.2	Dimensions of CLIP-A	14
Table 1.3	Specification of ALIP-1 and ALIP-2	15
Table 1.4	Details of IA 21 and IA 81	15
Table 1.5	Details of ALIP from Novatome	16
Table 1.6	Specification of 600 m ³ /h ALIP	16
Table 1.7	Candidate materials for sodium immersed EM pump	17
Table 1.8	Model pump design specifications	17
Table 1.9	Details of submersible 160 m ³ /min EM pump	18
Table 1.10	Rating of double stator EM pump	19
Table 1.11	Details of Self Cooled ALIP	19
Table 1.12	Details of 43.5m ³ /min electromagnetic pump	20
Table 1.13	Details of EM pump for Lithium pumping	21
Table 1.14	Specification of the electromagnetic pump manufactured in England	22
Table 1.15	Technical data of 50m ³ /h and 100m ³ /h EM pump	22
Table 1.16	Comparison of parameters of various EM pumps	23
Table 1.17	Specification of Indian FLIP	24
Table 1.18	Specification of Indian ALIP	24
Table 1.19	Specification of Indian DC Conduction Pump	25
Table 2.1	List of parameters / variables used in derivation	31
Table 3.1	Specifications of submersible ALIP	44
Table 3.2	Magnetic Reynolds Number for Submersible ALIP	63
Table 4.1	Technical details of the motor	66
Table 4.2	Tests on 1.5 mm MI cable roll	73
Table 4.3	Tests on 1.5 mm MI cable in wound condition	75
Table 5.1	Details of Pressure Pot Level Probes	89
Table 5.2	Details of Flow meter	90
Table 5.3	Details of Pressure Transmitter	90
Table 5.4	Control Logics	90

Glossary

MWe	Mega Watt electric
PHWR	Pressurized Heavy Water Reactors
AHWR	Advance Heavy Water Reactor
FBR	Fast Breeder Reactors
SFR	Sodium Cooled Fast Reactor
MOX	Mixed Oxide
ALIP	Annular Linear Induction Pump
SALIP	Submersible Annular Linear Induction Pump
DCCP	DC Conduction Pump
ACCP	AC Conduction Pump
FLIP	Flat Linear Induction Pump
MI	Mineral Insulated
MgO	Magnesium Oxide
FEM	Finite Element Method

List of Symbols

D_1	Radial annular width for liquid metal passage
D_2	Radial thickness of outer sodium duct
D_3	Radial gap between outer sodium duct and Stator bore
D_4	Thickness of stainless steel jacket surrounding the central core
D_5	Total non-magnetic gap
D_6	Pole Pitch
D_7	Mean diameter of Annulus
D_8	Bore diameter of stator surface
D_9	Diameter of central core
D_{10}	Width of stator tooth
D_{11}	Width of stator slot
D_{12}	Clearance between top of coil and top of slot
D_{13}	Depth of coil side
D_{14}	Slot Depth
D_{15}	Mean length of coil turn
N_1	Number of Poles produced by stator winding
N_2	Number of phases
N_3	Slots per pole per phase
N_4	Number of slots in stator
N_5	Number of teeth in stator
N_7	Number of turns per coil
N_8	Carter co-efficient
N_9	Multiplier for D_5 to account for apparent increase in D_5 due to slots
N_{sc}	Effective number of turns in series per phase in stator
R_1	Stator Winding Resistance per phase (Ω / ph)
R_j	Equivalent resistance of jacket around central core (Ω / ph)
R_w	Equivalent resistance of outer annulus wall (Ω / ph)
R_f	Equivalent resistance of liquid metal (Ω / ph)
R_{cf}	Equivalent resistance of R_w , R_j and R_f in parallel
X_1	Stator winding Leakage Reactance per phase (Ω / ph)
X_m	Magnetizing Reactance (Ω / ph)
ρ_{Cu}	Resistivity of copper wire
ρ_{SS}	Resistivity of Stainless Steel
ρ_{Na}	Resistivity of sodium
I_{mg}	Magnetising Current
k_p	Pitch factor
k_d	Winding distribution factor
p	No. of pole-pairs
V_{syn}	Synchronous velocity of traveling magnetic field
V_L	Velocity of liquid metal
V_R	Relative velocity between traveling magnetic field and liquid metal
ΔP	Differential pressure developed by pump
f	Stator electrical frequency (Hz)
μ_0	Permeability of vacuum

ϕ	Flux
I	Current
B_m	Peak value of flux density
H_m	Magnetic field intensity
F_a	Stator mmf
T_{ph}	Turns per phase
p	Pole pairs
E_A	voltage induced across X_m
τ	Pole pitch
U	Uranium
P_u	Plutonium
ω	Angular velocity
J	Current density
σ	Electrical conductivity
η	Efficiency

Chapter-1

CHAPTER – 1

INTRODUCTION AND REVIEW OF LITERATURE

1.1 Indian Nuclear Power Program

Nuclear energy is a viable alternative energy source to meet ever-growing demand for energy with less impact on environment [1]. Presently, nuclear energy provides over 15% of the world's total electricity. As of July 2014, there are around 435 nuclear reactors in 31 countries with a total installed capacity of 3.70 GigaWatt electric (GWe). In India, currently about 3% of total energy production is coming from nuclear energy. When a fissile element atom is bombarded by neutron, the fissile element breaks into low atomic mass elements and this gives approximately 200 MeV equivalent thermal energy. If this nuclear reaction is continued, it has capability to produce 200 MeV energy per fission continuously. Splitting of multiple atoms can produce high amount of energy proportional to number of fissile atoms split and this is the basis of producing nuclear energy in a nuclear reactor. U^{235} is naturally available fissile material while Pu^{239} and U^{233} are man made fissile materials by transmutation of U^{238} and Th^{232} respectively in a nuclear reactor. Transmutation is a radioactive phenomenon in which bombardment of neutrons on some element, results in conversion of element into other element. This happens because of absorption of neutron by the element leading to increase in atomic weight of element, hence converting the original element into other element. All the above mentioned three fissile materials give approximately 200 MeV energy per atom split on bombardment of neutron.

Uranium resources (~110,000 tonnes) in India are limited, which is around 2% of world uranium resources. But India has vast resources of thorium (~ 800,000 tonnes estimated) which is around 25% of world thorium resources. The available U^{235} resources can generate around 10 GWe for about 40 years according to Nuclear Power

Corporation of India Limited (NPCIL). According to Department of Atomic Energy (DAE), the country can produce more than 500 GWe for 400 years using country's economically extractable thorium reserves. In order to exploit the nuclear fuel resources for energy production, a sequential three-stage programme is envisaged in India based on a closed fuel cycle, where the spent fuel of one stage is reprocessed to produce fuel for the next stage. The first stage of Indian nuclear programme involves deployment of Pressurized Heavy Water Reactors (PHWRs), where natural uranium ($U^{238} + U^{235}$) in oxide form is used as fuel. It produces energy and some part of U^{238} gets transmuted to fissile element Pu^{239} [4,5].

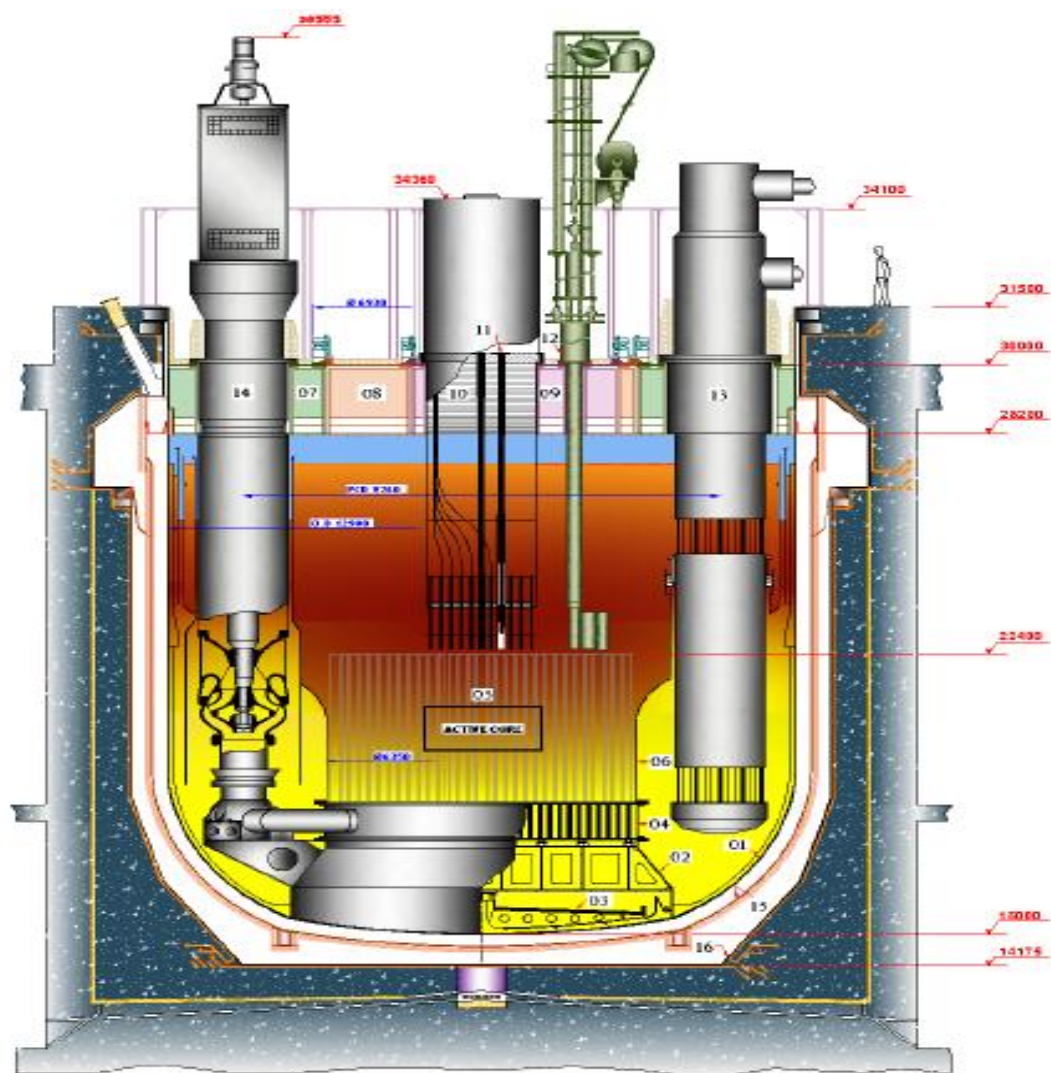
In the second stage, Fast Breeder Reactors (FBRs) employ mixed oxide (MOX) fuel made of Pu^{239} (recovered by reprocessing of spent fuel from the first stage) and uranium. In FBRs, Pu^{239} undergoes fission reaction to produce energy. Further, Pu^{239} is produced by transmutation of U^{238} present in the fuel. FBRs can produce more fuel than they consume and hence, termed breeders. Over a period of time, plutonium inventory can be built up by transmutation of U^{238} . Similarly Th^{232} is not a fissile element but can be converted to a fissile material (U^{233}) by transmutation in FBRs. The third stage of the programme will be based on advanced heavy water reactor in which U^{233} will be used as the fuel for producing electricity and Th^{232} will be transmuted to obtain U^{233} to form a self-sustaining series of Th^{232} and U^{233} fuelled reactors, with appropriate reprocessing programme.

Now, India is in the second stage of the nuclear program, where sodium cooled fast reactors are being used for power generation. The fast breeder reactor operates in fast neutron energy spectrum where high energy fast neutrons are used for the nuclear chain reaction. These fast neutrons bombard the fissile elements present in the fuel for producing nuclear energy. Since the reactor has to operate in fast neutron energy spectrum,

the nuclear fuel (Plutonium and Uranium) are placed in a compact manner, so that fast neutrons have to travel lesser distance without losing much of energy for remaining in fast spectrum energy level, before meeting fissile atoms for chain reaction. This makes the FBR core very small but enriched with plutonium, resulting in volumetric high power density. The coolant in the FBR should not reduce the energy of fast neutrons i.e. it should not moderate the neutrons. The typical linear fuel power density in FBR can be of the order of 450 W/cm. This high power density heat can be efficiently removed only by a coolant that has very good heat transfer property. Hence in Indian FBR, sodium is used as a coolant due to its excellent heat transfer property and favourable neutronic property which does not moderate the neutrons. Sodium is a highly reactive element and it reacts violently when it comes in contact with oxygen and moisture. Hence, it has to be kept always in inert atmosphere. Proto type Fast Breeder Reactor (PFBR) uses sodium as coolant. Sodium will be continued to be used as coolant for several other future fast reactors [2,3,6]. Use of large amount of sodium in primary coolant system is also advantageous from the standpoint of safety, because of high heat capacity of sodium and natural circulation flow. Sodium has good electrical conductivity and this facilitates the use of electromagnetic pumps for pumping sodium in fast reactors as well as in experimental sodium facilities. In a FBR, sodium has to be pumped from cold zone to hot zone for heat transfer. The pumping of sodium is done by centrifugal mechanical pumps and by electromagnetic (EM) pumps. The centrifugal mechanical pumps are used in main heat transport circuits while EM pumps are used in auxiliary purification circuits in FBRs. EM pumps are also used for pumping sodium in experimental facilities where various fast reactor components are tested for their performance evaluation.

1.2 Description of Prototype Fast Breeder Reactor (PFBR)

India is on the verge of commissioning of prototype fast breeder reactor (PFBR) which forms the second stage of India's nuclear program [2]. Fig.1.1 shows the PFBR reactor assembly and Fig.1.2 shows the PFBR flow sheet. About 1200 t of primary sodium (main coolant) is contained in the main vessel.



LEGEND

- | | |
|----------------------------|------------------------------------|
| 01. MAIN VESSEL | 09. SMALL ROTATABLE PLUG |
| 02. CORE SUPPORT STRUCTURE | 10. CONTROL PLUG |
| 03. CORE CATCHER | 11. CONTROL & SAFETY ROD MECHANISM |
| 04. GRID PLATE | 12. IN-VESSEL TRANSFER MACHINE |
| 05. CORE | 13. INTERMEDIATE HEAT EXCHANGER |
| 06. INNER VESSEL | 14. PRIMARY SODIUM PUMP |
| 07. ROOF SLAB | 15. SAFETY VESSEL |
| 08. LARGE ROTATABLE PLUG | 16. REACTOR VAULT |

Fig.1.1 PFBR Reactor assembly [2]

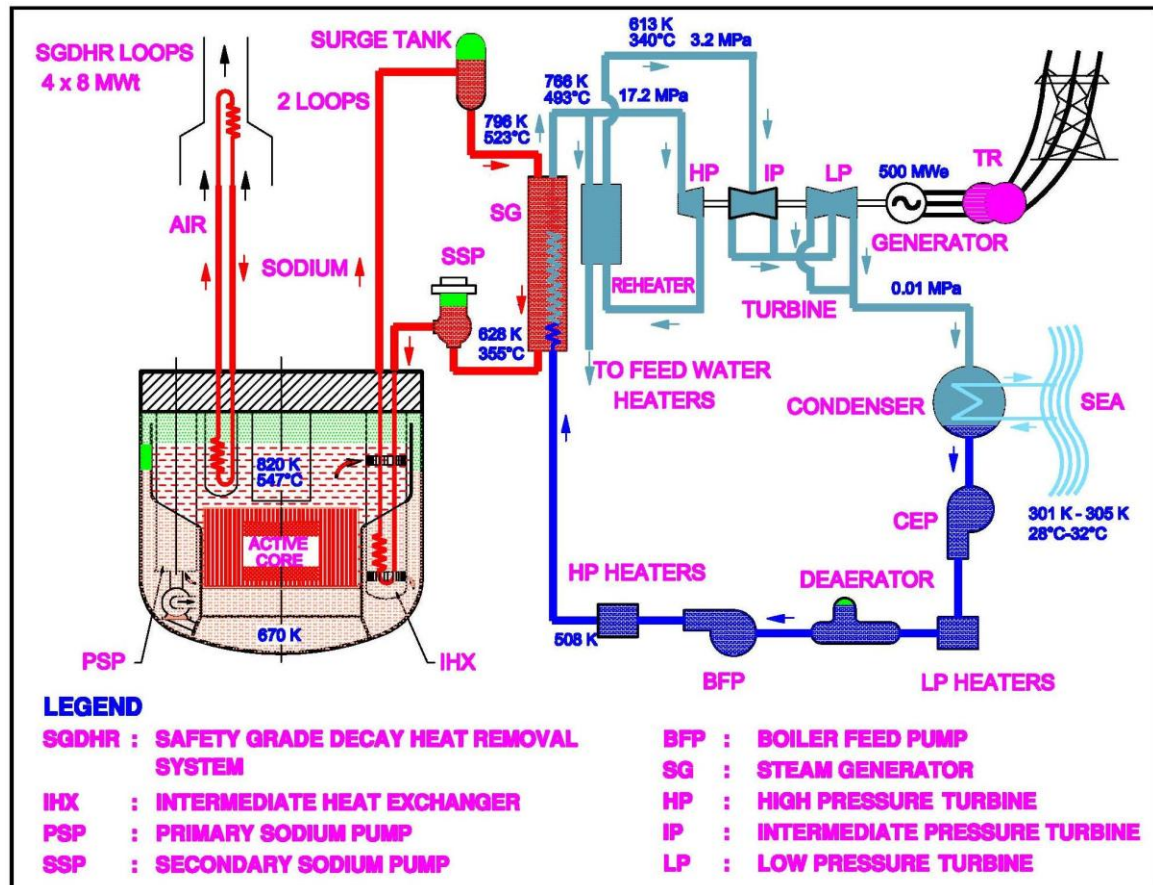


Fig.1.2 PFBR Flow Sheet [2]

The nuclear fuel core, primary sodium pump, intermediate heat exchanger (IHX) and fuel transfer machine are housed in main vessel. The secondary sodium circuit and steam water circuit are outside the main vessel as shown in Fig.1.2.

The main vessel is divided into two zones, namely, cold pool and hot pool. The primary sodium pump sucks cold sodium (397°C) from cold pool and pumps out to the fuel core zone. The pumped cold sodium extracts heat from the fuel core and attains a temperature of 547°C . This hot sodium passes through the intermediate heat exchanger (IHX) which transfers the heat to secondary sodium that is pumped out by other sodium pump called, secondary sodium pump. The hot primary sodium, after losing the heat in IHX, becomes cold and comes back to the cold pool for recirculation. The secondary sodium transfers the heat to steam-water circuit to generate the steam which rotates the turbine and alternator for generating the electricity. The primary sodium always remains

in the primary sodium pool contained in the main vessel and pumped by the mechanical sodium pump [2,3].

1.3 Research Objective

In PFBR, hot pool primary sodium is maintained at 547 °C and cold pool sodium is maintained at 397 °C during full power operation. The primary sodium is maintained at 200 °C during fuel handling period, which is minimum temperature of sodium permitted in PFBR. As stated earlier, primary radioactive sodium is always contained in the main vessel through out the reactor life of 40-60 years. In case of any untoward incident, requiring visual inspection of the fuel sub-assembly head using periscope or for reactor decommissioning, the primary sodium has to be drained outside the main vessel to a storage tank. Presently, there is no provision for large scale draining of primary sodium to outside storage tank. This needs pumping device which has to be submerged in sodium and operate at 200 °C without provision of any external cooling arrangement. The pumping device has to be placed inside the reactor through available inspection canal of maximum diameter of 450 mm. The pump shall be capable of operating in radiation field. The drained sodium shall also come out through pump outlet line passing through the inspection canal through which the pump is inserted [7]. Hence the technological challenges to be considered while designing the device for draining the primary sodium from the main vessel of FBRs are:

- 1) operation in sodium submerged condition
- 2) operation to withstand sodium temperature upto 200 °C
- 3) operation without any external cooling
- 4) slender and compact construction which can be inserted inside reactor through inspection canal of 450 mm diameter
- 5) operation in high radiation field present in the reactor

Keeping the above constraints in mind, the research objective was set to design and develop a sodium submersible pump capable of operating in radiation field at 200 °C sodium without any external cooling facility and with a maximum diameter of 400 mm.

Preliminary studies were carried out to finalize the option available for achieving the above mentioned aim. The primary sodium pump, even though submerged in primary sodium, can only circulate sodium within the main vessel and it can not drain primary sodium out side the main vessel. Hence, existing primary sodium pump is not considered. The draining of sodium using present purification circuit and its electromagnetic pump is not possible because it can not drain the primary sodium upto fuel sub-assembly head level and below. Use of small centrifugal pump which can be inserted through the inspection canal for draining is not possible due to space constraints because it is difficult to have the pump shaft and outlet line through same inspection canal. Deployment of a mechanical jet pump inside reactor for pumping out sodium is not possible because it needs extra pumps working outside the reactor and needs priming which is not possible in PFBR configuration. DC conduction pump is a possibility. However, its bulkiness and requirement of high power DC power supply makes it unattractive. The option of annular linear induction pump has potential of overcoming all the above constraints. Hence, this research work is aimed at development of a radiation resisitant sodium submersible annular linear induction pump (ALIP) which can operate at 200 °C without any external cooling and which is compact enough (400 mm dia) for insertion through inspection canal.

1.4 Motivation for the Present Study

Compact, high temperature sodium submersible ALIP which can be operated in high radiation field is technological challenge. Presently there is no device which meets all the challenges mentioned above and hence none of the fast reactor has been provided

with a system which can completely drain primary sodium from SFR main vessel. Partial draining has been achieved by existing EM pump in the primary purification circuit of the reactor. In present day scenario, draining of sodium upto sub-assembly head is desired safety creiteria for enhanced reactor safety. The challenges stated motivated to take up research work for development of ALIP capable of operating in high temperature sodium submerged condition and radiation environment. In present application, the winding temperature of ALIP may go as high as 550 °C. Conventional organic electrical insulation can only withstand temperatures upto 200 °C. Hence, selection of non organic mineral insulation, which can withstand high temperature and radiation field [14] is one of the research problem.

1.5 Brief Description of Electromagnetic Pumps

For pumping of liquid metal, mechanical or electromagnetic (EM) pumps are used. Sodium, which finds application in fast reactors as coolant, is a good conductor of electricity and this property is exploited in the design and development of electromagnetic pumps. The function of EM pump is to force the liquid sodium to flow through a defined path. Mechanical sodium pump imparts the pumping energy to sodium by means of mechanical movement of the impeller. There is a relative motion between the stationary parts and the moving impeller of pump. Hence, complete sealing of sodium is difficult. Presence of physical moving parts in the mechanical pump makes it prone to failures, and this demands more maintenance.

1.5.1 Principle of EM pumps

In EM pumps, an electric current is forced (either conduction or induction) to flow through a liquid metal. When the current carrying liquid metal is placed in the magnetic field, it experiences an electromagnetic body force (Lorentz force) as per Eqn.1.1. The direction of the force is decided by Fleming's left-hand rule.

$$\text{Force}(F) = BIL \quad (1.1)$$

where B is the flux density, I is the current and L is the length of current carrying liquid metal. All the parameters mentioned above are 90° to each other. The above principle is exploited in all types of electromagnetic pumps.

The electromagnetic pumps have no moving parts, and this makes it maintenance free. Sodium is hermetically sealed in EM pumps, and this eliminates the problem of sodium leakage. However, EM pumps have lower efficiency as compared to the mechanical pumps. World over, EM pumps are preferred in purification circuits because they do not need oil seal and have no narrow gaps like hydrostatic bearing of mechanical pumps, eliminating the possibility of impure sodium plugging in the narrow gap. In mechanical pump, narrow gap exists in hydrostatic bearing where possibility of plugging of impure sodium always exists. Due to this reason, EM pumps are used for purification/other auxiliary sodium circuits of the reactor and experimental sodium loops which are of comparatively low capacity where lower efficiency is not of concern.

1.5.2 Classification

EM pumps are classified into two broad categories, viz, conduction pump and induction pump. Principal classification of the EM pumps is shown in Fig.1.3. Conduction pumps are the simplest type in construction where the current through the liquid metal is fed directly from the source. The induction pumps are those in which, the current induced in the liquid metal is by transformer action.

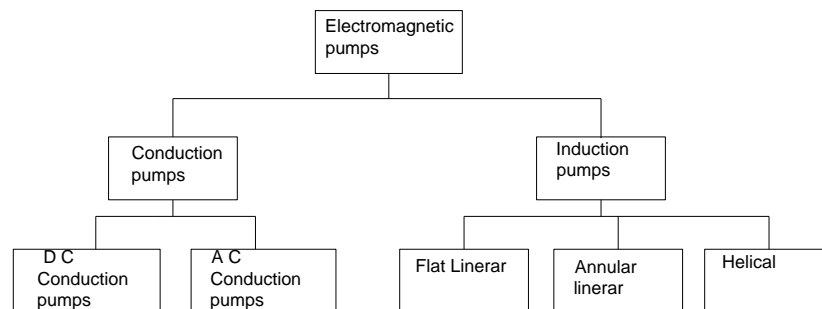


Fig. 1.3 Broad classification of the electromagnetic pumps [12]

1.5.3 DC conduction pump

Schematic of a DC conduction pump is shown in Fig.1.4 [12]. In D.C. conduction pump, current is forced through sodium kept in the pump duct placed in magnetic field. Hence, force is developed in sodium, which pumps the sodium. The magnetic field is produced by an electromagnet or permanent magnet such that the field direction is mutually perpendicular to the current and direction of the desired flow. The electrical conductivity of the duct material and liquid metal contributes to the leakage current parallel to the duct current. The fringing flux at the end also contributes to the braking action due to the eddy currents. This, in addition to other ohmic losses, gives rise to very low efficiency. These types of pumps find application where the ambient temperature is high. The operating current in this type of pump will be of the order of few kA and the operating voltage will be of order of few Volts [8,13].

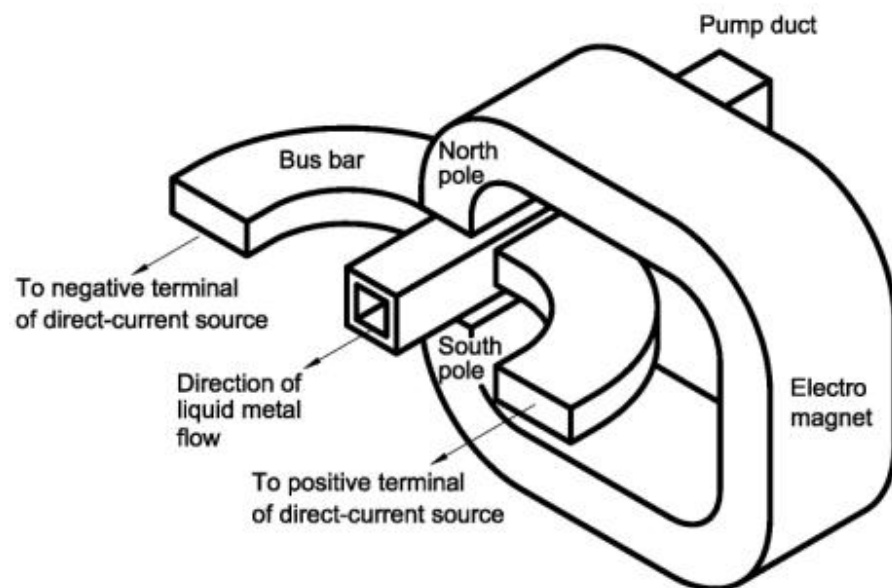


Fig. 1.4 Schematic of a DC conduction pump [12]

1.5.4 AC conduction pump

Working principle of AC conduction pump is similar to that of a DC conduction pump except the current and the flux which will be of alternating nature. In AC conduction pump, there are two windings placed over a laminated silicon steel core. They

are primary multi-turn coil and secondary single-turn coil. Sodium is placed in the duct. Secondary current alternating in nature is induced in single turn short circuited secondary coil due to linking of primary main flux. The secondary alternating current also passes through sodium placed in the duct since duct is part of secondary single turn coil. The primary winding produces pulsating field in the same core. This field interacts with the alternating current in sodium resulting in a unidirectional pumping force. The pressure developed in the pump pulsates at twice the supply frequency as explained below. Magnetic force acting on sodium is calculated as per Eqn. 1.1, where B and I are alternating in nature as given below.

$$B = B_{\max} \sin \omega t \quad (1.2)$$

$$I = I_{\max} \sin (\omega t \pm \theta) \quad (1.3)$$

where $\omega t = 2\pi f t$ and f is the supply frequency. Then the force Eq. 1.1 yields

$$F = B_{\max} \sin \omega t \times I_{\max} \sin (\omega t \pm \theta) \times L \quad (1.4)$$

by using trigonometric identities, we can write

$$F = B_{\max} \times I_{\max} \times \left[\frac{(1 - \cos \omega t) \cos \theta \pm \sin \omega t \sin \theta}{2} \right] \quad (1.5)$$

The term ωt gives rise to double frequency pulsation in developed pressure which can create noise and vibration. AC conduction pumps find applications in various experimental liquid metal loops having low head and flow rate. Conduction pumps are not normally used except in certain high temperature requirements due to their lower efficiency in the order of 2 – 5 %.

1.5.5 Flat linear induction pump (FLIP)

Flat linear induction pump is the simplest form of linear induction pump. The schematic of FLIP [12] is shown in Fig.1.5. The FLIP consists of duct carrying sodium and a three phase stator winding placed in slots perpendicular to the direction of flow

which generates a traveling magnetic field. A copper bar is brazed at both sides of duct along the length which plays the role of end ring like in conventional cylindrical induction motor. When the stator is excited from a three phase power supply, it creates a traveling magnetic field along the pump duct, inducing electric current in the conducting liquid sodium. The interaction between the traveling magnetic field of stator and the induced current in sodium produces an electromagnetic body force, pumping the liquid sodium through the duct.

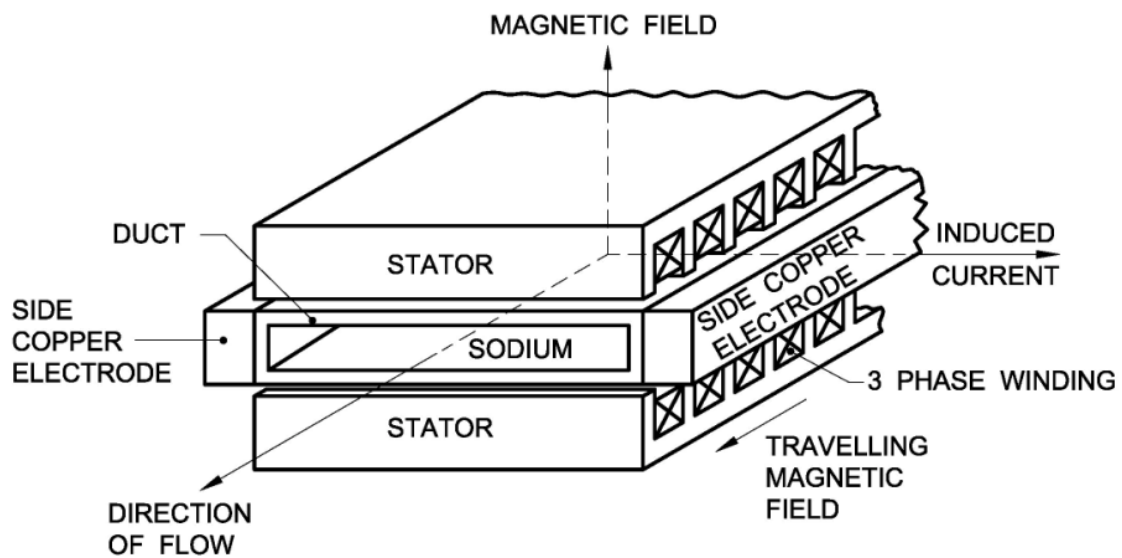


Fig. 1.5 Schematic of FLIP [12]

1.5.6 Annular linear induction pump (ALIP)

The general assembly of an Annular Linear Induction Pump (ALIP) [12] is shown in Fig.1.6. In ALIP, the annular duct contains the liquid sodium. The stator consists of three-phase circular distributed winding over the duct. The coils are placed in the slots of laminated stator stacks. The working principle of ALIP is similar to that of FLIP. The stator produces a radial magnetic field in annular duct region, travelling linearly along the length of annulus and linking with sodium in annular gap, which induces current in the sodium filled in annulus. Interaction of this induced current in sodium with the stator magnetic field produces a pumping force in sodium. ALIP has potential to operate as

sodium submersible pump at higher temperatures. Hence, this type of pump is chosen for development to meet the objective of research work [12].

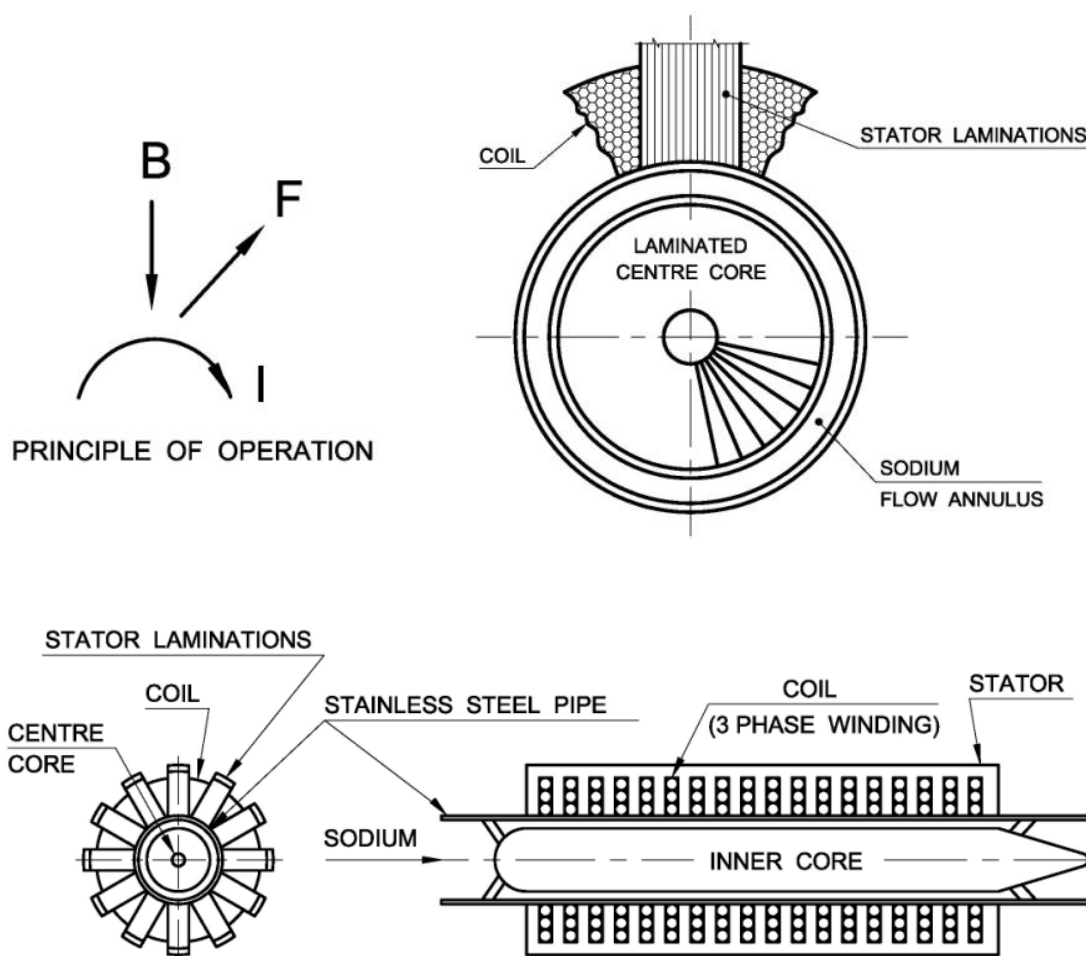


Fig. 1.6 : General Assembly and Principle of an ALIP [12]

1.6 Status of EM Pumps - a review

Electromagnetic pumps of various types have been designed, manufactured and tested in various countries. Many of these pumps were used in experimental facilities and many in nuclear reactors. Electromagnetic pumps are mainly used for pumping sodium metal. The literature on electromagnetic pump development is quite scattered since not many details are available at one place in open literature. Therefore, it was considered to list the available details of various electromagnetic pumps developed around the globe. The survey of electromagnetic pumps is arranged country-wise. The pumps of various countries cannot be compared in all respects since they were designed to meet specific

application of each country's program, moreover these pumps were developed in different periods of time also. Therefore, some of the relevant parameters of the pumps developed in various countries are presented in this chapter.

1.6.1 Development of EM Pumps in Russia

In Russia, many electromagnetic pumps have been designed and developed at D.V. Efremov Scientific Research Institute of Electrophysical Apparatus (NIIEFA) [40]. They are naturally cooled pumps. The technical parameters of these pumps are given in Table 1.1.

Table 1.1 Technical details of pumps from NIIEFA [40]

Nominal pressure, MPa	0.4	0.8	1.6	0.4	0.4	0.4	0.4	0.4
Nominal flow rate, m ³ /h	2.5	2.5	2.5	32	50	80	125	200
Power consumption, kW	1.65	2.64	6.43	14.3	19.8	31	50	76
Length, m	0.45	0.6	0.5	0.7	0.84	0.84	0.93	0.93
Diameter, m	0.25	0.25	0.4	0.4	0.4	0.41	0.43	0.5

Kirillov and et al. have described a two dimensional numerical model for analysis of the local and integral characteristics of linear EM pumps [18]. This pump called CLIP-A, has got the dimensions as shown in Table 1.2.

Table 1.2 Dimensions of CLIP-A [18]

Pump active length (m)	0.9376
Number of Poles (Nos.)	6
Tooth width (mm)	8.8
Slot width (mm)	17
Duct mean Diameter (m)	0.173
Non-magnetic Gap Height (mm)	17
Supply Frequency (Hz)	30

Hideo Araseki et al. reported experimental results of electromagnetic pumps (EMPs) pressure and flow rate pulsation as well as duct and pipes vibrations [28]. They have conducted studies on EMPs namely ALIP-1 and ALIP-2. Both pumps have annular

ducts of return flow type, i.e. sodium is pumped upward in an outer duct between inner and outer magnetic structure and then is flowing downward over the central duct. The details of the pumps are given in Table 1.3.

Table 1.3 Specification of ALIP-1 and ALIP-2 [28]

Nominal Parameters	ALIP-1	ALIP-2
Flow Rate (m ³ /min)	2.1	7.2
Developed pressure (MPa)	0.2	0.15
Frequency (Hz)	20	50
Phase Voltage (V)	225	380
Phase Current (A)	60	180
Stator Length (m)	0.938	0.85
Duct Average Diameter (m)	0.173	0.296
Duct Width (m)	0.01	0.012
Number of winding poles	6	6
Number of winding slots	36	36

1.6.2 Development of EM Pumps in France

Two Annular Linear Induction Pumps have been described in the specifications of French company Novatome [45]. The pumps have got the trade names IA 21 and IA 81 and its details are given in Table 1.4. Details of other pumps are given in Table 1.5.

Table 1.4 Details of IA 21 and IA 81 [45]

Nominal Parameters	IA 21	IA 81
Flow Rate (m ³ /hr)	4	8
Na Temperature (°C)	600	600
Differential Pressure rise (bars)	1.3	1.5
Active Power (kW)	2	2.5
Current at nominal flow (A)	4.5	6
Preheating Secondary circuit voltage (V)	6.5	13

Table 1.5 Details of ALIP from Novatome [45]

Description	IA 124	IA 251	IA 501	IA 1401
Delivery (m ³ /h)	12	25	50	140
Na Temperature (°C)	600	600	600	600
Differential pressure (bars)	3	5	5	4
N.P.S.H. (bars)	0.8	0.8	0.8	1
Active Power (kW)	8	25	45	80

Construction and tests in sodium of a 600 m³/h ALIP were carried out. The specifications of the pump are in Table 1.6.

Table 1.6: Specification of 600 m³/h ALIP [41]

Overall length (mm)		3930	
Overall transverse dimensions (mm)		740 x 790	
Pump weight inclusive of frame (tons)		4.5	
Connecting duct diameter (mm)		219	
Cooling mode		Axial air cooling	
Air flow rate (m ³ /hr)		4990	
Head loss in cooling (mbar)		34	
Power supply		Cyclo-converter 460 kVA Frequency range 0-15 Hz	
Calculated performance	Pump with no end pole	Pump with end pole	Pump with end pole
Sodium temperature (°C)	200	200	400
Nominal flow rate (m ³ /hr)	480	480	600
Differential pressure (bar)	4.42	5.17	5.45
Frequency (Hz)	8	8	10
Voltage per phase (V)	265	265	365
Current per phase (A)	295	295	295
Power requirement (kW)	143	144	193
Efficiency (%)	41.1	47.8	47
Power factor	0.611	0.615	0.597
Sodium velocity (m/s)	5.2	5.2	6.5

1.6.3 Development of EM Pumps in Japan

Nakazaki et al. [25] have described a sodium immersed self-cooled electromagnetic pump. The pump diameter is about 0.5 m and length about 1 m. About 90 % of the total heat generated at the stator is calculated to be transferred to the sodium inside the duct. The candidate materials proposed by Nakazaki et al. for sodium immersed self-cooled electromagnetic pump are given in Table 1.7. Model pump design specifications are provided in Table 1.8.

Table 1.7 Candidate materials for sodium immersed EM pump [25]

Electrical Components	Operating Temperature	Required Functions	Candidate Materials
Conductor	550°C	High Electrical Conductivity & Mechanical Strength	Alumina-Dispersion Strengthened Copper
Insulation	550°C	High BOV Characteristics, High Resistivity, Mechanical Strength	Alumina-Cloth Backed Mica-Tape
Lamination	550°C	Magnetic Characteristics.	Ceramic-Coated Electrical Steel

Table 1.8 Model pump design specifications [25]

Parameter	Self-cooled ALIP specifications
Flow rate (m ³ /min)	1
Developed head (MPa)	0.37
Sodium temperature (°C)	350
NPSH (m Sodium)	10
Voltage (V)	350
Current (A)	85
Power factor	0.53
Input power (kVA)	51
Efficiency (%)	22

A 160 m³/min capacity sodium immersed self cooled electromagnetic pump has also been developed for application as a main circulation pumps of FBR [26]. This

advanced pump is a submersible annular linear induction pump designed to be self-cooled by immersing into sodium and applying high temperature electrical insulation. Almost all the internal electrical losses were transferred to the surrounding sodium which can be recovered as electricity by turbine generators. The boundary between flow stability and instability of the EM pump operation has been defined by peak position of the Q-H curve, which was specified by magnetic Reynolds' number times slip of 1.4 to 1.5 at 335 °C. The specifications of the pump are indicated in Table 1.9.

Table 1.9 Details of submersible 160 m³/min EM pump [26]

Parameter	ALIP Specifications
Flow rate (m ³ /min)	160
Developed pressure (MPa)	0.25
Sodium temperature (°C)	335
Input power (kW)	1680
Terminal voltage (V)	1350
Phase current (A)	884
Frequency (Hz)	20
Number of poles	14
Flow gap (mm)	77
Flow velocity (m/s)	10.4
Number of coils	84 x 2
Outer dia. of casing (mm)	1900
Boundaries	SUS 304, ALLOY 625
Stator iron	Electrical Steel
Coil electrical insulations	Alumina Cloth, glass cloth and mica tape
Coil conductors	Copper

1.6.4 Development of EM Pumps in USA

A double stator electromagnetic pump has been described in [29] for the primary system of the Advanced Liquid Metal Reactor. The ratings of the pump are in Table 1.10.

Table 1.10 Rating of double stator EM pump [29]

Parameter	Double Stator ALIP
Flow rate (m ³ /minute)	43.5
Pressure (kPa)	793
Inlet sodium temperature (°C)	338
Frequency (Hz)	17.7
Gross operating efficiency (%)	56.9
Peak insulation temperature for inner stator (°C)	441
Peak insulation Temperature for outer stator (°C)	447

A self-cooled sodium submersible electromagnetic pump was reported by C. Deverge et al. [42] with primary materials of construction as stainless steel Type 304 and 316 (used for the pump outer housing and ducts, respectively), low carbon electrical iron for the stator laminations, electrolytic tough pitch copper for the conductors, and phlogopite (amber) mica tapes for the conductor insulation amber mica and Nextel (trade name) ceramic tape for coil insulation. Secon-5 (trade name) potting compound is used as a binder for the coil insulation. In addition, mica sheets are used to separate the upper and lower coil tiers and placed between the coils and lamination rings. The use of mica/Secon-5 insulation system has resulted in acceptable performance. The details of the pump are in Table 1.11.

Table 1.11 Details of self cooled ALIP [42]

Parameter	Once through ALIP details
Flow rate (m ³ /hr)	8100
Net circulating head (bar)	2.65
Operating temperature (°C)	345
Voltage (V)	950
Frequency (Hz)	10
Efficiency (%)	45
Power factor	0.5
Active power consumption (MW)	1.34
Weight (kg)	20000

Testing of a 43.5 m³/min EM pump in sodium has been described in [27]. The testing was carried at various v/f ratios. Details of the EM pump are given in Table 1.12.

Table 1.12 Details of 43.5 m³/min electromagnetic pump [27]

Flow (m ³ /min)	43.5
Pressure (kPa)	98
Sodium temperature (°C)	352
Net positive suction head (m-Na)	13.3
Input (kVA)	317
Terminal voltage (V)	850
Frequency (Hz)	18.7
Flow velocity (m/s)	9.2

GEC-REL direct current conduction pumps are designed for sodium and NaK liquid metals at operating temperatures up to 650°C. Four standard sizes cover a range of outputs, the maximum nominal output of 20 m³/h with a developed head of 6.7 kg/cm². With low voltage electric supply, the conductors need no insulation and therefore these pumps are suitable for application at high temperatures without the need for cooling, provided that the magnet temperature does not rise above 550°C. The D.C. pump has a characteristic of non-pulsating flow and can operate free from cavitation at an inlet pressure as low as 0.3 kg/cm² absolute.

The magnetic field of the pump is produced by a stabilized permanent magnet manufactured from Alcomax III. The duct is made of stainless steel 316. Two oxygen free copper electrodes are nickel plated to prevent their corrosion. They are brazed to the duct using high temperature vacuum technique.

Three annular linear induction pumps namely MK-1, MK-II and Auxiliary EM Lithium pump were developed by Liquid Metal Engineering. The MK-1 pump was operated flawlessly for 8600 h. Maximum temperature rise in the pump was about 55 °C, during pumping of lithium at 270 °C. Efficiency at the design point was 48 %.

Changes in MK-II include higher flow and heat capability (750 gpm, 62 psi) and re-design of inlet region to achieve improved hydraulic characteristics were incorporated. Improved hydraulic design of MK-II included magnetically graded end poles to reduce the end losses. A streamlined flux-return torpedo resulted in less hydraulic pressure drop through the pump. Due to the above changes, the pump was able to operate at lower NPSH with lithium as a pumping fluid. Details of EM pump for lithium pumping are given in Table 1.13.

Table 1.13 Details of EM pump for Lithium pumping

Parameter	MK-I	MK-II	Auxiliary pump
Structural design basis	Requirements of ASME Code Section III, Class 1; except no "N" stamp required.		
Fluid	Lithium		
Line voltage (V AC)	480	660	200
Line current (A)	90	200	40
Input power (kW)	60	200	20
Phases	3	3	3
No. of poles	6	6	6
Design point	0.038 m ³ /s at 228 kPa	0.047 m ³ /s at 428 kPa	0.00063 m ³ /s at 276 kPa
Duct diameter (cm)	15.2	15.2	5.08
Length (cm)	101	213	91.44
Diameter (cm)	40.6	40.6	25.4
Weight (kg)	522.7	613.63	75.91
Maximum Temperature (°C)	538	648	538
Cooling	Natural convection in air, radiation and heat transfer to lithium		
External environment	Air at ambient conditions		

1.6.5 Development of EM Pumps in England

Electromagnetic pumps were designed and manufactured in England mainly for DFR and PFR. FLIP, ALIP, DC Conduction pumps have been described in [13,20]

Details of one EM pump manufactured in England are given in Table 1.14 [13].

Table 1.14 Specification of the electromagnetic pump manufactured in England [13]

Fluid	Sodium
Pump output (hp)	14
Maximum metal temperature (°C)	500
Capacity (gpm)	400
Generated pressure head (lb/in ²)	50
Frequency (Hz)	50
Power factor	0.3
Efficiency in %	36

1.6.6 Development of EM Pumps in Germany

The manual of Interatom describes two electromagnetic pumps of capacities 50 m³/h and 100 m³/h [43]. The pumps described are reflux types. At the end of the pump length, the liquid metal flow is deflected and flows through the inner pipe to the outlet. The magnetic frame can be removed or mounted at the free end without interfering in the closed pipe system. Due to the eddy current losses in the annular gap, the pump can be started up without external trace heating. The technical data are given in Table 1.15.

Table 1.15: Technical data of 50 m³/h and 100 m³/h EM pump [43]

Design (m ³ /h)	100		50	
Operating temperature (°C)	200	550	200	550
Discharge capacity (m ³ /h)	100		50	
Discharge pressure (bar)	6.4	9.7	3.2	4.6
Power consumption in (kVA)	108	160	54	80
Operating voltage (V)	256	380	255	380
Power factor	0.77	0.85	0.76	0.83
Efficiency (%)	15.3	17	13.8	15.3
Weight (kg)	280		180	
Number of coils	36		18	

Comparison regarding MHD instability has been made in [21] among i) Soviet CLIP-3 / 3500 with a maximum sodium delivery of 3600 m³/h, ii) a French Prototype with a maximum delivery of 700 m³/h and iii) a West German EMP of 600 m³/h built by Interatom Society. Parameters of all the three electromagnetic pumps are provided in Table 1.16.

Table 1.16 Comparison of parameters of various EM pumps [21]

Parameters	Prototype French	CLIP-3/ 3500 Russian	Interatom NWA German
Temperature (°C)	200	300	350
Delivery (m ³ /h)	600	3600	609
Frequency (Hz)	10	50	40
Velocity (m/s)	6.5	12.9	9.52
Pole pitch (mm)	450	156	210
Wave number k (m ⁻¹)	6.98	20.14	14.96
Rm	3.33	0.96	3.09
Duct height (mm)	32.4	26	14.9
Mean radius (mm)	125.8	475	190
Length of the inductor (mm)	2270	5000	1000

It is seen that Russian pump is having capacity much higher than other two pumps hence length and diameter are high. All the three pumps operate at different frequency. Design velocity in the Russian pump is 12.9 m/s which is higher than the conventional design value of 10.0 m/s [12]

1.6.7 Development of EM Pumps in India

In India, developmental work related to EM Pump started with the development of Flat Linear Induction Pump (FLIP) of 20 m³/h, 5 kg/cm² capacity at Indira Gandhi Centre for Atomic Research, Kalpakkam. The pump was manufactured, tested and is being used in an experimental sodium loop. Further development of FLIP was not pursued because of stringent requirement of stainless steel duct to copper welding required in it, hence

attention switched over to annular linear induction pump (ALIP) which does not need stainless steel to copper welding and manufacturing is comparatively easy. ALIPs of 5 m³/h, 5 kg/cm² capacity and 170 m³/h, 4 kg/cm² capacity were developed and tested. Further, DC Conduction Pump of 0.36 m³/h, 1.45 kg/cm² capacity was developed and tested. The pumps developed proved indigenous design and manufacturing capability for sodium application. These ALIPs and FLIPs were designed and manufactured using conventional electrical insulation in the pump winding. The developed pumps were used in auxiliary circuits of Prototype Fast Breeder Reactor. The developed DC conduction pump can operate in sodium submerged condition. Specifications of FLIP, ALIP and DC Conduction Pump developed are given in Table 1.17, Table 1.18 and Table 1.19 respectively [8, 19].

Table 1.17 Specification of Indian FLIP

Flow (m ³ /h)	20
Pipe size (mm)	63
Differential pressure (kg/cm ²)	5
Fluid	Sodium
Temperature (°C)	530
Rating (kVA)	36
Efficiency (%)	20
Insulation	Class H

Table 1.18 Specification of Indian ALIP [19]

Flow (m ³ /h)	5	170
Head (kg/cm ²)	5	5
3 Phase line voltage (V)	415	360
Sodium temperature (°C)	400	450
Input power (kW)	11.5	98
Power factor	0.47	0.5
Efficiency (%)	6.8	19
Phase current (A)	21	308
Winding Insulation	Class H	Class H

Table 1.19 Specification of Indian DC Conduction Pump [8]

Nominal flow rate (m^3/hr)	0.36
Operating temperature ($^{\circ}\text{C}$)	560
Head developed by the pump at nominal flow and temperature (kg/cm^2)	1.45
Shut-off head at 2000 A, (kg/cm^2)	1.8
Operation	Continuous
Mounting position	Vertical
Pump design pressure at 600 $^{\circ}\text{C}$ (internal) (kg/cm^2)	5
Duct material	SS 316
Duct thickness (mm)	1.5

1.7 Knowledge Gained from the Literature Survey

It is learnt from literature that different types of electromagnetic pumps have been developed/manufactured by various countries depending on diverse need. Single phase AC induction pumps are used for low flow operation. DC conduction pumps are used for low flow and high temperature operation inclusive of sodium submerged condition. FLIP and ALIP are used in auxiliary circuits of sodium cooled fast reactors and sodium experimental facilities. Literature survey has indicated development of a few sodium submersible ALIPs but there is no mention of their use in reactor and under radiation field. Literature survey has not revealed provision of any pump in any sodium cooled fast reactor, right from beginning of its life for sodium draining during normal operation of reactor. However, survey has indicated the use of primary purification circuit EM pump for partial draining during decommissioning stage. Hence, the research work on design and development of sodium submerible annular linear induction pump for draining of sodium during normal operation and during decommissioning of sodium cooled fast reactor is a technological challenge and first-of-its-kind. The research work targeted to develop a compact annular linear induction pump for draining sodium at high temperature

without external cooling and to operate at intense radiation field in the reactor, to overcome the technological challenge.

1.8 Organization of Thesis

The aim of the present research is to design and develop a compact high temperature sodium submersible annular linear induction pump which can be used for draining of primary sodium from main vessel of PFBR.

Chapter 2 deals with development of a mathematical model for annular linear induction pump. In this chapter, various equations of the pump parameters are derived using basic principles.

Chapter 3 comprises of design of submersible annular linear induction pump and analysis.

Chapter 4 gives a detailed account of annular linear induction pump development and manufacture. Various aspects of the pump development are dealt here.

Chapter 5 illustrates the experimental sodium facility used for testing the developed submersible ALIP. This chapter also deals with experimental performance evaluation of the submersible ALIP developed.

Chapter 6 briefs about summary and future prospects.

Chapter-2

CHAPTER – 2

DEVELOPMENT OF MATHEMATICAL MODEL FOR ANNULAR LINEAR INDUCTION PUMP (ALIP)

2.1 Introduction

The aim of research work is to develop sodium submersible device which can pump out radioactive sodium at 200 °C from main vessel of PFBR [2]. Literature survey and study of various systems lead to the conclusion that annular linear induction pump (ALIP) has the potential to achieve the research aim. Use of mineral insulated winding can overcome the challenges associated in the development of ALIP for operation at high temperature and radiation field. Literature survey also indicated that use of mineral insulated cable in ALIP is first of its kind and is not reported in open literature. Parametric studies on conventional ALIP [9, 10, 11, 15, and 19] was carried out for understanding the functionality of ALIP and development of mathematical model was carried out.

This chapter deals with derivation of governing equations used in design of ALIP.

2.2 Design Methodology of Annular Linear Induction Pump (ALIP)

Generally, design and performance evaluation of ALIP are being done using equivalent circuit analysis similar to analysis being carried out for an induction motor [16, 17]. The equivalent circuit approach is based on lumped model of ALIP and is used for determining various parameters [12].

2.3 Working Principle and Equivalent Circuit of ALIP

Schematic construction of ALIP is shown in Fig. 2.1. It consists of annular stainless steel duct over which three phase winding is placed. Laminated stator core and centre core provide high permeance path for magnetic flux. The sodium to be pumped is placed in a stainless steel annular duct. ALIP has a 3-phase distributed winding which

produces a linearly traveling magnetic field. This traveling magnetic field induces current in sodium. Interaction of the induced current in sodium with the traveling magnetic field gives rise to a pumping force as per equation 1.1.

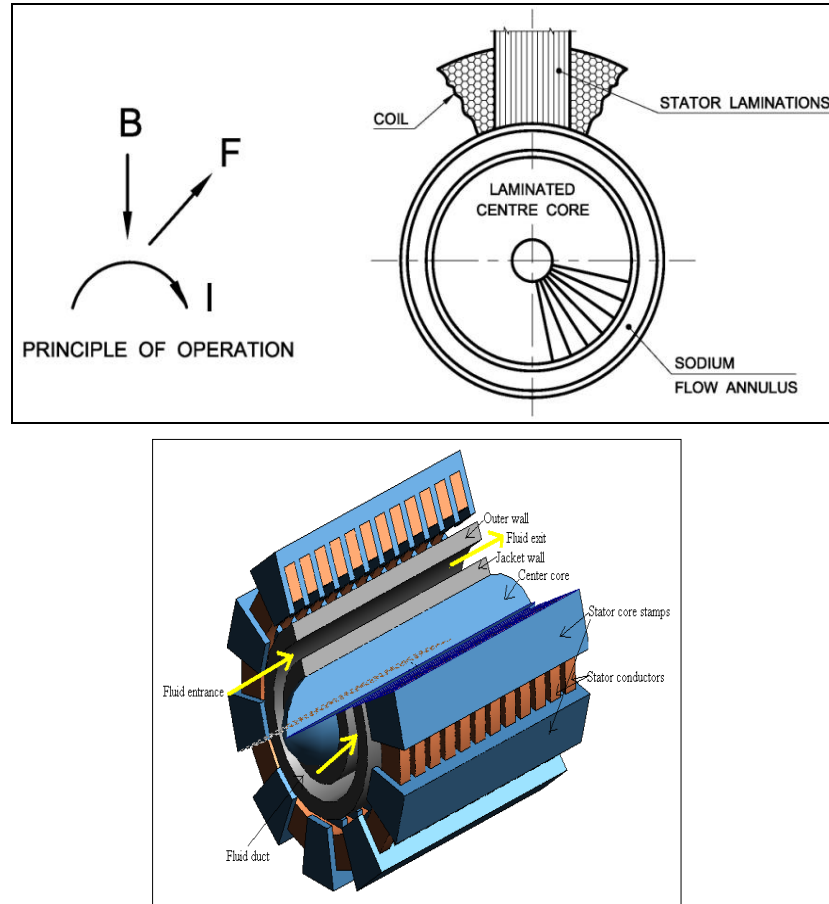


Fig. 2.1: Schematic construction and working principle of ALIP [12]

2.3.1 Equivalent circuit of ALIP

The equivalent circuit of ALIP, similar to equivalent circuit of an induction motor is depicted in Fig. 2.2. The symbol E_b in the equivalent circuit (Fig. 2.2) represents applied phase voltage. The constructional details of ALIP along with definition of various parameters are shown in Fig. 2.3 and Fig. 2.4 [12, 20]. The coil in ALIP is a circular pan-cake type which surrounds the central core and sodium completely. The coils are placed in slots and are thermally and electrically insulated from the stainless steel duct. The conductor in the coil does not occupy full space due to insulation. The entire flux produced by primary winding does not link the secondary and hence, the primary winding

has got a leakage reactance. The magnetic circuit is completed by cold rolled grain oriented (CRGO) laminations which are stacked together and arranged along the periphery of the duct as shown in Fig. 2.4. The non-magnetic stainless steel duct forms the annular space through which liquid sodium flows. This duct also has circulating current and it acts as short circuited secondary. The sodium in the duct is equivalent to a single turn secondary.

In the equivalent circuit, all the parameters of the secondary are referred to the primary side. Leakage inductance of secondary is assumed to be negligible. The symbols used in figures and derivations are given in Table- 2.1. The equivalent circuit analysis is carried out per phase basis with the assumption of symmetrical phase distribution of voltage and current in all the three phases. The end-effects are neglected in this approach. The cross-section view of ALIP is shown in Fig. 2.4.

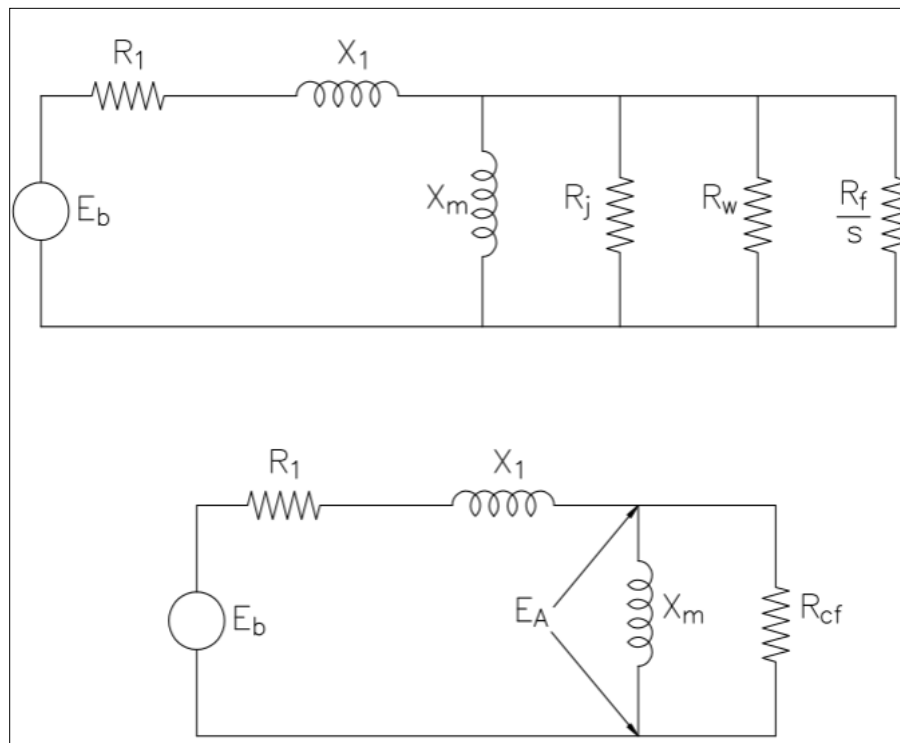


Fig. 2.2: Equivalent circuit of ALIP

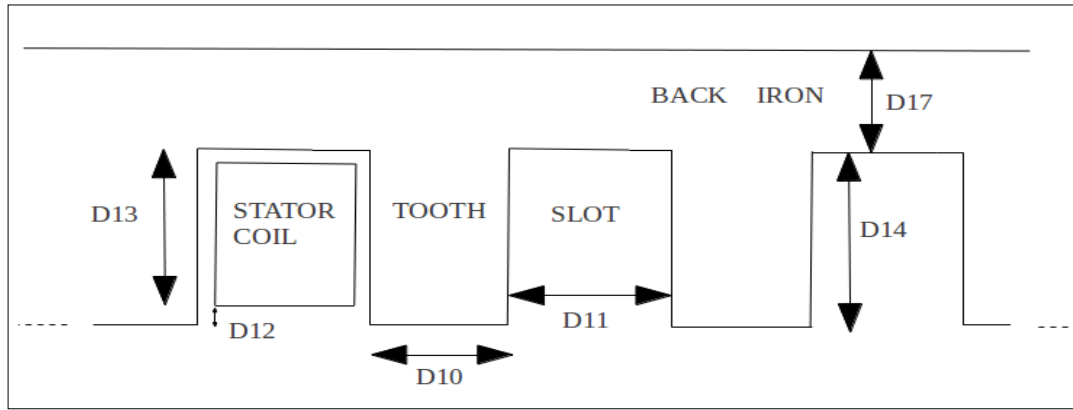


Fig. 2.3 Definition of parameters related to coils and slots

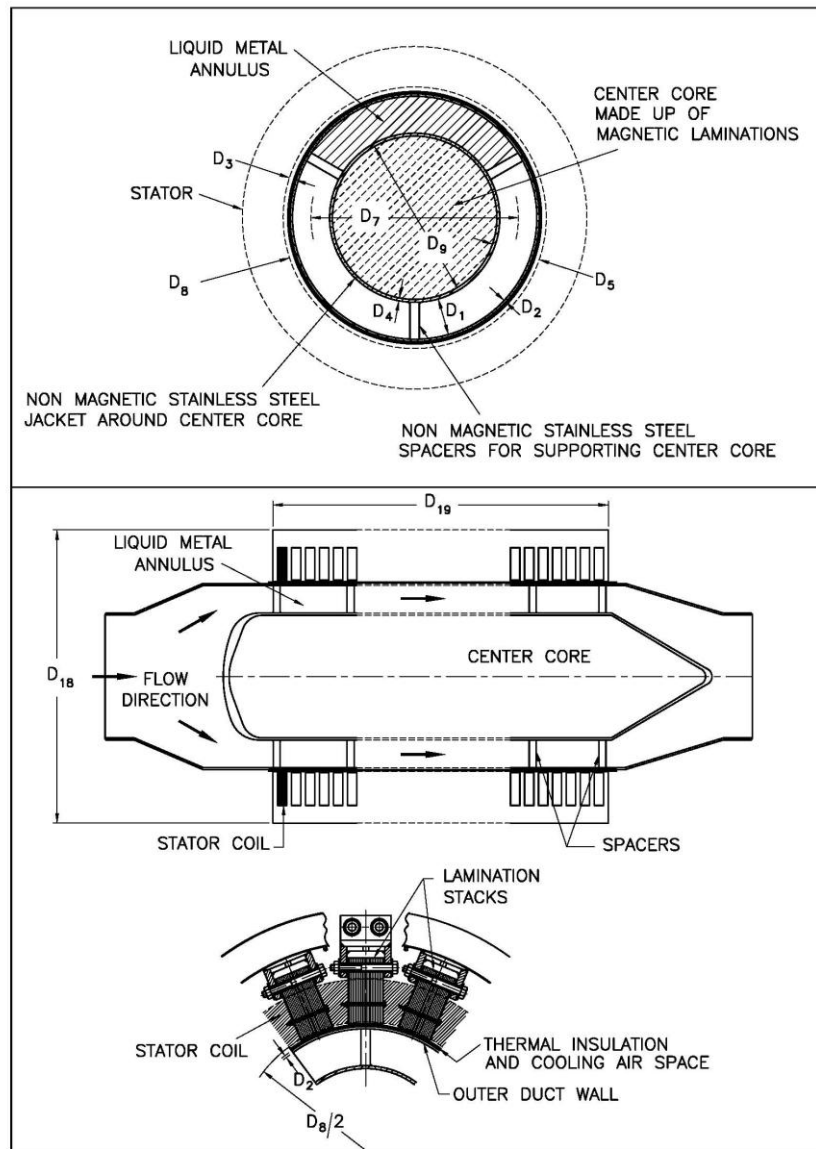


Fig. 2.4 Cross-section view of ALIP along with definition of various parameters

Table 2.1 List of parameters/variables used in derivation

D ₁	Radial annular width for liquid metal passage	N ₉	Multiplier for D ₅ to account for apparent increase in D ₅ due to slots
D ₂	Radial thickness of outer sodium duct	N _{sc}	Effective number of turns in series per phase in stator
D ₃	Radial gap between outer sodium duct and Stator bore	R ₁	Stator Winding Resistance (Ω / ph)
D ₄	Thickness of stainless steel jacket surrounding the central core	R _j	Equivalent resistance of jacket around central core (Ω / ph)
D ₅	Total non-magnetic gap	R _w	Equivalent resistance of outer annulus wall (Ω / ph)
D ₆	Pole Pitch	R _f	Equivalent resistance of liquid metal (Ω / ph)
D ₇	Mean diameter of Annulus	R _{cf}	Equivalent resistance of R _w , R _j and R _f in parallel
D ₈	Bore diameter of stator surface	X ₁	Stator winding Leakage Reactance (Ω / ph)
D ₉	Diameter of central core	X _m	Magnetizing Reactance (Ω / ph)
D ₁₀	Width of stator tooth	ρ_{Cu}	Resistivity of copper wire
D ₁₁	Width of stator slot	ρ_{SS}	Resistivity of Stainless Steel
D ₁₂	Clearance between top of coil and top of slot	ρ_{Na}	Resistivity of sodium
D ₁₃	Depth of coil side	I _{mg}	Magnetising Current
D ₁₄	Slot Depth	k _p	Pitch factor
D ₁₅	Mean length of coil turn	k _d	Winding distribution factor
N ₁	Number of Poles produced by stator winding	p	No. of pole-pairs
N ₂	Number of phases	V _{syn}	Synchronous velocity of traveling magnetic field
N ₃	Slots per pole per phase	V _L	Velocity of liquid metal
N ₄	Number of slots in stator	V _R	Relative velocity between traveling magnetic field and liquid metal
N ₅	Number of teeth in stator	ΔP	Differential pressure developed by pump
N ₇	Number of turns per coil	f	Stator electrical frequency (Hz)
N ₈	Carter co-efficient	μ_0	Permeability of vacuum

2.4 Estimation of Equivalent Circuit Parameters – A First Principle Approach

Design and performance evaluation of ALIP is done using the equivalent circuit approach, from the first principles.

2.4.1 Stator winding resistance (R_1)

Conventional ALIP has circular pan-cake winding which is made of enameled insulated copper wire. This circular winding is housed in stator slot. The expression for conventional ALIP winding resistance is obtained from the formula

$$\text{Resistance}(R_1) = \frac{\text{resistivity } (\rho) \times \text{Length } (L)}{\text{Area}(A)} \quad (2.1)$$

$$\text{Total length of one phase of primary winding} = \frac{D_{15}N_7N_4}{N_2} \quad (2.2)$$

Assuming 60% of slot cross-sectional area is occupied by copper

$$\text{Copper area in one slot} = \frac{D_{14}D_{11} \times 0.6}{N_7} \quad (2.3)$$

As a standard practice in design, $D_{14} = 5D_{11}$

$$\text{Wire cross-section } (A) = \frac{5D_{11} \times D_{11} \times 0.6}{N_7} = \frac{3D_{11}^2}{N_7} \quad (2.4)$$

$$R_1 = \frac{\rho l}{A} = \frac{\rho_{Cu} \times \frac{D_{15}N_7N_4}{N_2}}{\frac{3D_{11}^2}{N_7}} = \frac{\rho_{Cu}D_{15}N_7^2N_4}{3N_2D_{11}^2} \quad (2.5)$$

The assumption of 60% of slot cross-section area occupied by copper and equality $D_{14} = 5D_{11}$ are made to have similarity of expression for R_1 given in Handbook of Electromagnetic Pump Technology [12]. However this expression is not used in the design calculation for the developed ALIP. R_1 is calculated using Eq 2.1 and actual cross-section of copper in MI cable without considering the slot fill factor of 60%. The calculation carried out is indicated in Annexure-A Eqn. (A-22) in Page no. 120.

2.4.2 Stator winding leakage reactance

The leakage reactance (X_1) is due to the fact that some of the primary flux is leaked from main flux path resulting in leakage reactance of the winding. The total leakage flux ϕ mainly consists of two components (ϕ_1 and ϕ_2) as shown in Fig. 2.5 where ϕ_1 is the leakage flux passing through winding portion and ϕ_2 is the leakage flux where winding is not present.

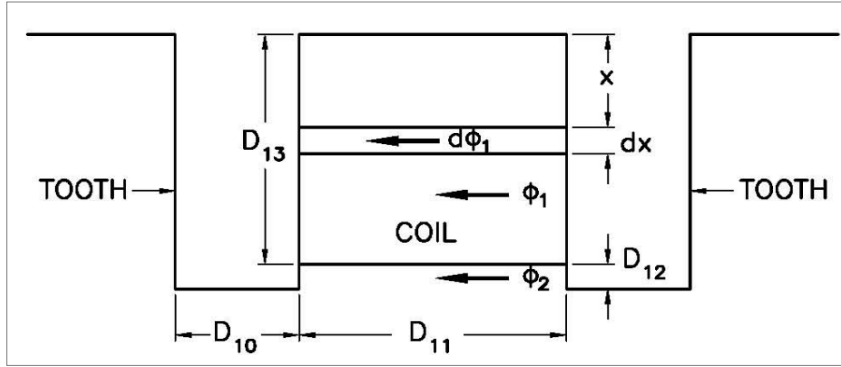


Fig. 2.5 Different leakage fluxes of primary winding

Let L be the inductance per coil and I current in the winding, then

Primary winding leakage reactance per phase becomes

$$X_1 = 2\pi f L N_1 N_3 \quad (2.6)$$

$$L = N_1 \frac{\phi}{I} = N_1 \frac{\phi_1}{I} + N_1 \frac{\phi_2}{I} = L_1 + L_2 \quad (2.7)$$

where, I is the current in the conductor of the winding & ϕ is the total leakage flux.

$$L_1 = N_1 \frac{\phi_1}{I} \quad \text{and} \quad L_2 = N_1 \frac{\phi_2}{I} \quad (2.8)$$

$$\text{Amp-turns at strip (refer Fig. 2.5)} \quad d\phi_1 = I \cdot \frac{N_1}{D_{13}} \cdot x \quad (2.9)$$

$$\text{Reluctance of the strip} = \frac{\text{Length of Flux Flow}}{\mu_0 \text{ Area of flux flow}} = \frac{D_{11}}{\mu_0 \text{ Area of Flux Flow}} \quad (2.10)$$

Area for flux flow $= \pi D_g dx$, (flux flow referred in Eq 2.10 is parallel to pump longitudinal axis)

This is because, the perimeter of stator lamination at the stator bore diameter through which the flux passes (magnetic material width) is πD_8 , where D_8 is the diameter of the stator bore surface and height of the strip is dx .

$$d\phi_1 = \frac{\text{mmf at strip}}{\text{reluctance of strip}} = I \cdot \frac{N_7}{D_{13}} \cdot x \cdot \frac{\mu_0 \pi D_8 dx}{D_{11}} \quad (2.11)$$

$$\text{Turns enclosed by } d\phi_1 = \frac{N_7}{D_{13}} \cdot x \quad (2.12)$$

$$\text{turns} \times d\phi_1 = \frac{N_7}{D_{13}} \cdot x \cdot I \cdot \frac{N_7}{D_{13}} \cdot x \cdot \frac{\mu_0 \pi D_8}{D_{11}} dx$$

$$\text{turns} \times d\phi_1 = \frac{N_7^2 \pi D_8 \mu_0 I x^2}{D_{13}^2 D_{11}} dx \quad (2.13)$$

$$N_7 \phi_1 = \text{flux linkage of } \phi_1 = \int \text{turns} \times d\phi_1$$

$$\int \text{turns} \times d\phi_1 = \int \frac{N_7^2 \pi D_8 \mu_0 I x^2}{D_{13}^2 D_{11}} dx \quad (2.14)$$

$$L_1 = \frac{N_7 \phi_1}{I} = \int \frac{\text{turns} \cdot d\phi_1}{I} = \int \frac{N_7^2 \pi D_8 \mu_0 I x^2}{D_{13}^2 D_{11} I} dx = \frac{\pi \mu_0 N_7^2 D_8}{D_{13}^2 D_{11}} \int x^2 dx = \frac{\pi \mu_0 N_7^2 D_8}{D_{13}^2 D_{11}} \left[\frac{x^3}{3} \right]_0^{D_{13}} \quad \dots (2.15)$$

$$L_1 = \frac{\pi \mu_0 N_7^2 D_8 D_{13}}{3 D_{11}} \quad (2.16)$$

For flux ϕ_2 which is enclosed by the entire ampere turns of the slot.

$$\text{Amp - turns} = N_7 I$$

$$\text{Reluctance} = \frac{\text{Length of flux } \phi_2 \text{ flow}}{\mu_0 \text{ Area of flux } \phi_2 \text{ flow}} = \frac{D_{11}}{\mu_0 \text{ Area of flux } \phi_2 \text{ flow}} = \frac{D_{11}}{\mu_0 \pi D_8 D_{12}} \quad (2.17)$$

Area for flux ϕ_2 flow = $\pi D_8 D_{12}$ where D_8 is the diameter of the stator bore surface and D_{12} is height as shown in Fig. 2.5.

$$\phi_2 = \frac{\text{mmf}}{\text{reluctance}} = N_7 I \times \frac{\mu_0 \pi D_8 D_{12}}{D_{11}} \quad (2.18)$$

$$\frac{N_7 \phi_2}{I} = \frac{N_7 \cdot N_7 I}{I} \times \frac{\mu_0 \pi D_8 D_{12}}{D_{11}} = \frac{N_7^2 \mu_0 \pi D_8 D_{12}}{D_{11}} \quad (2.19)$$

Total inductance

$$L = N_7 \frac{\phi_1}{I} + N_7 \frac{\phi_2}{I} = L_1 + L_2 = \frac{N_7^2 \pi \mu_0}{D_{11}} \left[\frac{D_8 D_{13}}{3} + D_8 D_{12} \right] \quad (2.20)$$

Total Leakage Impedance of stator

$$X_1 = 2\pi f L N_1 N_3 = 2\pi f N_1 N_3 \frac{N_7^2 \pi \mu_0}{D_{11}} \left[\frac{D_8 D_{13}}{3} + D_8 D_{12} \right]$$

$$X_1 = \frac{2.48 \times 10^{-5} f \times N_1 N_3 N_7^2}{D_{11}} \left[\frac{D_8 D_{13}}{3} + D_8 D_{12} \right] \quad (2.21 \text{ a})$$

Multiplying and dividing the Eq (2.21 a) by 2, above expression for X_1 becomes

$$X_1 = \frac{4.96 \times 10^{-5} f \times N_1 N_3 N_7^2}{D_{11}} \left[\frac{D_8 D_{13}}{6} + \frac{D_8 D_{12}}{2} \right] \quad (2.21 \text{ b})$$

It can be observed that expression of X_1 indicated in Eq (2.21 b) is same as of expression of X_1 given in Handbook of Electromagnetic Pump [12], this confirms the correctness of methodology followed for estimation of expression for X_1 from first principle approach.

2.4.3 Magnetizing reactance (X_m)

Magnetizing reactance (X_m) is responsible for producing flux in air gap.

Let flux per pole be Φ then Average air-gap flux density = ϕ / A

Peak value of flux density $B_m = (\pi/2)(\phi/A)$ (assuming a sinusoidal flux distribution)

Effective air gap length = $N_9 \times D_5$

where N_9 is the multiplier to account for apparent increase in air-gap D_5 due to the presence of slots

$$\text{Amp - turns} = H_m N_9 D_5 = \frac{B_m}{\mu_0} \times N_9 D_5 = \frac{\pi \phi}{2 A \mu_0} \times N_9 D_5 \quad (2.22)$$

Fundamental component of stator mmf (F_a)

$$F_a = \frac{1.35IT_{ph}k_mK_e}{p} \text{ amp turn per pole} \quad [17] \quad (2.23)$$

Where, F_a – amplitude of fundamental component

I – Magnetising current (rms) = I_{mg}

T_{ph} – Turns per phase = N_{sc}

k_m – distribution factor = k_d

k_e = span factor = k_p

p – pole pairs = $N_1/2$

In terms of the notations used in this thesis

$$F_a = \frac{1.35I_{mg}N_{sc}k_dK_p}{\frac{N_1}{2}} = \frac{1.35 \times 2 \times I_{mg}N_{sc}k_dK_p}{N_1} \quad (2.24)$$

Equating equations (2.22) & (2.24)

$$\begin{aligned} \frac{1.35 \times 2 \times I_{mg}N_{sc}k_dK_p}{N_1} &= \frac{\pi \phi}{2 A \mu_0} \times N_9 D_5 \\ I_{mg} &= \frac{\pi}{2} \times B_g \times \frac{1}{\mu_0} \times \frac{N_9 D_5 N_1}{1.35 \times 2 \times N_{sc} k_p k_d} = \frac{\pi}{2} \times \frac{1}{\mu_0} \times \frac{1}{1.35} \times \frac{1}{2} \times \frac{N_9 N_1 D_5 B_g}{N_{sc} k_p k_d} \\ I_{mg} &= \frac{\pi}{2} \times \frac{10^7}{4\pi} \times \frac{1}{1.35} \times \frac{1}{2} \times \frac{N_9 N_1 D_5 B_g}{N_{sc} k_p k_d} = 0.463 \times 10^6 \times \frac{N_9 N_1 D_5 B_g}{N_{sc} k_p k_d} \end{aligned} \quad (2.25)$$

E_A – voltage induced across X_m

$$E_A = \frac{1}{\sqrt{2}} \times \frac{\pi}{2} \times 2f \times k_d \times k_p \phi_T \frac{N_{sc}}{N_1} \quad (2.26)$$

$$\phi_T = B_g \pi D_7 D_6 N_1 \quad (2.27)$$

$$E_A = 2.22 f k_d k_p \frac{N_{sc}}{N_1} B_g \pi D_7 D_6 N_1 = 2.22 \pi f B_g \pi D_7 D_6 N_{sc} k_d k_p \quad (2.28)$$

$$X_m = \frac{E_A}{I_m} = \frac{2.22 \pi f B_g \pi D_7 D_6 N_{sc} k_d k_p}{0.463 \times 10^6 \times \frac{N_1 N_9 D_5 B_g}{N_{sc} K_p K_d}} = 15.06 \times 10^{-6} \times \frac{f (N_{sc} k_d k_p)^2 D_6 D_7}{N_1 N_9 D_5} \quad (2.29)$$

Multiplying and dividing by N_2 i.e. Number of phases which are normally 3

$$X_m = \frac{15.06 \times 10^{-6}}{N_2} \times \frac{N_2 \times f (N_{sc} k_d k_p)^2 D_6 D_7}{N_1 N_9 D_5} = \frac{15.06 \times 10^{-6}}{3} \times \frac{N_2 \times f (N_{sc} k_d k_p)^2 D_6 D_7}{N_1 N_9 D_5}$$

In the above expression, one N_2 has been taken as 3 to have similarity with the expression given in Handbook of Electromagnetic Pump[12].

$$X_m = 5.02 \times 10^{-6} \times \frac{N_2 \times f (N_{sc} k_d k_p)^2 D_6 D_7}{N_1 N_9 D_5} \quad (2.30)$$

The above expression (2.30) is valid for a 3 phase machine only.

2.4.4 Equivalent resistance of outer annulus wall (R_w):

$$\text{Mean diameter of outer pipe} = D_7 + \frac{D_1}{2} \times 2 + \frac{D_2}{2} \times 2 = D_7 + D_1 + D_2 \quad (2.31)$$

$$\text{The circumference length of outer pipe} = \pi (D_7 + D_1 + D_2) \quad (2.32)$$

$$\text{Pipe cross-section area (pump length x wall thickness)} = D_2 (N_4 D_{11} + N_5 D_{10}) \quad (2.33)$$

$$\text{Cross-section Area /phase} = \frac{D_2 (N_4 D_{11} + N_5 D_{10})}{N_2} \quad (2.34)$$

$$R_w = \frac{\rho l}{A} \times \left(\frac{N_{primary}}{N_{secondary}} \right)^2 = \frac{\rho_{ss} \pi (D_7 + D_1 + D_2) N_2 (N_{sc} k_p k_d)^2}{D_2 (N_4 D_{11} + N_5 D_{10})} \quad (2.35)$$

2.4.5 Equivalent resistance of jacket around central core (R_j)

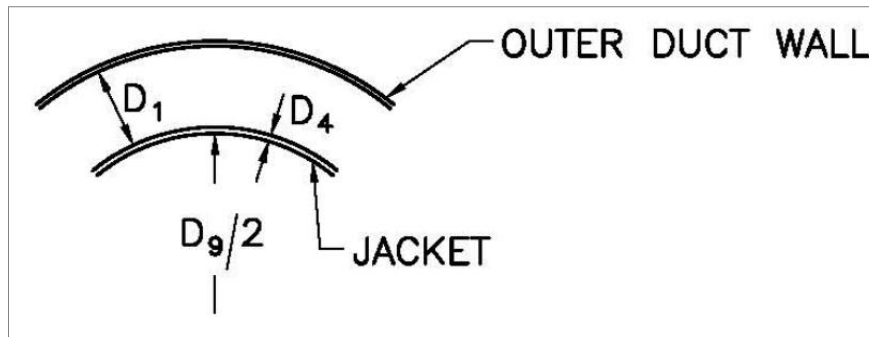


Fig. 2.6 Non-magnetic jacket over central core

As per Fig. 2.6,

$$\text{Mean circumferential length of jacket} = \pi \left(D_9 + \frac{D_4}{2} \times 2 \right) = \pi(D_9 + D_4) \quad (2.36)$$

$$\text{Jacket cross-section area} = \text{pump length} \times \text{wall thickness} = \frac{D_4(N_4 D_{11} + N_5 D_{10})}{N_2} \quad (2.37)$$

$$R_j = \frac{\rho l}{A} \times \left(\frac{N_{\text{primary}}}{N_{\text{secondary}}} \right)^2 = \frac{\rho_{SS} \pi (D_9 + D_4) N_2 (N_{sc} k_p k_d)^2}{D_4 (N_4 D_{11} + N_5 D_{10})} \quad (2.38)$$

2.4.6 Equivalent resistance of liquid metal (R_f):

$$\text{Mean circumferential length of liquid metal} = \pi D_7$$

$$\text{Cross-section of liquid metal per phase} = \frac{D_1 (N_4 D_{11} + N_5 D_{10})}{N_2} \quad (2.39)$$

$$R_f = \frac{\rho_{Na} \pi D_7 N_2 (N_{sc} k_p k_d)^2}{D_1 (N_4 D_{11} + N_5 D_{10})} \quad (2.40)$$

$$\text{Mean length of annular space} = \pi D_7$$

Stator length = $\tau \times N_1$ where τ is pole pitch, so R_f can also be expressed as

$$R_f = \frac{\rho_{Na} \pi D_7 N_2 (N_{sc} k_p k_d)^2}{D_1 \tau N_1} \quad (2.41)$$

2.4.7 Derivation of differential pressure developed on liquid sodium by ALIP

The differential pressure developed on liquid sodium by ALIP was derived using schematic shown in Fig 2.7.

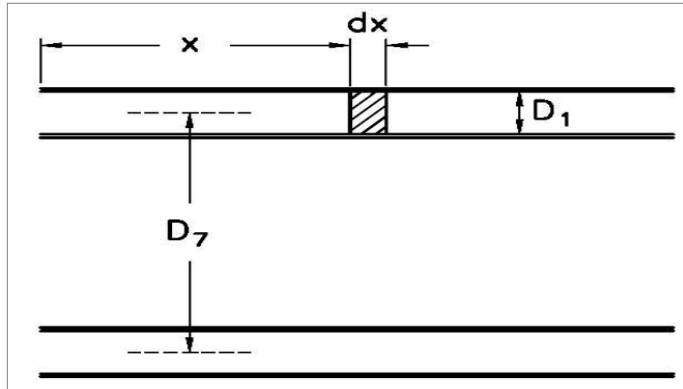


Fig. 2.7: Schematic of annular gap D_1

D_1 is annular gap where liquid sodium is filled

At a point x , gap flux density = B_x

$$B_x = B_m \sin(\omega t - \beta x) \quad (2.42)$$

where, $\beta = \frac{2\pi}{2\tau} = \frac{\pi}{\tau}$

Synchronous velocity = $2 f \tau = V_{\text{syn}}$

$$\text{slip } s = \frac{V_{\text{syn}} - V_L}{V_{\text{syn}}} \quad (2.43)$$

and relative velocity

$$V_R = V_{\text{syn}} - V_L = s V_{\text{syn}}$$

At point x emf induced = $B_x L V_R$ (in this section L is the length)

$$\text{Current in the element } dx = I_x = \frac{B_x L V_R}{\rho_{Na} \times \frac{\pi D_1}{D_1 dx}} = \frac{B_x L V_R D_1 dx}{\rho_{Na} \pi D_1} \quad (2.44)$$

$$\text{Force on the element } dx = dF = B_x L I_x = \frac{B_x^2 L^2 V_R D_1}{\rho_{Na} \pi D_1} dx \quad (2.45)$$

$$\text{Force over a pole pair} = F_p = \frac{L^2 V_R D_1}{\rho_{Na} \pi D_1} \int B_x^2 dx \quad (2.46)$$

$$\int B_x^2 dx = \int B_m^2 \sin^2(\omega t - \beta x) dx = B_m^2 \int \frac{1 - \cos 2(\omega t - \beta x)}{2} dx \quad (2.47)$$

$$= \frac{B_m^2}{2} \left(\int dx - \int \cos 2(\omega t - \beta x) dx \right) \quad \text{applying limit 0 to } 2\tau$$

$$= \frac{B_m^2}{2} \left[x - \frac{\sin 2(\omega t - \beta x)}{-2\beta} \right]_0^{2\tau} = \frac{B_m^2}{2} \left[2\tau + \frac{\sin 2(\omega t - \beta 2\tau)}{2\beta} - \frac{\sin 2\omega t}{2\beta} \right]$$

$$= \frac{B_m^2}{2} \left[2\tau + \frac{\sin 2(\omega t - 2\pi)}{2\beta} - \frac{\sin 2\omega t}{2\beta} \right] = \frac{B_m^2}{2} \left[2\tau + \frac{\sin 2(\omega t)}{2\beta} - \frac{\sin 2\omega t}{2\beta} \right]$$

$$= B_m^2 \tau$$

Therefore,
$$F_p = \frac{L^2 V_R D_1}{\rho_{Na} \pi D_7} \int B_x^2 dx = \frac{L^2 V_R D_1}{\rho_{Na} \pi D_7} B_m^2 \tau \quad (2.48)$$

Total force on $(N_1/2)$ pole pairs = $F = F_p \times \frac{N_1}{2} = \frac{L^2 V_R D_1}{\rho_{Na} \pi D_7} \frac{B_m^2 \tau N_1}{2} \quad (2.49)$

Differential pressure = $\Delta p = \frac{F}{area} = \frac{F}{\pi D_7 D_1} = \frac{L^2 V_R D_1}{\rho_{Na} \pi D_7} \frac{B_m^2 \tau N_1}{2\pi D_7 D_1} \quad (2.50)$

$L = \pi D_7$ and $V_R = s V_{syn}$ substituting these values in the above equation

$$F = \frac{\pi^2 D_7^2 s V_{syn} D_1}{\rho_{Na} \pi D_7} \frac{B_m^2 \tau N_1}{2\pi D_7 D_1} \quad (2.51)$$

Re-arranging the equation

$$F = \frac{D_1 \tau N_1}{\pi \rho_{Na} D_7} \frac{B_m^2 \pi^2 D_7^2 V_{syn} s}{2\pi D_7 D_1} \quad (2.52)$$

Equivalent resistance of liquid metal R_f is given by

$$R_f = \frac{\rho_{Na} \pi D_7 N_2 (N_{sc} k_p k_d)^2}{D_1 \tau N_1}$$

Re-arranging the terms we get the following equation

$$\frac{D_1 \tau N_1}{\pi \rho_{Na} D_7} = \frac{N_2 (N_{sc} k_p k_d)^2}{R_f} \quad (2.53)$$

The rms voltage induced in fluid per phase at synchronous velocity

$$e_a = \frac{B_m}{\sqrt{2}} \pi D_7 V_{syn} \quad (2.54)$$

Equivalent voltage referred to primary winding (i.e. voltage across X_m)

$$E_A = e_a (N_{sc} k_p k_d) = \frac{B_m}{\sqrt{2}} \pi D_7 V_{syn} (N_{sc} k_p k_d) \quad (2.55)$$

$$E_A^2 = \frac{B_m^2 \pi^2 D_7^2 V_{syn}^2 (N_{sc} k_p k_d)^2}{2} \quad (2.56)$$

Re-arranging the above equation the following equation is obtained

$$B_m^2 \pi^2 D_7^2 V_{syn} = \frac{2E_A^2}{V_{syn}(N_{sc} k_p k_d)^2} \quad (2.57)$$

Substituting values derived in eqn (2.53) and (2.57) in (2.50) the following equation is obtained

$$\Delta p = \frac{N_2(N_{sc} k_p k_d)^2}{R_f} \times \frac{2E_A^2}{V_{syn}(N_{sc} k_p k_d)^2} \times \frac{s}{2\pi D_7 D_1}$$

$$\Delta p = \frac{N_2(N_{sc} k_p k_d)^2}{R_f} \times \frac{2E_A^2}{V_{syn}(N_{sc} k_p k_d)^2} \times \frac{s}{2\pi D_7 D_1} \quad (2.58)$$

$$\Delta p = \frac{N_2 s E_A^2}{R_f \pi D_7 D_1 V_{syn}} = \frac{N_2 s E_A^2}{R_f Q_{syn}} \quad (2.59)$$

The above expression (Eqn. 2.59) for differential pressure does not take into account the hydraulic losses and entry and exit end-effect losses. The entry and exit losses decrease with increase in number of poles and this effect has been accounted empirically by the factor $(N_1-1)/(N_1+1)$ [12]. After taking into account the exit and entry end-effect losses, expression for pressure developed in ALIP is derived as;

$$\Delta P = \left(\frac{N_1 - 1}{N_1 + 1} \right) \frac{N_2 s E_A^2}{R_f Q_{syn}} \quad (2.60)$$

2.5 Summary

Mathematical model for annular linear induction pump using first principle approach was made. Derivation of formulae for equivalent circuit parameters like winding resistance, leakage reactance, magnetizing reactance, resistance of wall, jacket, pumped fluid and pressure developed by the pump were used in design. Derivation of the formulae gives more in-sight of design of the pump and also it makes base for modification in equivalent circuit for incorporating effect of eddy current loss in stainless steel sheath of winding in newly designed pump.

Chapter-3

CHAPTER – 3

SUBMERSIBLE ANNULAR LINEAR INDUCTION PUMP DESIGN AND ANALYSIS

3.1 Design Requirement

Using equivalent circuit approach, design and development of sodium submersible annular linear induction pump for draining of sodium from PFBR Main Vessel is taken up. This necessitated the development of annular linear induction pump which is totally enclosed in stainless steel enclosure and its winding made of mineral insulated stainless steel sheathed cable capable of withstanding temperature upto 550 °C. The design is aimed for compact, hermetically sealed annular linear induction pump to achieve sodium submersible operation at sodium temperature of 200 °C. An ALIP of 2.0 m³/h flow and 4.0 kg/cm² pressure head is designed for sodium draining. While designing, care was taken to achieve pump diameter less than 450 mm to facilitate easy insertion through available inspection canal in PFBR roof slab.

3.2 Design of Submersible Annular Linear Induction Pump

The flow rate of 2.0 m³/h was selected for the pump to maintain compactness of pump having reasonable drain time. Pressure head of 4.0 kg/cm² was selected to overcome static head in PFBR vessel and frictional losses in the drain pipe. Design of ALIP was carried out as per flow chart shown in Fig. 3.1 and the design calculations are provided in Appendix-A. ALIP is designed with winding made from mineral insulated stainless steel sheathed cable which can withstand temperature upto 550 °C and intense radiation field. Retainer plates are used to retain the windings made from the mineral insulated stainless steel sheathed cable since this cable is not flexible as conventional winding cable. Introduction of mineral insulated stainless steel sheathed cable facilitates ALIP for high temperature operation but also introduces higher loss due additional loss in stainless steel sheath and retainer plate.

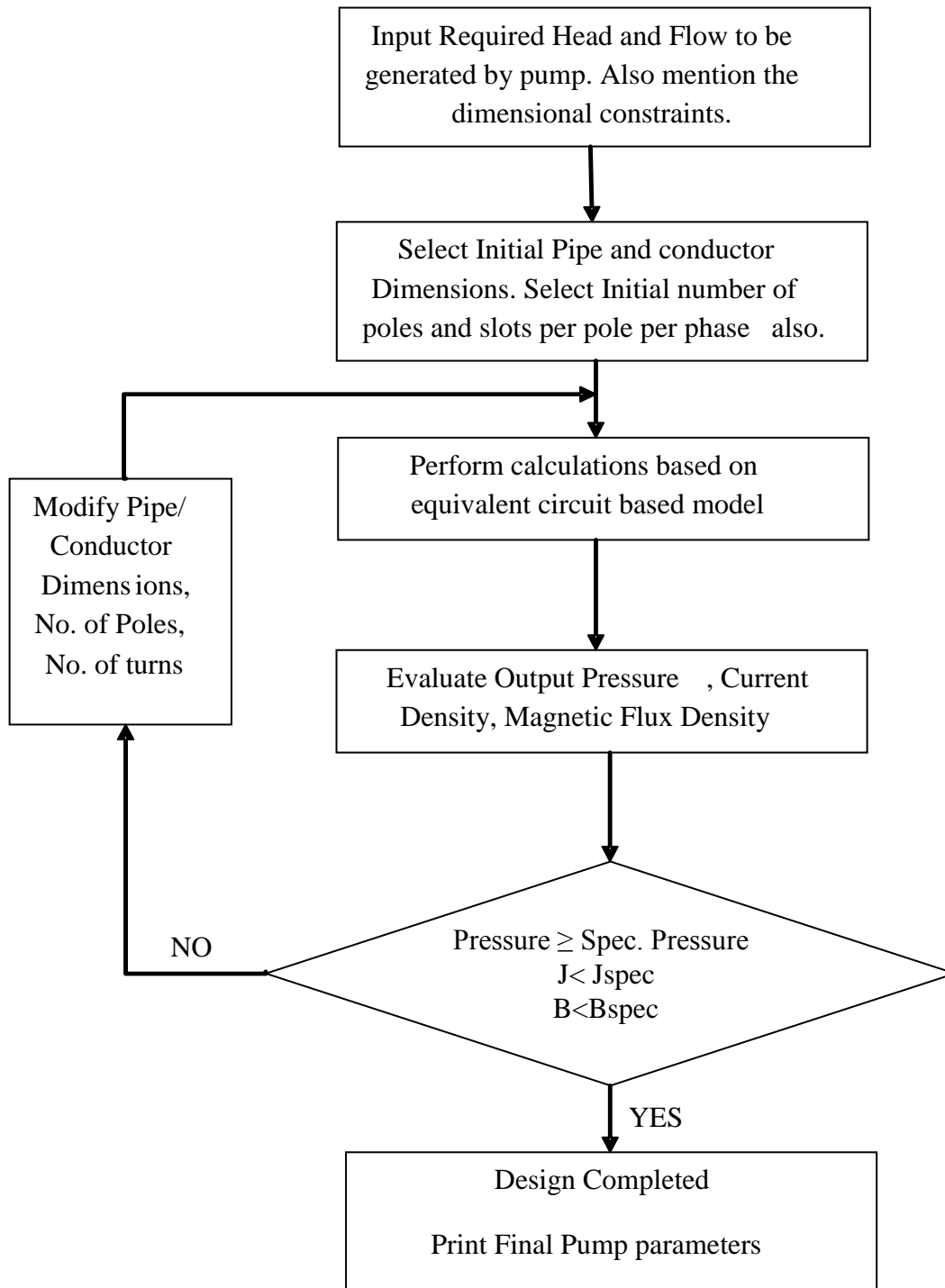


Fig.3.1 Flow chart for ALIP design calculations

3.3 Dimensions of Designed ALIP

General assembly of designed submersible ALIP is shown in Fig. 3.2. As per the design calculations (Appendix-A), pump develops a pressure of 4.0 kg/cm^2 at 150 volts per phase input voltage and a phase current of 60.5 A which meets the design requirement. The flux

density in the core is within the permissible limit of 1.2 T. The specification of developed submersible ALIP is given in Table 3.1.

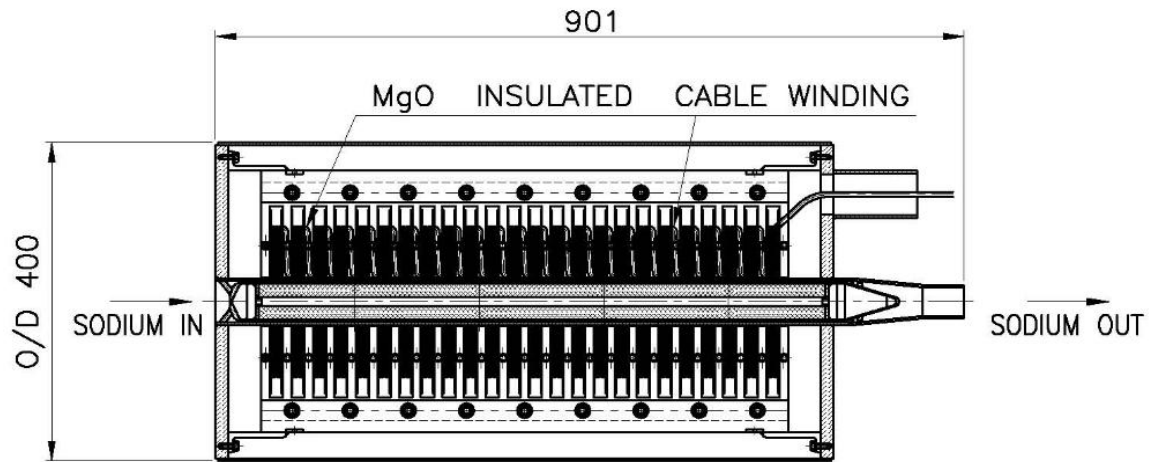


Fig. 3.2 General assembly of submersible ALIP

Table 3.1 Specifications of submersible ALIP

Designation of Pump	Submersible ALIP
Normal Flow rate	2.0 m ³ /h
Head to be Developed at Nominal flow Rate and Temperature	0.4 MPa
Rated Voltage	150 V, 3 Phase, 50 Hz
kVA Rating	30 kVA
Line Current	105 Amps (phase current – 60 Amp)
Insulation	Mineral Insulated SS Sheathed Copper Conductor
Cooling	No external cooling required
Maximum Sodium Temperature Permissible	873 K(600 °C)
Normal Sodium Temperature	473K (200 °C)
Shut off head of pump	0.5 MPa
Duct design Pressure	1.2 MPa at 873 K
Type of ALIP	Once Through Type

3.4 Simulation of Submersible ALIP

This section deals with simulation of submersible annular linear induction pump. In order to house the MI cable winding 1.0 mm thick SS plates are provided in the slots. The design of submersible ALIP was done using the equivalent circuit approach. Finite element based simulation was carried out to compare with the analytical design calculations. The convergence of the two diverse techniques helps in enhancing the confidence for building the pump design.

Following assumptions were made in the finite element model of ALIP.

- i. 2-D axisymmetry was assumed. The central core and duct are axisymmetric but the stator lamination stacks are not. Though, the arrangement of stator laminations is such that when the magnetic flux enters the sodium duct, it is axisymmetric. Therefore, the assumption of axisymmetry is justified.
- ii. The individual conductors and turns of MI cable winding were not modeled, rather conductor area and number of turns in each slot were given as input. This implies that the SS sheath surrounding the copper was not modeled.
- iii. The winding was housed in a stainless steel plate housing. This housing was not modeled.
- iv. The MI cable has additional length of leads (approximately 20 m on both start and finish ends of the winding). This lead length was not included. This means that the actual winding will have more resistance than that in the model. This additional length of the winding has been added in the winding resistance in the equivalent circuit based calculations.
- v. Magnetic properties of the materials were assumed to be linear. This means that B-H curves of material used is linear. Magnetic properties are assumed to be independent of temperature though, electrical conductivity of material varies with temperature in the simulation model.

vi. Grain orientation of magnetic material was not modeled.

3.4.1 Geometric details of finite element based model

The geometry of the pump as modeled in COMSOL is shown in Fig. 3.3. The pump has been modeled as an axisymmetric object.

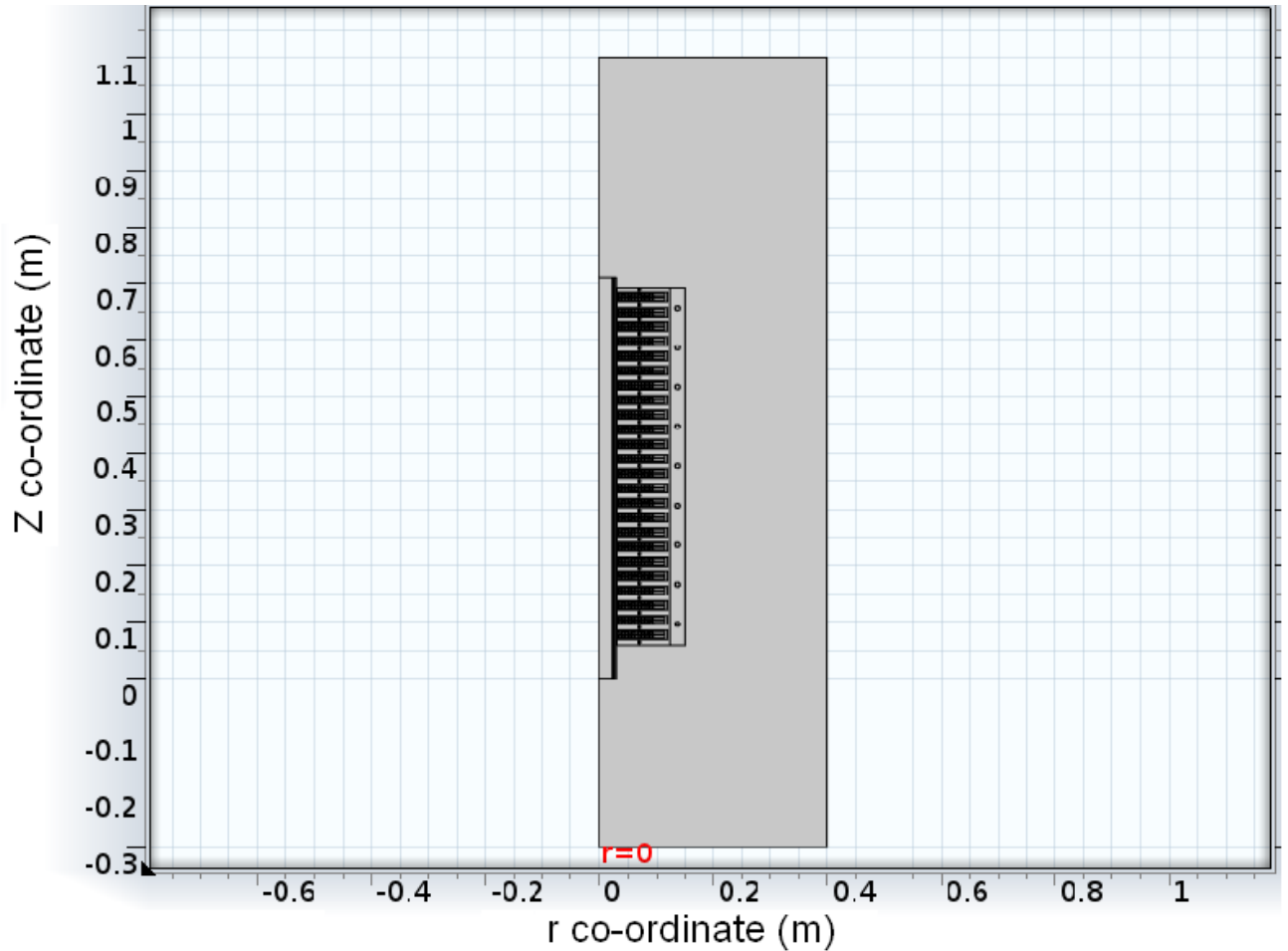


Fig. 3.3: Simulation model in COMSOL

3.4.2 Applicable equations

The simulation model solves both the electromagnetic and turbulent flow equations but not simultaneously. The simulation of ALIP has been done in the following three stages in COMSOL.

- a. First Navier Stokes equations are solved for flow (in Turbulent Region) and the velocity profile is obtained for the specified flow.

- b. Electromagnetic force is computed for the velocity obtained in a.
- c. Flow equations are once again solved for the electromagnetic force obtained in b and the pressure developed at the pump exit is obtained.

The simulation of ALIP has been done in time harmonic domain and coupled with steady state hydrodynamic Navier Stokes equations. Following are the applicable Maxwell's equations.

$$\nabla \times H = J \quad (3.1)$$

$$\nabla \times E = - \frac{\partial B}{\partial t} \quad (3.2)$$

$$J = \sigma(E + V \times B) \quad (3.3)$$

$$\nabla \cdot B = 0 \quad (3.4)$$

$$f_{EM} = J \times B \quad (3.5)$$

Navier Stokes equation for steady state flow is given by

$$\rho(V \cdot \nabla) V = -\nabla p + \eta \nabla^2 V + f_{EM} \quad (3.6)$$

For incompressible steady state flow, the mass conservation equation becomes

$$\nabla \cdot (\rho V) = 0 \quad (3.7)$$

The coupling between electromagnetic field and the fluid flow is simulated by adding the volume electromagnetic force f_{EM} to the force term of the Navier Stokes equation. The effect of velocity on the magnetic field is simulated by adding the term $V \times B$ to the ohms' law $J = \sigma E$.

3.4.3 Boundary conditions

3.4.3.1 Electromagnetic Boundary Conditions

For electromagnetic boundary conditions the central axis is assigned axisymmetry boundary condition where as the outer boundaries are assigned magnetic insulation boundary condition which makes the magnetic field tangential to the outer boundary or in other words the magnetic field does not cross the outer boundary. The outer boundary is a rectangular box

whose edges are 250 mm away from the pump outer boundary. Since the simulation is in low frequency range ($<1000\text{Hz}$) this distance was found to be acceptable.

COMSOL feature of multi-turn domain was used to model the coils with specified number of turns. The conductivity of the conductor material (i.e. copper) was set as per temperature. Voltage was given as input to the coil. All the 3-phase coils were excited by the same voltage but displaced in phase by 120° electrical.

3.4.3.2 Fluid flow Boundary Conditions

The central axis was assigned axisymmetry boundary condition. The walls of the pipe were assigned logarithmic wall function to account for the variation of flow velocity in turbulent region. The fluid flow has been solved using the k - ε turbulence model. The inlet was assigned a pressure of zero Pascal and the outlet boundary was assigned the velocity corresponding to the desired flow rate.

3.4.4 Coupling Between Electromagnetic and Fluid Models

The electromagnetic force produced in the liquid metal is coupled to the fluid flow by adding the electromagnetic force to the Navier-Stokes equation as a volume force. Then the resultant pressure obtained from solving Navier Stokes equation yields the pressure developed by the pump. The hydraulic losses are already accounted in the Navier Stokes equation.

In COMSOL simulation first flow is simulated without the electromagnetic field and the velocity profile in the annular duct region is obtained. Thereafter, the electromagnetic force corresponding to the obtained velocity is computed. In the third stage, Navier-Stokes equation is solved once again and the pressure developed by the pump is obtained. Thus, the effect of velocity profile and end effects due to motion of conducting liquid metal in magnetic field are accounted in the simulation model.

A mesh consisting of 351767 triangular elements was created using the FEM based software COMSOL. The total degrees of freedom was 703627. The number of edge elements in the mesh was 44965 and the number of vertex elements was 2798.

3.4.5 Simulation results

The simulation has been carried out at 50 Hz frequency at rated flow of $2 \text{ m}^3/\text{h}$. The developed pressure was calculated. Simulation results at 200°C and voltage of 150 volts are presented below.

The axisymmetric model made in COMSOL is shown in Fig. 3.4. A view of the mesh is depicted in Fig. 3.5. The mesh consists of 351767 triangular elements. The simulation was run on an Itanium 5 processor in a PC having 8 GB of RAM and took 5 minutes to solve.

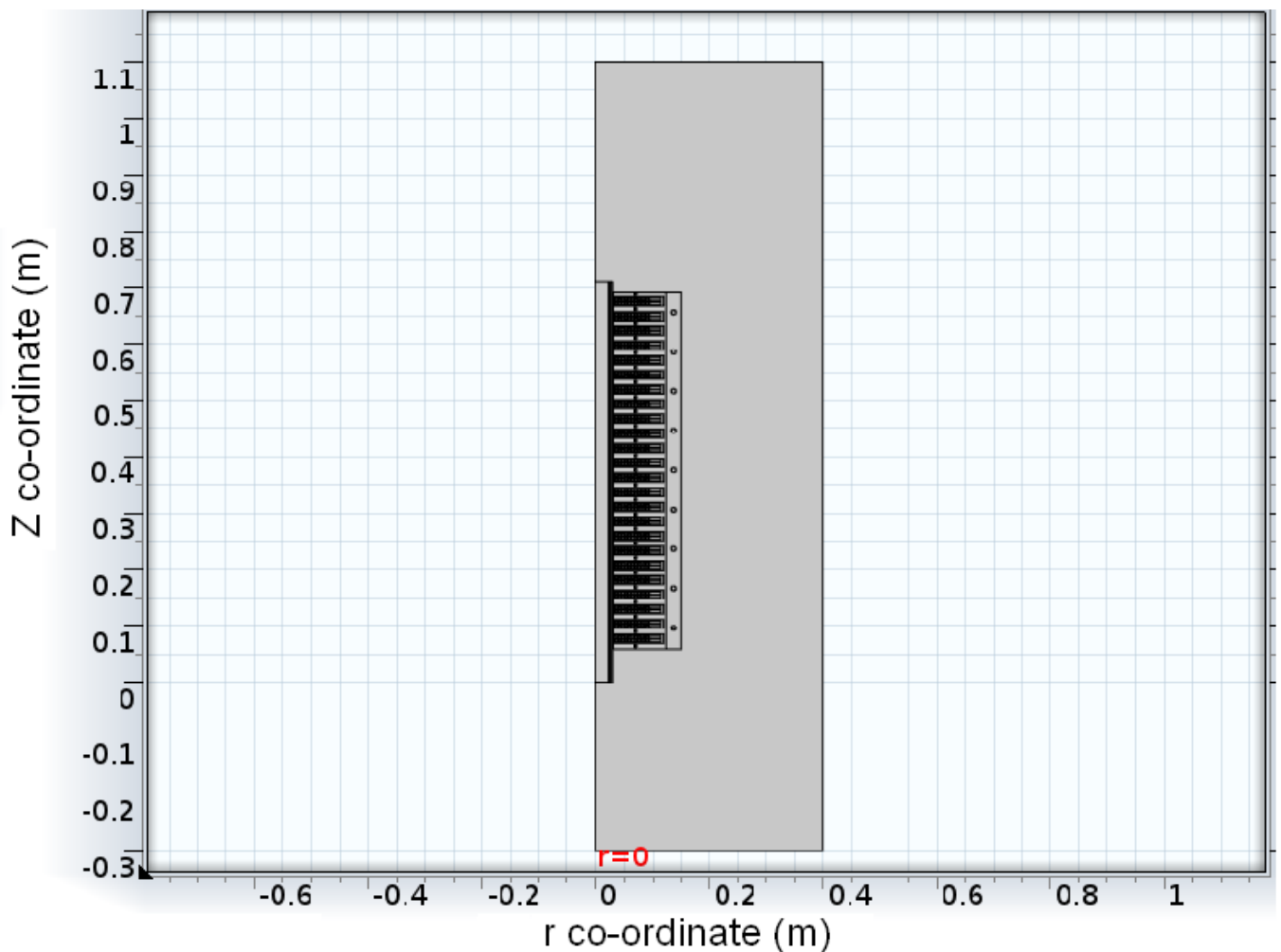


Fig. 3.4 Simulation model of ALIP

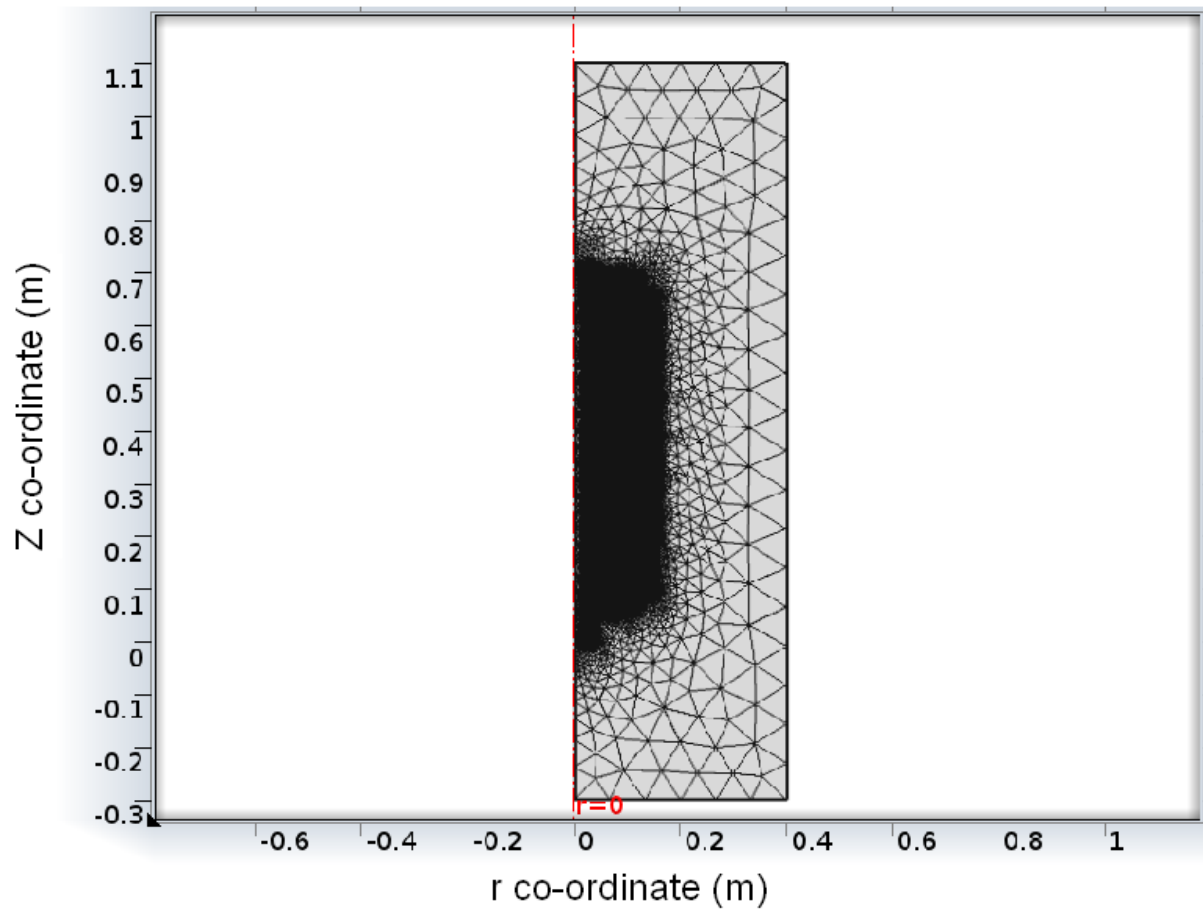


Fig. 3.5 Mesh used in simulation

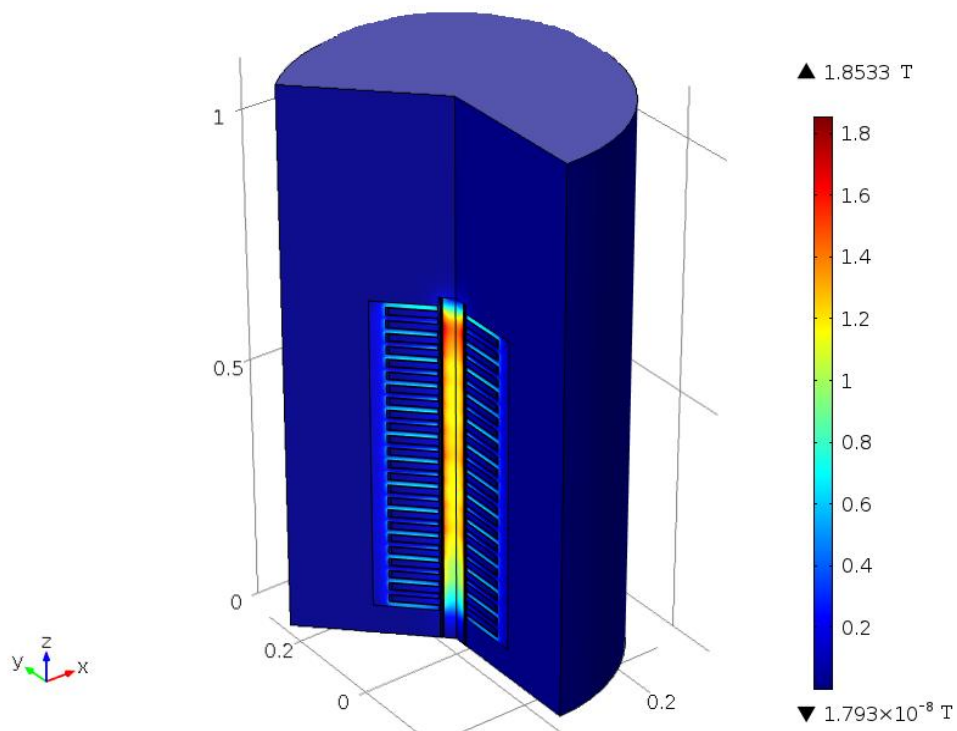


Fig. 3.6 Flux density at $2.0 \text{ m}^3/\text{h}$ flow

An isometric cut-view of flux density in SALIP is shown in Fig. 3.6. It can be observed from Fig. 3.6 that the maximum flux density is in the central core and this value is slightly above the knee of the B-H curve of CRGO lamination used. The flux density in teeth and back iron portion is well below the knee of the B-H curve. Magnetic flux magnitude in annular duct is plotted in Fig. 3.7 where it can be observed that the flux density is oscillating around a mean value. The oscillating variation in B is due to slots in the stator. The flux density is more beneath a tooth compared to that beneath a slot due to air gap variation between tooth and slot.

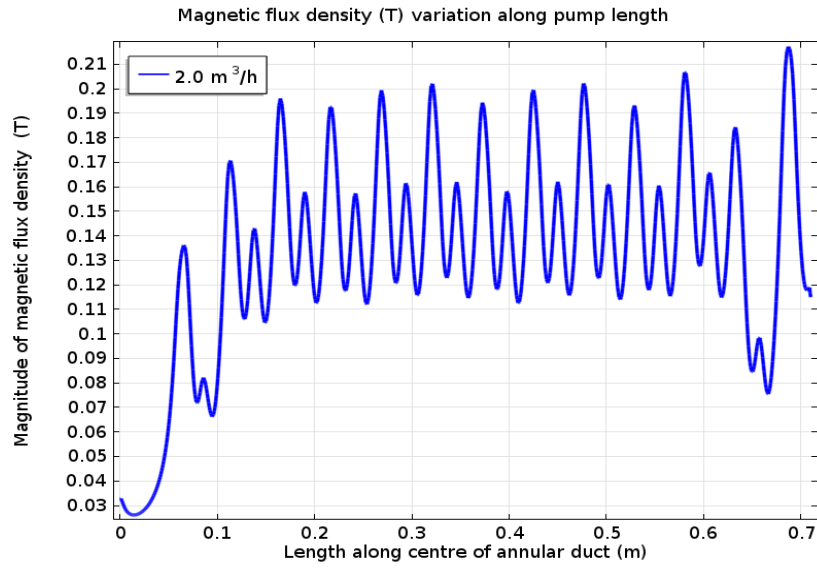


Fig. 3.7 Magnitude of magnetic flux density in sodium duct at 2.0 m³/h

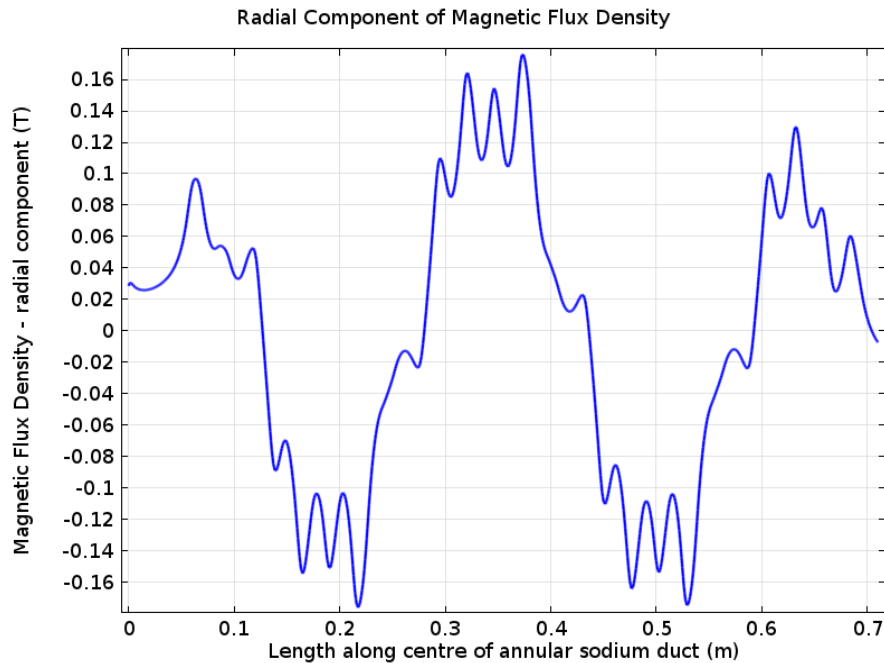


Fig. 3.8 Variation of radial component of magnetic flux density in duct

Variation in radial component of magnetic flux density is shown in Fig. 3.8. The field is having a predominant fundamental component along with harmonics imposed due to slots. From the variation of magnetic field it can also be observed that the winding produces 4 magnetic poles.

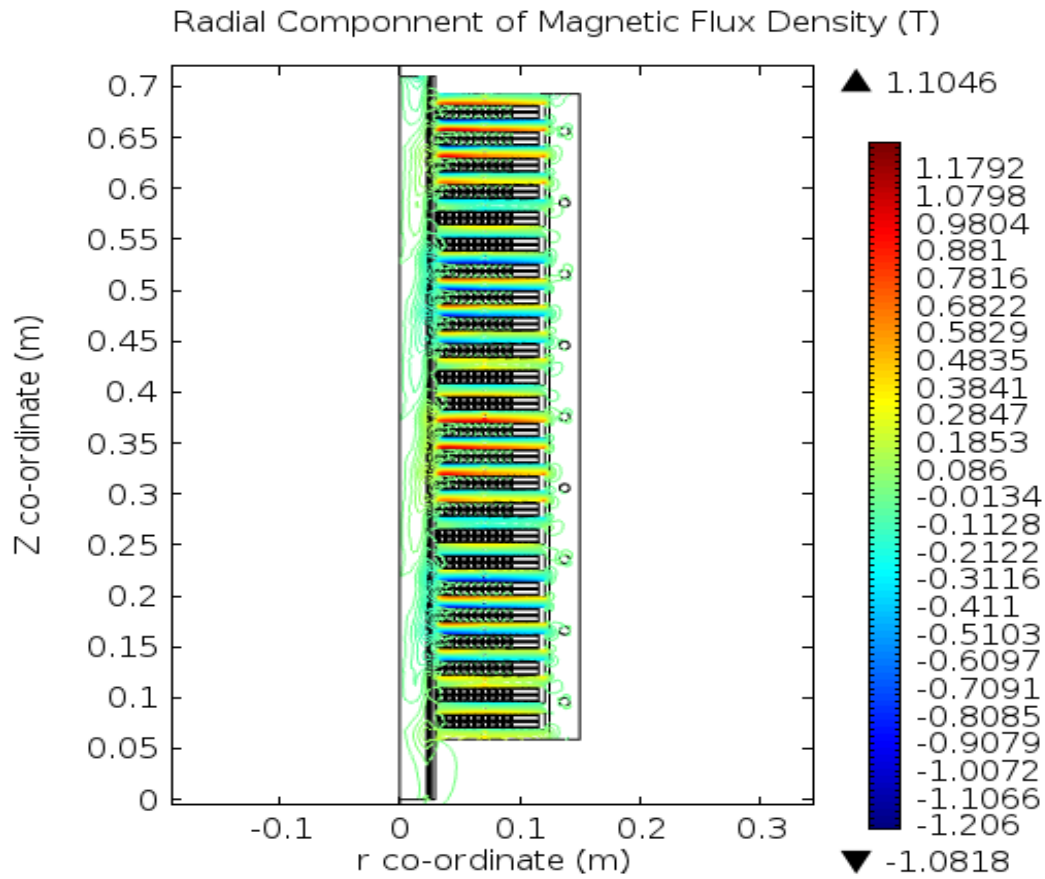


Fig. 3.9 Contour plot of radial component of magnetic flux density

Contour plot of radial component of magnetic flux density is shown in Fig. 3.9 where it is observed that the maximum radial magnetic flux density is 1.2 T well below the knee of the B-H curve. The arrow plot of Fig. 3.10 depicts the flow of magnetic flux from tooth to central core and from central core back to tooth. Crowding of flux (higher flux densities) is observed in the central core region compared to that in the teeth region.

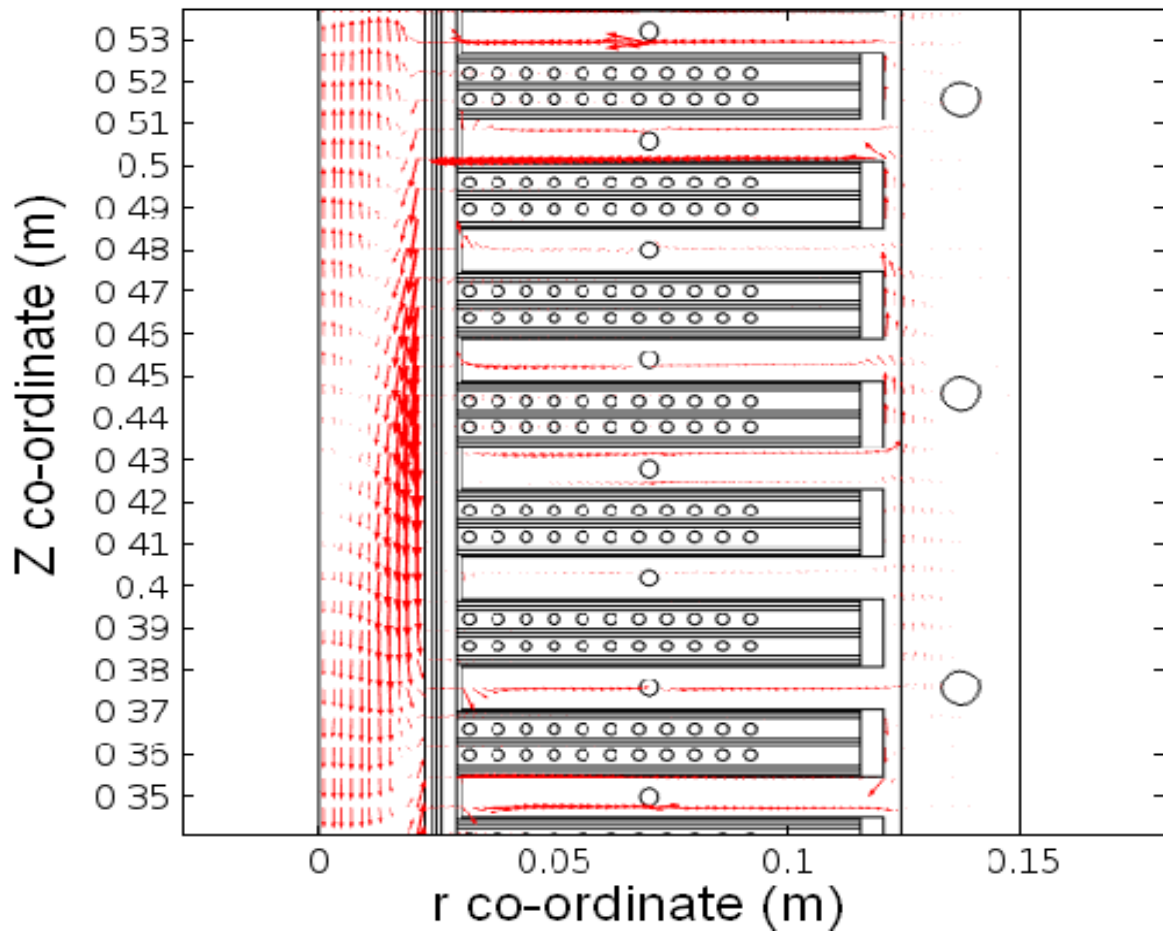


Fig. 3.10 Arrow plot depicting the magnetic flux density lines

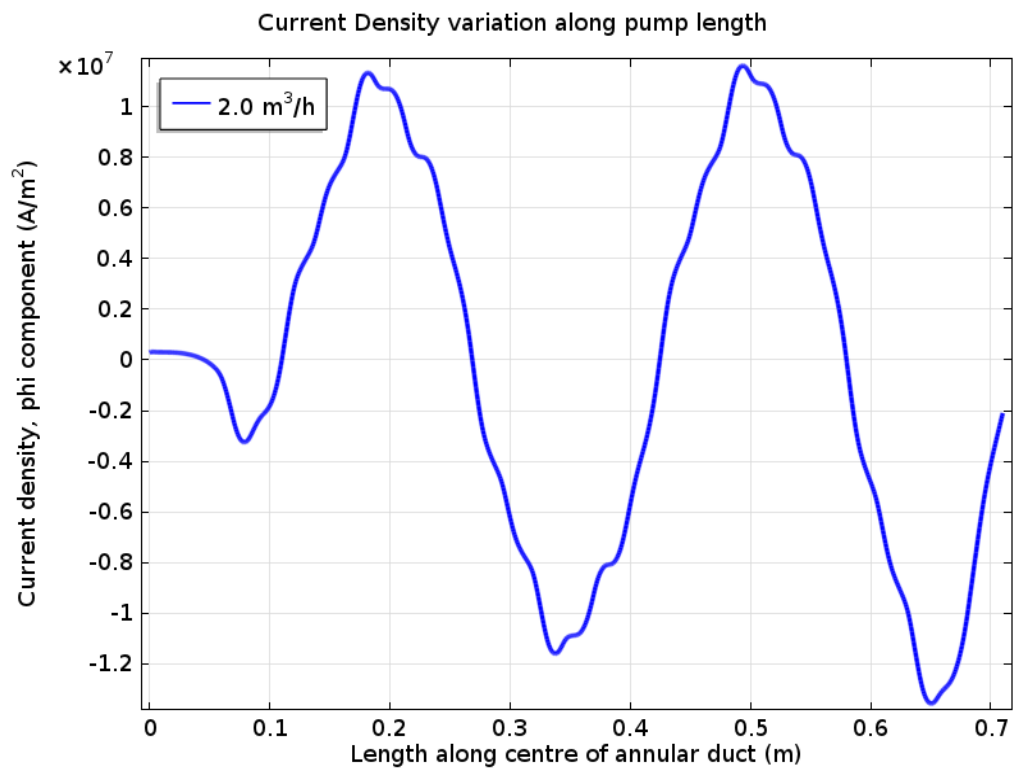


Fig. 3.11 Model predicted current density in sodium duct

Induced current density plot in annular sodium duct is shown in Fig. 3.11. The variation is approximately sinusoidal in nature. The interaction of this induced current with magnetic field produced by the winding results in volume force on liquid sodium as per the equation 3.5.

The volume force generation in the sodium duct is shown in Fig. 3.12. The negative volume force at the entry and exit of the pump is due to the so called “end- effects” which occur due to discontinuity in magnetic field. These effects are not present in an induction motor since the magnetic circuit is closed. The oscillation in force along the length is due to the presence of slots and teeth. These oscillations do not result in any observable fluctuations in sodium flow due to the inertia of sodium and it flows as per the average force produced.

The developed pressure, as a result of this volume force on liquid sodium is plotted and shown in Fig. 3.13. It can be observed that the pressure increases linearly with length of the pump. The variation in output pressure at different flow rates is shown in Fig. 3.14. The reduction in pressure at higher flow rates is due to the end-effects which gain prominence at higher liquid metal velocity.

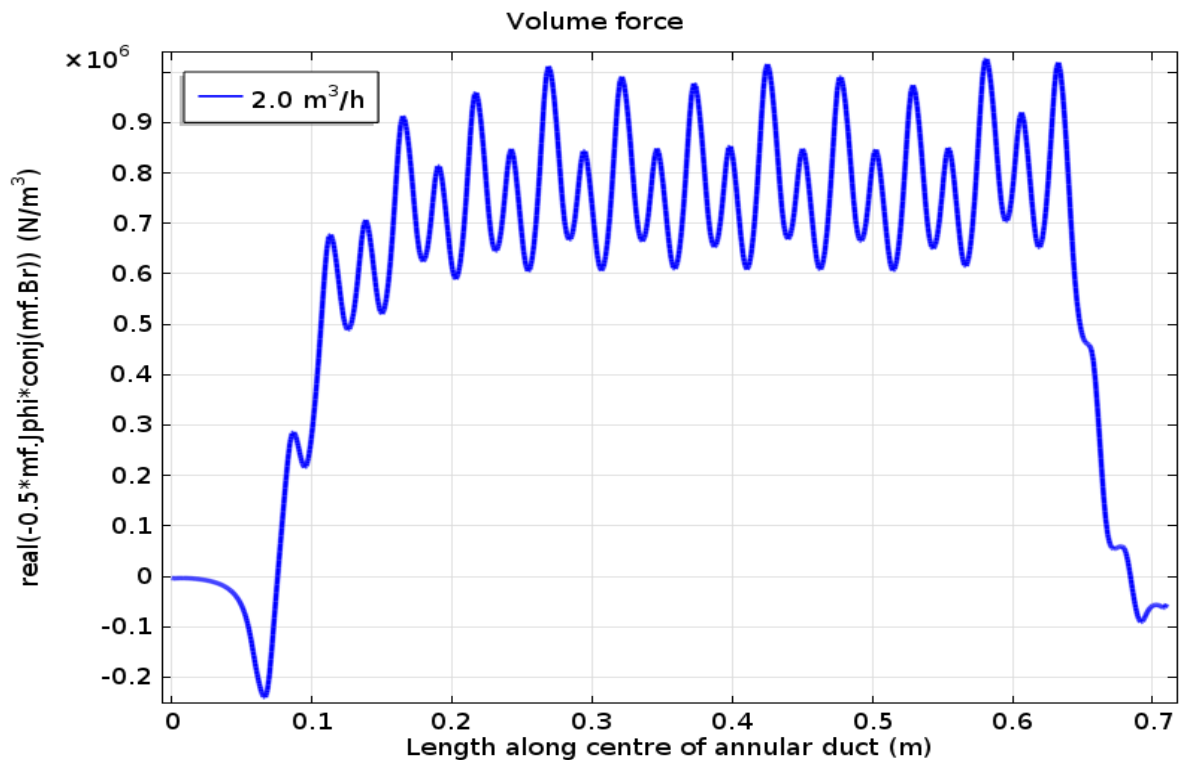


Fig. 3.12 Volume force in sodium duct at 2.0 m³/h

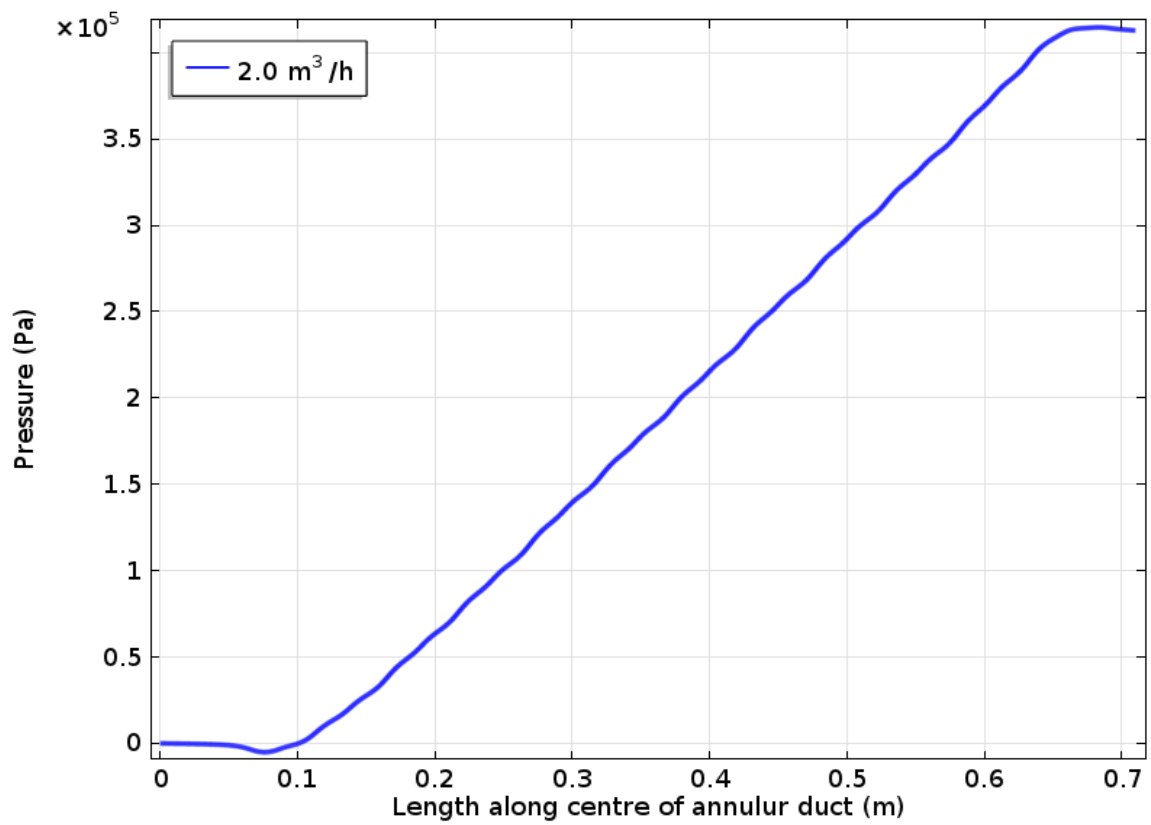


Fig. 3.13 Pressure development in sodium duct at $2.0 \text{ m}^3/\text{h}$

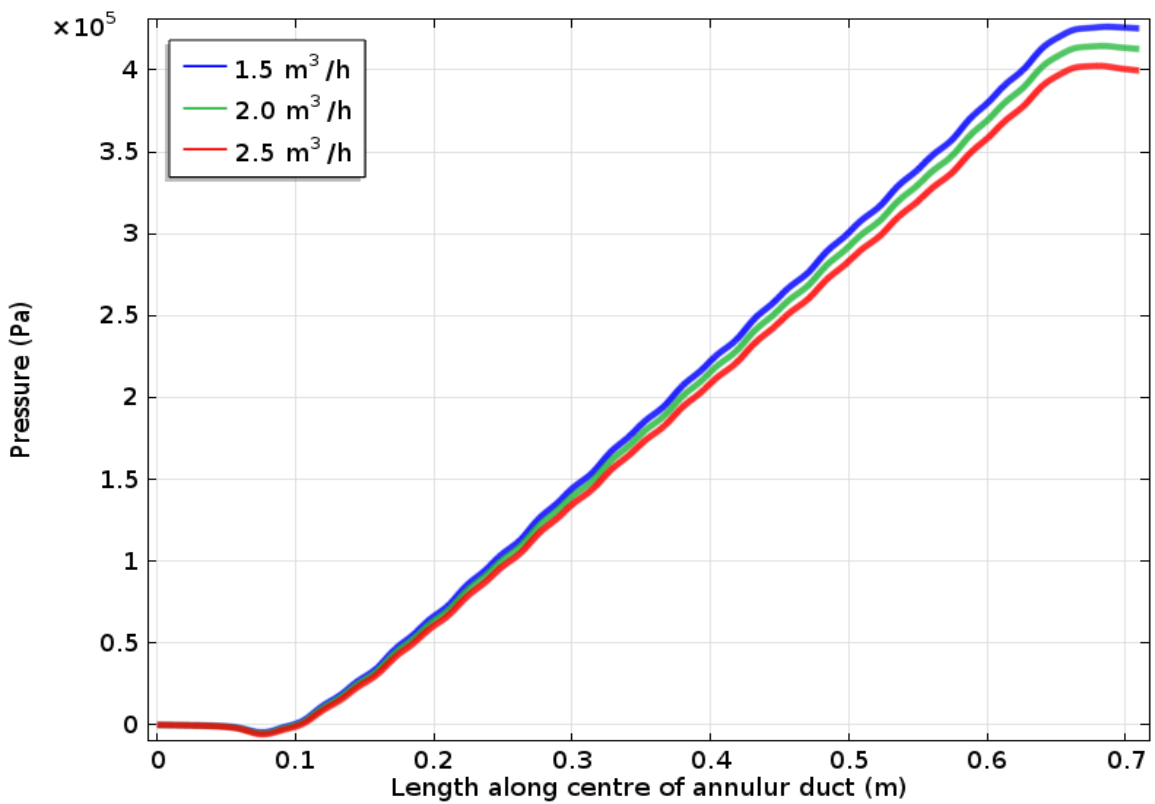


Fig. 3.14 Variation in developed pressure with flow

3.4.6 Discussion on simulation results

It can be observed that as the flow increases the induced current density gets reduced, which is leading to reduction in volume force and also in developed pressure. This is due to end effects which become prominent as sodium velocity in the duct increases. These effects are not accounted for sufficiently in the equivalent circuit approach. The simulation model also provides a deeper understanding into the working of electromagnetic pumping phenomenon taking place under different operating conditions.

3.4.7 Comparison of equivalent circuit model and COMSOL model

Theoretical calculation of pressure developed by the pump during design stage was carried out using equivalent circuit model. The applied voltage was 150 V to the input of the pump which has 130 mtr length MI cable. Around 20 mtrs of MI cable is left for the extra terminal length of the pump since this pump has to be dipped in main vessel which is of 12 mtr height. Hence around 110 mtr of MI cable is used in pump winding which participate in electromagnetic action. In theoretical calculation of pressure developed the applied voltage is 150 at input terminal of the pump but the voltage applied to magnetizing inductance is around 105 volt which is obtained after subtracting resistive drop of MI cable utilized for lengthy terminal cable. In COMSOL simulation, the length of winding is calculated internally based on slot dimensions and dimensional data given for MI cable. In COMSOL extra terminal length of winding wire cannot be fed (connecting cable lead). Hence for pressure calculation during COMSOL simulation, input voltage fed is 105 volt so that voltage across magnetizing inductance is same for both COMSOL simulation and equivalent circuit model. The theoretical pressure drop calculation of both models is shown in Fig 3.15.

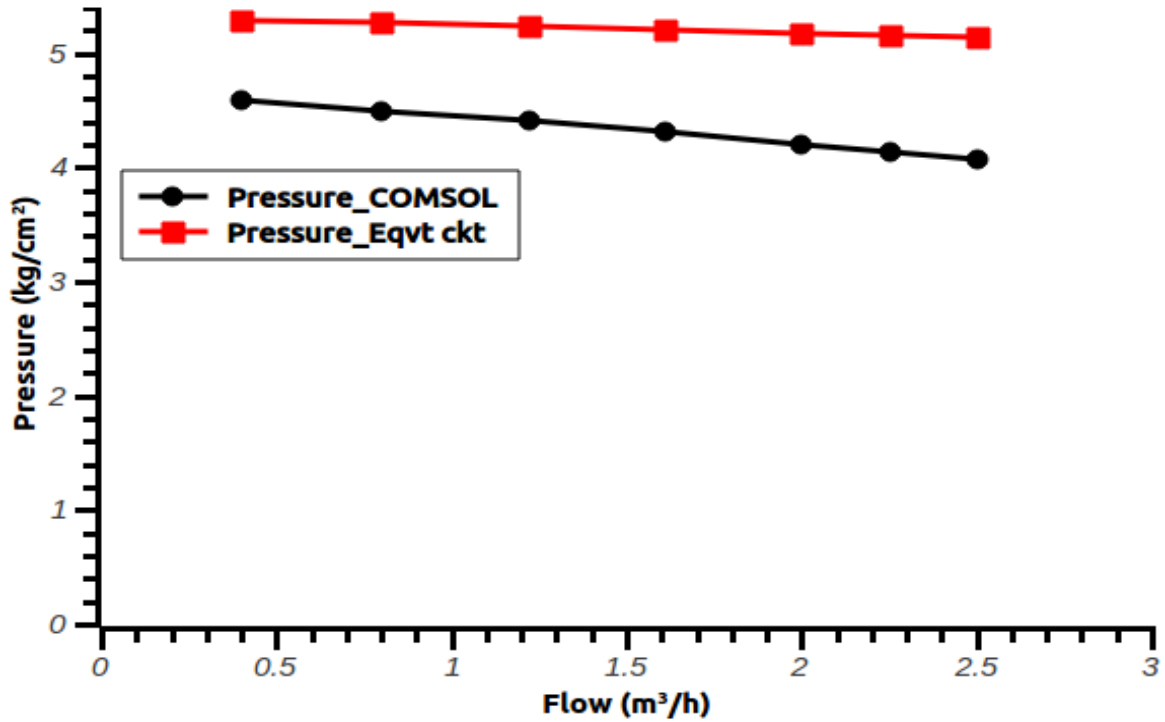


Fig. 3.15 Comparison of theoretical developed pressure by COMSOL and equivalent circuit model

The calculation shows that COMSOL model gives little less pressure developed than equivalent circuit model. One probable reason may be that magnetic losses and hydraulic loss are not accounted in the equivalent circuit model whereas the same have been accounted in COMSOL.

3.5 Effect of Stainless Steel Sheath of Winding and Winding Retainer Plate on ALIP and Derivation of Modified Equivalent Circuit for MI Cable Wound ALIP

Winding of the developed annular linear induction pump is made from stainless steel sheathed cable. The winding is placed in the stator slot and two stainless steel plates of 1.0 mm thick are used as winding retainer plate in the stator slot because the cable used for winding is stiff. This type of arrangement is not present in the conventional ALIP. The stator leakage flux of ALIP passes through the winding retainer stainless steel plates and the stainless steel sheath of the cable resulting in production of eddy current in the stainless steel sheath of cable and the stainless steel winding retainer plates. The effect of eddy current circulating in winding retainer plates and cable sheath which is not present in the conventional ALIP has to

be accounted while predicting theoretical performance of the ALIP. The presence of two layers of stainless steel sheath of winding and two winding retainer plates are approximated as presence of total six stainless steel plates of 1.0 mm thick present in the slot for determining eddy current effect. The winding arrangement in the slot is shown in Fig. 3.16. To account effect of eddy current in winding and retainer plate, the equivalent circuit of ALIP is modified as shown in Fig. 3.17 and theoretical performance is evaluated based on modified equivalent circuit [23].

3.5.1 Calculation of eddy current in sheath and plates and its equivalent resistance referred to primary

ϕ_1 is the leakage flux in the slot which causes eddy current in the sheath and plate.

ϕ_1 as given below can be obtained from equations 2.15 & 2.16 of chapter 2.

$$\phi_1 = \frac{N_7 I \pi \mu_0 D_8}{3} \frac{D_{13}}{D_{11}} \quad (3.8)$$

Where $N_7 = 22$, $I = 60$ A, $\mu_0 = 4\pi \times 10^{-7}$, $D_8 = 62.48 \times 10^{-3}$ m, $D_{13} = 77 \times 10^{-3}$ m, $D_{11} = 16 \times 10^{-3}$ m

$$\phi_1 = \frac{22 \times 60 \times \pi \times 4\pi \times 10^{-7} \times 77 \times 10^{-3}}{3} \frac{62.48}{16}$$

$$\phi_1 = 5.22 \times 10^{-4} \text{ wb}$$

$$e_{\text{ms}} = \phi_1 \times \omega = 5.22 \times 10^{-4} \times 2 \times \pi \times 50 = 0.16399 \text{ V} \quad (3.9)$$

Resistance of retainer disc is calculated as follows

$$R_{\text{disc}} = \rho \frac{\text{Length}}{\text{Area}} \quad (3.10)$$

OD of Disc = 230.0 mm

ID of Disc = 60.0 mm

Therefore, inner radius of disc, $r_1 = 30.0$ mm

Outer radius of disc, $r_2 = 115.0$ mm

Width of disc for current flow = $r_2 - r_1 = 85.0$ mm

$$\text{Mean Radius} = r_1 + \frac{r_2 - r_1}{2} \quad (3.11)$$

$$\text{Mean Radius} = 72.5 \text{ mm}$$

$$\text{Mean Length} = 2 \pi \times 72.5 \times 10^{-3} = 455.5 \times 10^{-3} \text{ m} \quad (3.12)$$

area = thickness x height

$$\text{area} = 1 \times 10^{-3} \times 85 \times 10^{-3} = 85.0 \times 10^{-6} \text{ m}^2$$

$$R_{\text{disc}} = \rho \frac{\text{Length}}{\text{Area}} = 1.1144 \times 10^{-6} \frac{455.5 \times 10^{-3}}{85 \times 10^{-6}} = 5.971 \times 10^{-3} \Omega \quad (3.13)$$

$$I_{\text{eddy}} = \frac{e_{\text{rms}}}{R_{\text{disc}}} = \frac{0.16399}{5.971 \times 10^{-3}} = 27.46 \text{ Amp} \quad (3.14)$$

Loss in one Disc

$$I_{\text{eddy}}^2 R_{\text{disc}} = 27.46^2 \times 5.971 \times 10^{-3} = 4.5 \text{ watt} \quad (3.15)$$

There are 8 slots per phase having 6 equivalent discs (this includes SS discs and sheathed cables)

$$\text{Therefore, Eddy Current Loss per phase} = 4.5 \times 6 \times 8 = 216.0 \text{ watt} \quad (3.16)$$

$$\text{Total mmf in all discs in a slot} = 6 \times 27.46 = 164.76 \text{ Amp Turn} \quad (3.17)$$

$$\text{Total mmf of disc in per phase} = 164.76 \times 8 = 1318 \text{ Amp Turn} \quad (3.18)$$

$$\text{No. of Turns in primary per phase} = N_{\text{sc}} \times I_{\text{eq eddy current in primary}} = 1318 \quad (3.19)$$

$$I_{\text{eq eddy current in primary}} = \frac{1318}{176} = 7.5 \text{ Amp} \quad (3.20)$$

R'_{eddy} = Resistance of disc reflected to primary side

$$7.5^2 \times R'_{\text{eddy}} = 216.0 \quad (3.21)$$

$$R'_{\text{eddy}} = 3.84 \Omega$$

R'_{eddy} is designated as R_{sp} in the modified equivalent circuit. R_{sp} represents resistance of SS sheath of cable and retainer plate in the slot referred to primary.

3.5.2 Calculation for effect of opposing MMF due to eddy current

$$e_{\text{rms}} = \frac{\pi \mu_0}{3} \frac{N_7 D_8 D_{13} \omega}{D_{11}} I_{\text{rms}} \quad (3.22)$$

$$I_{\text{eddy}} = \frac{\pi \mu_0}{3} \frac{N_7 D_8 D_{13} \omega}{D_{11}} \frac{I_{\text{rms}}}{R_{\text{eddy}}} \quad (3.23)$$

The eddy currents oppose the main mmf in the slot

Therefore, the net effective mmf in the slot

$$\text{Net Slot MMF} = N_7 I_{\text{rms}} - N_p \frac{\pi \mu_0}{3} \frac{N_7 D_8 D_{13} \omega}{D_{11}} \frac{I_{\text{rms}}}{R_{\text{eddy}}} \quad (3.24)$$

$N_p = \text{No. of equivalent SS plates} = 6$

$$\text{Net Slot MMF} = \left(1 - N_p \frac{\pi \mu_0}{3} \frac{D_8 D_{13} \omega}{D_{11}} \frac{1}{R_{\text{eddy}}} \right) N_7 I_{\text{rms}} \quad (3.25)$$

For the dimensional parameters of the designed Submersible ALIP

$$\mu_0 = 4\pi \times 10^{-7}, D_8 = 62.48 \times 10^{-3} \text{ m}, D_{13} = 77.0 \times 10^{-3} \text{ m}, D_{11} = 16.0 \times 10^{-3} \text{ m},$$

$$R_{\text{eddy}} = 5.971 \times 10^{-3} \Omega, N_p = 6$$

Therefore, Net Slot MMF

$$= \left(1 - \frac{6 \times \pi \times 4\pi \times 10^{-7}}{3} \times \frac{62.48 \times 10^{-3} \times 77 \times 10^{-3} \times 2\pi \times 50}{16 \times 10^{-3}} \times \frac{1}{5.971 \times 10^{-3}} \right) N_7 I_{\text{rms}}$$

$$\text{Net Slot MMF} = (1 - 0.1249) N_7 I_{\text{rms}} = 0.875 \times N_7 I_{\text{rms}} \quad (3.26)$$

This implies that the effective number of primary turns in the slots becomes 87.5 % of the wound turns due to the effect of eddy currents in the stator winding as well as in the retainer plates. Theoretical performance of the pump is calculated based on this effective number of primary turns in the slot. While calculating the performance, the $i^2 R$ loss in the equivalent sheath plates is also taken into account. Hence, based on the effect of sheath plate, the equivalent circuit of the pump is modified and shown in Fig. 3.17.

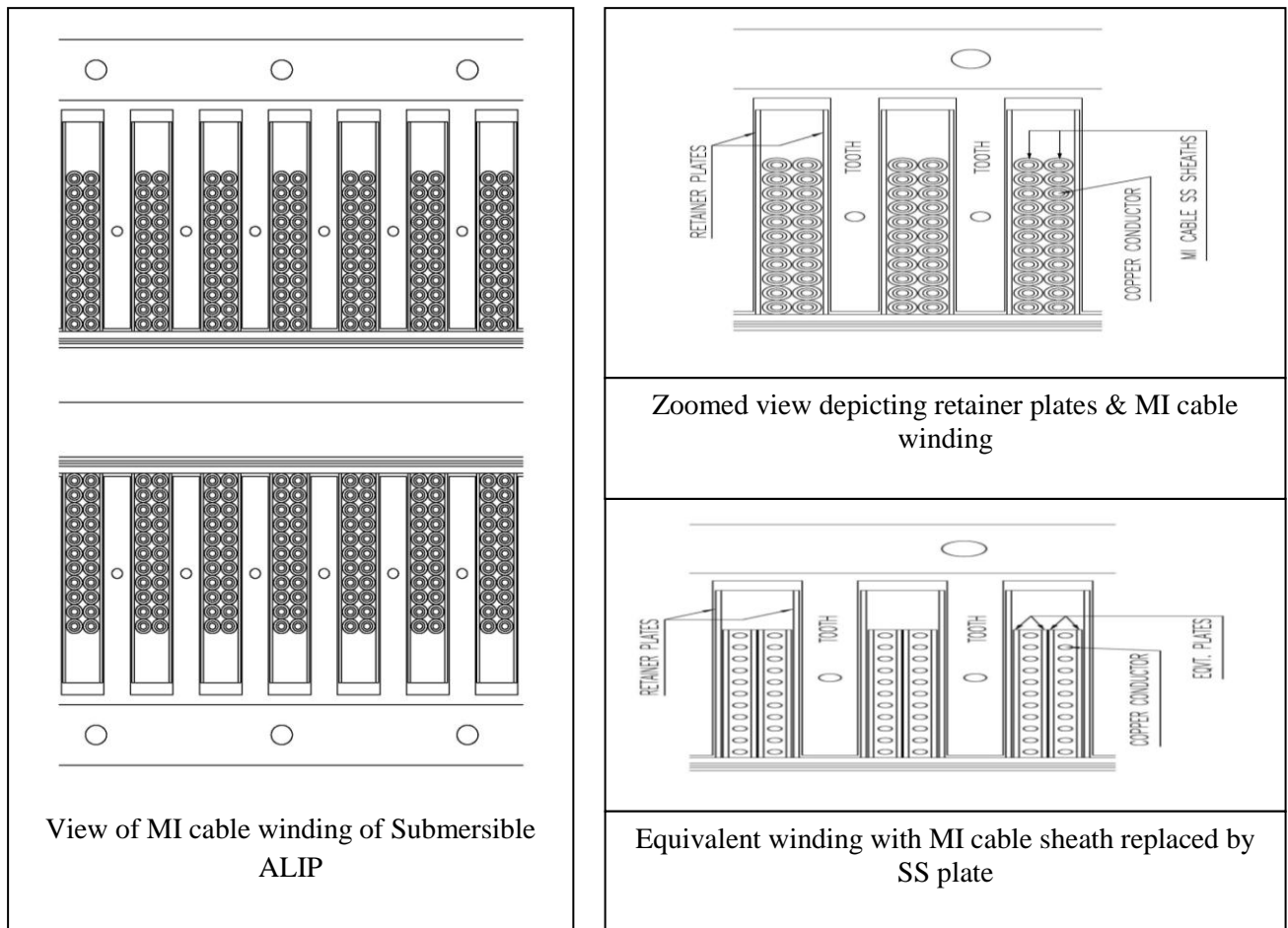


Fig. 3.16 Winding arrangement in the slot

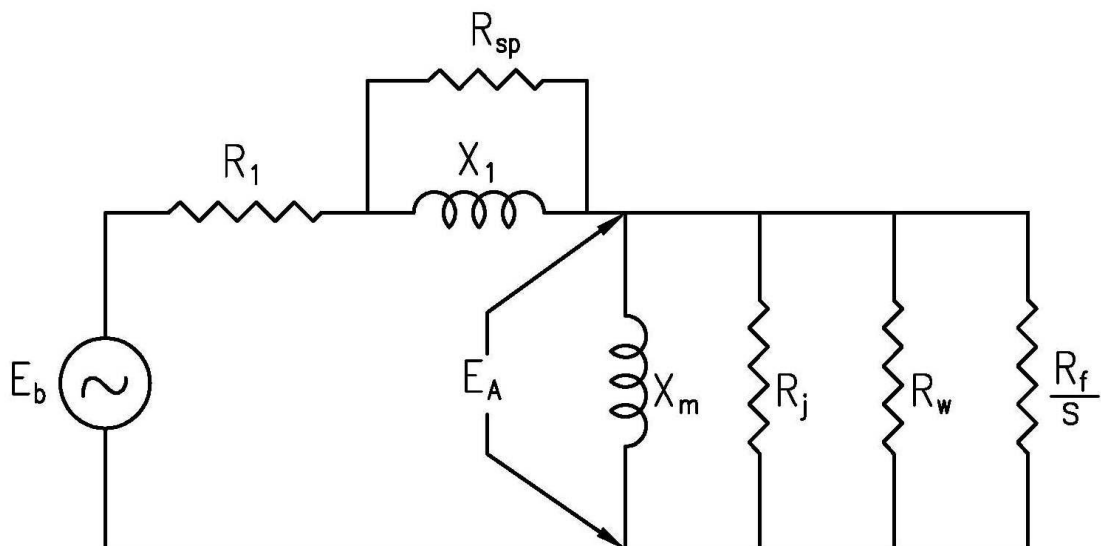


Fig. 3. 17 Modified equivalent circuit of ALIP for taking into account the losses taking place in SS sheath of MI cable and in SS retainer plates.

3.6 Theoretical Characteristics of Developed Submersible ALIP

Theoretical characteristics (Pressure Head, Input Power and Efficiency Vs Flow) of the designed sodium submersible ALIP were obtained using the empirical formula used in the design at 200 °C. Pressure Head Vs Flow, Input power Vs Flow and Efficiency Vs Flow characteristics are shown in Fig. 3.18, Fig. 3.19 and 3.20 respectively.

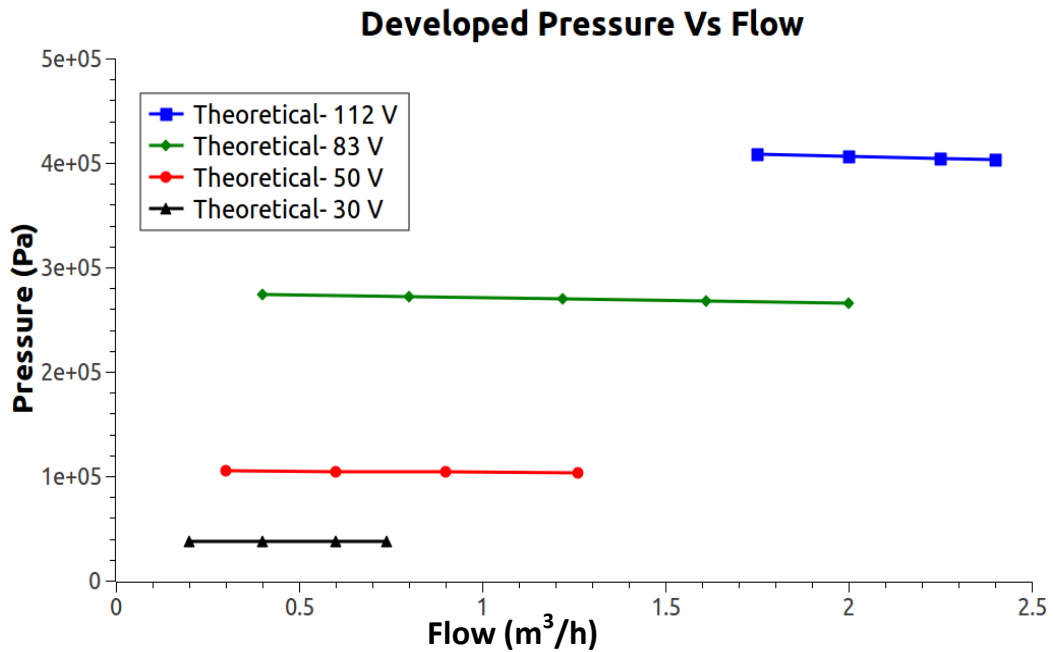


Fig. 3.18 Theoretical Head Vs Flow curve at 200 °C

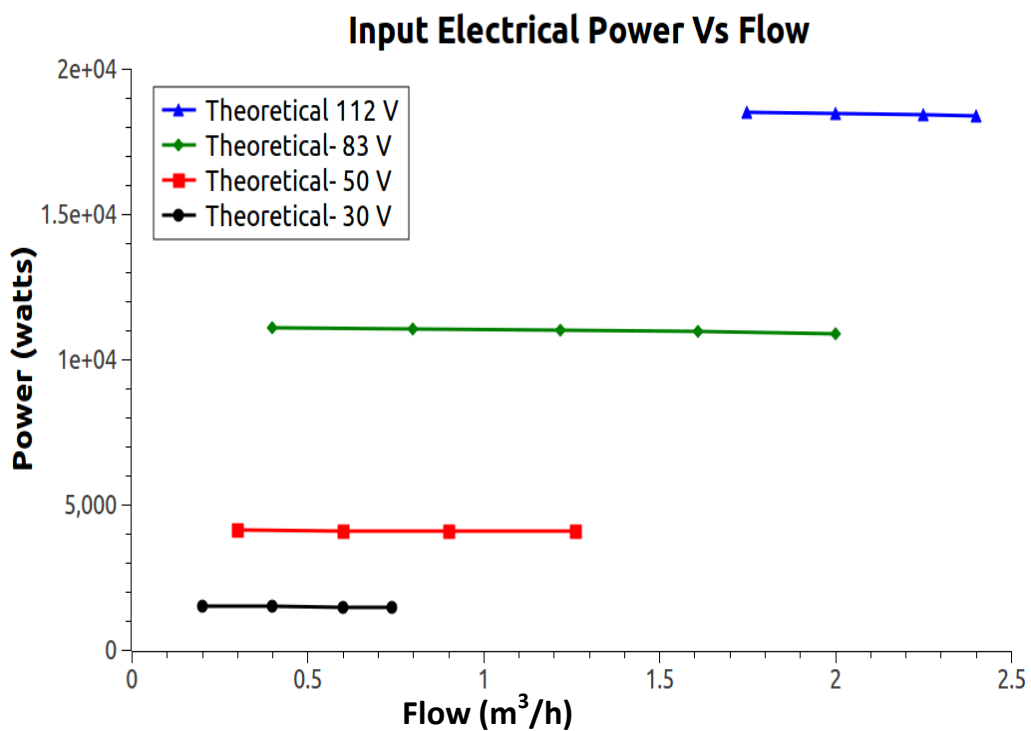


Fig. 3.19 Theoretical Input Electrical Power Vs Flow at 200 °C

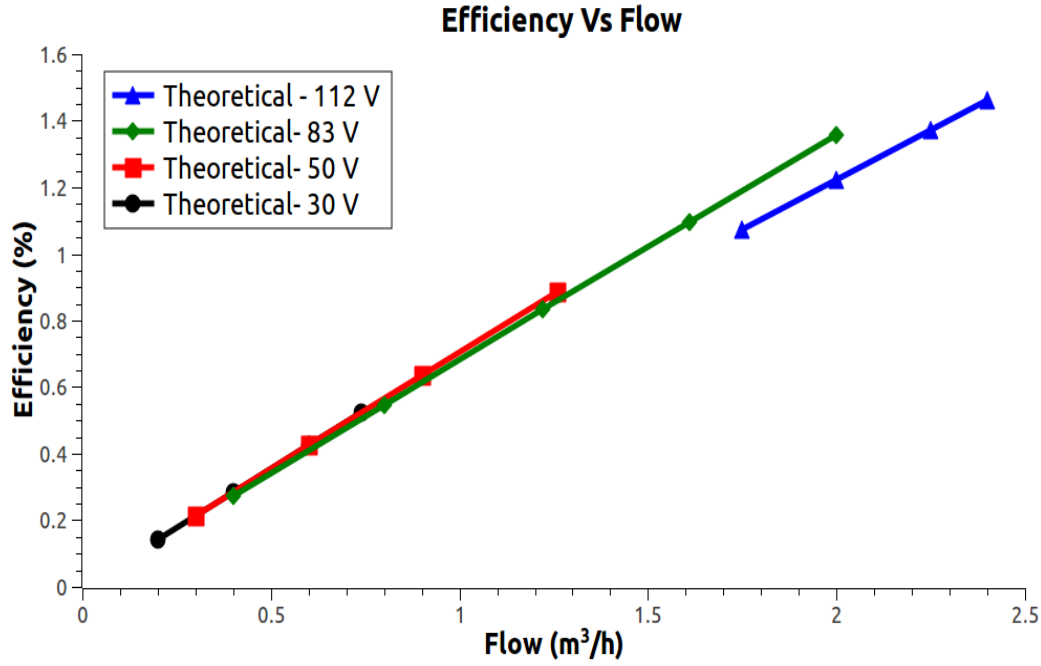


Fig. 3.20 Theoretical Efficiency Vs Flow at 200 °C

3.7 Calculation of Magnetic Reynolds Number for the developed Submersible ALIP

A. Gailitis and O.Lielāusis [47], showed that the flow becomes unstable, if magnetic Reynolds number is higher than unity. Later H. Araseki et al.[48] confirmed results derived in analytical work [47] by broad experimental and numerical investigations of MHD instability in ALIP. Hence calculation of Magnetic Reynolds Number for the developed Submersible ALIP is carried out as in Table 3.2

Table : 3.2 Magnetic Reynolds Number for Submersible ALIP

Temperature of liquid Na (°C)	300
Pole-pitch (m) - τ	0.156
Duct Height (m) - δ_h	2.09×10^{-3}
Non-magnetic gap height (m) - δ_m	8.74×10^{-3}
Duct Mean Diameter ($2 * R_{av}$) (m)	0.05039
R_{av}/τ	0.1615064
Tooth pitch (t_z) (m)	26×10^{-3}
Tooth width (b_z) (m)	10×10^{-3}
Carter co-efficient (k_δ) $k_\delta = (t_z + 10\delta_m)/(b_z + 10\delta_m)$	1.164
Liquid metal conductivity (S/m) (σ)	5671506.4
Flow (m³/h)	2
Frequency (Hz)	50

Angular Frequency (ω)	314.15
synchronous velocity (m/s)	15.6
flow velocity (m/s)	1.6784156
Slip (s)	0.8924093
magnetic permeability (μ)	1.257×10^{-6}
$\alpha=\pi/\tau$ (i.e. π /pole pitch)	20.137821
Magnetic Reynolds Number, $Rms = \frac{\delta_h}{\delta_m k_\delta} \frac{\sigma \mu \omega}{\alpha^2} s$	1.00

It is seen from calculation that Magnetic Reynolds Number is not higher than unity. Theoretical Pressure Vs Flow characteristic obtained as shown in Fig. 3.18 shows dP/dQ negative. Other condition for unstable flow is that dP/dQ should be positive[47]. Since Magnetic Reynolds Number is not higher than unity and also dP/dQ is negative, it is concluded that developed flow will not become unstable. Theoretically it is foreseen that pump will develop stable flow in its operating region.

3.8 Summary

Sodium submersible ALIP having $2.0 \text{ m}^3/\text{h}$ flowrate and 4.0 kg/cm^2 pressure head was designed. A lateral dimension of 400.0 mm was achieved. The winding of pump is made of stainless steel sheathed mineral insulated cable capable of withstanding 550°C . Its performance was evaluated using FEM analysis. Comparison of theoretical pressure developed by the designed pump using equivalent circuit model and by the FEM analysis using COMSOL was carried out. The effect of eddy currents in the sheath of winding on the pump performance was carried out. Modification of the equivalent circuit to take account of effect of eddy currents is brought out and this is an important aspect in this research work. Theoretical pump characteristics are also obtained using empirical formula used in the design. Theoretical calculation has indicated that pump flow will be stable and pump instability is not predicted.

Chapter 4

CHAPTER- 4

ANNULAR LINEAR INDUCTION PUMP DEVELOPMENT AND MANUFACTURING

Annular linear induction pump having stator winding made from mineral insulated stainless steel sheathed cable capable of withstanding high temperature sodium atmosphere as per the research aim was manufactured in three stages. In first stage, a compact three phase induction motor with mineral insulated cable winding was developed to prove the concept of motor winding made from mineral insulated stainless steel sheathed cable. In second stage, mineral insulated stainless steel sheathed cable of 6 mm diameter required as per designed ALIP was developed. In third stage, compact stainless steel enclosed ALIP having stator winding made from mineral insulated stainless steel sheathed cable as per design was developed.

4.1 Development of Induction Motor with MI Cable Winding (Stage-1)

In the first stage, design, fabrication and testing of a compact three phase 50 W, 110 V, 3600 rpm squirrel cage induction motor with Mineral Insulated (MI) cable winding were carried out in two phases. In the first phase, one compact induction motor with class-H insulation winding was developed. In second phase, stator windings of the motor were replaced with MI cable winding to make it suitable for operation in high temperature environment.

4.2. Design of Induction Motor with class H insulation

4.2.1 Induction motor design

One 50 W, 3 ϕ , 110 V, 3600 rpm, squirrel cage induction motor was designed as per technical details given in Table. 4.1. The overall dimensions of the motor were fixed as per process requirements. CRNGO lamination of 0.35 mm thickness was used to form the stator

core and stator teeth of desired dimensions to avoid magnetic saturation of stator of the motor. Class-H type insulation was used in stator winding. Stator frame is made of stainless steel 316 (SS 316) to withstand high temperatures and corrosive environments. Twelve semi closed type stator slots were chosen to reduce the magnetizing current and tooth pulsation losses. Schematic of the stator cross section of the induction motor is shown in Fig. 4.1. Salient equations used in stator design are given below. Technical details of the motor are given in Table. 4.1

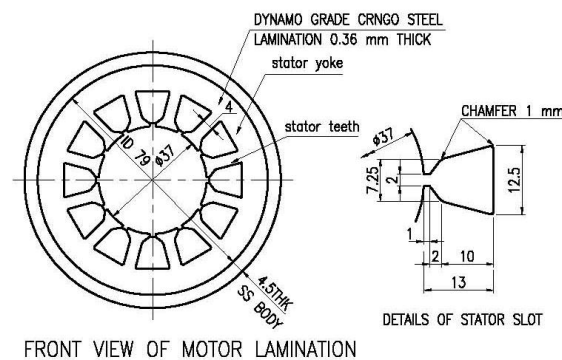


Fig. 4.1 Cross sectional view of stator

Table 4.1 Technical details of the motor

Power	50 W
Voltage (line to line)	110 V
Rated Phase current	0.9 A
Phase	3 phase
Frequency	65 Hz
Motor Syn Speed	3900 rpm
Insulation type	Class-H
OD of motor	88 mm
Length of motor	164 mm (body)
Length of rotor shaft	262.2 mm
Outer body of motor	SS 316
Laminations	0.35 mm (CRNGO)
Bare copper conductor (Dia)	0.63 mm
Enamelled copper wire (Dia)	0.85 mm

$$\text{KVA input} = Q = \frac{\text{Motor power output}}{\eta \times \cos(\phi)} \quad (4.1)$$

$$D^2 L = \frac{Q}{C_0 n_s} \quad (4.2)$$

$$C_0 = 11 \times K_w \times B_{av} \times ac \times 10^{-3} \quad (4.3)$$

$$\text{Pole pitch } (\tau) = \frac{\pi D}{P} \quad (4.4)$$

$$\text{Flux per pole } (\phi_m) = B_{av} \times \tau \times L \quad (4.5)$$

$$\text{Flux density at stator teeth} = \frac{\phi_m}{(S_s/P) \times W_{ts} \times L_i} \quad (4.6)$$

$$\text{Turns per phase } T_{ph} = \frac{E_s}{4.44 \times f \times \phi_m \times K_w} \quad (4.7)$$

$$\text{Stator current per phase } I_s = \frac{Q (\text{input KVA})}{\sqrt{3} \times V_L} \quad (4.8)$$

$$\text{Current density in stator} = \frac{I_s}{a_s} \quad (4.9)$$

where

C_0 Output coefficient

D Armature diameter or stator bore

L Stator core length

η Efficiency

$\cos(\phi)$ Power factor

P Number of poles

K_w Winding factor

B_{av} Specific magnetic loading

τ Pole pitch

ac Specific electric loading

n_s Synchronous speed (r.m.s)

f Frequency

S_s	Number of stator slots
W_{ts}	Width of tooth
L_i	Net iron length
V_L	Line voltage
I_s	Stator line current

CRNGO lamination of 0.35 mm thickness, die cast Aluminium rotor bar and end rings were used in rotor of the motor. Rotor with seventeen semi closed rectangular slots was chosen to avoid magnetic locking, for better overload capacity and high starting torque. Rotor cross section is shown in Fig. 4.2 and Fig. 4.3. Rotor bars shape chosen helps in higher starting torque and lower operating losses. Pictorial view of the developed low power induction motor is shown in Fig. 4.4. Equations used for rotor design are given below.

$$l_g = 0.2 + 2\sqrt{DL} \quad (4.10)$$

$$D_r = D_{si} - 2 \times l_g \quad (4.11)$$

Where

l_g Length of air gap

D_r Diameter of rotor

D_{si} Inner diameter of stator

$$\text{Rotor slot pitch at air gap} = \frac{\pi D}{S_r} \quad (4.12)$$

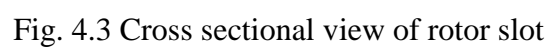
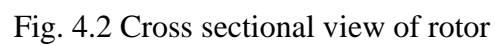
$$I_b = \frac{2 \times m_s \times K_{ws} \times T_{ph} \times I_s \times \cos(\phi)}{S_r} \quad (4.13)$$

$$a_b = \frac{I_b}{\delta_b} \quad (4.14)$$

$$B_{\max} (\text{Rotor teeth}) = \frac{\phi_m}{\frac{S_r}{P} \times \text{rotor teeth} \times L_i} \quad (4.15)$$

$$a_e = \frac{I_e}{\delta_e} \quad (4.17)$$

I_b	Rotor bar current
a_b	Area of rotor bar
I_e	End ring current
a_e	Area of end ring
δ_b	Current density in rotor bar



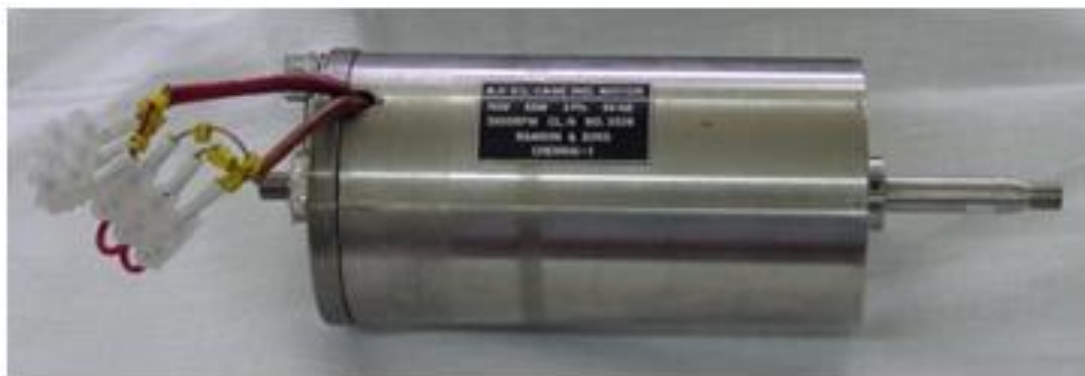


Fig. 4.4 Low power induction motor

The induction motor developed was tested. The test set up for measuring various electrical parameters of the motor is shown in Fig. 4.5. Input current and power measurements were carried out at no load and locked rotor conditions.



Fig. 4.5 Test set up for induction motor.

4.3. Design of High Temperature Induction Motor with Mineral Insulated Cable Winding

After successful testing of the compact motor, the work on development of high temperature induction motor was taken up. The conventional winding of the developed motor was replaced with mineral insulated cable winding. Stator winding of the motor was fabricated with Mineral Insulated (MI) cables of 1.0 mm outer diameter. MI cable consists of Stainless Steel (SS) sheath, MgO powder and copper conductor at the center of the cable. The MI cable does not undergo any major changes in the radiation field and being used in various sensors for high temperature application up to 550 °C. Use of MI cable in electromagnets of

the shut down systems submerged in sodium and operating at high temperature is a classical example of suitability of MI cable under hostile environments.

4.3.1 Properties and testing of MI cable

4.3.1.1 Properties of MI cable

MI cable consists of central copper conductor concentrically placed inside a SS tube. SS tube and central copper conductor are electrically insulated by a densely packed high pure Magnesium Oxide. The SS sheath of required thickness on the cable is formed by drawing a single tube. Both ends of the cable are sealed using epoxy sealants. MI cable was tested for conductor resistance, insulation resistance at room and high temperatures, SS sheath integrity and high voltage.

4.3.1.2 Current carrying capacity test on MI cable

In order to utilize the MI cable for high current density applications, experiment was conducted to determine the current carrying capacity of the MI cable of 1.5 mm outer diameter and 0.8 mm conductor diameter. The schematic of the test set-up is shown in Fig. 4.6. The pictorial view of the test set-up is shown in Fig. 4.7, Fig. 4.8 and Fig. 4.9. A thermocouple (K type) was used to monitor the temperature of the MI cable coil. A rheostat with ratings of 50 Ω and 10A was used in series with MI cable coil to vary the current in the coil.

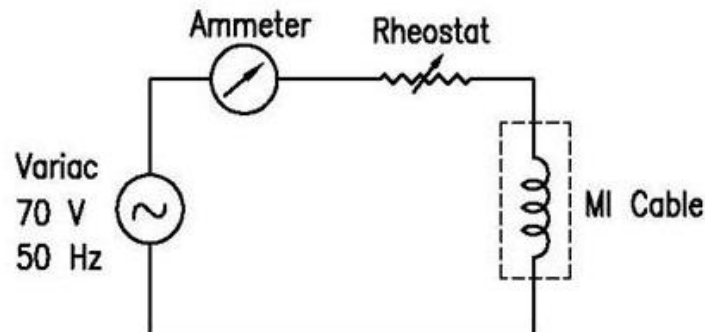


Fig. 4.6 Schematic of test set-up for MI cable

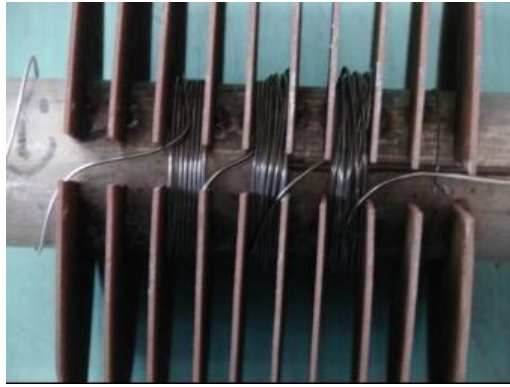


Fig. 4.7 MI Cable in wound condition over a pipe and slot arrangement



Fig. 4.8 Test set up without wound condition

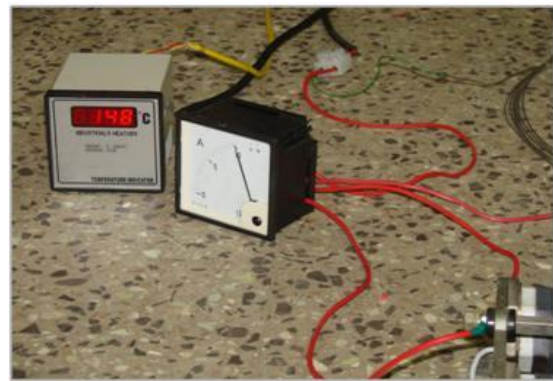


Fig. 4.9 Thermocouple reading at 10 A

During the testing, voltage upto 70 V was applied to the MI cable winding. The current in the winding was increased in steps by varying the resistance of rheostat and readings of thermocouple were recorded at regular intervals. Testing was done for 29 h (total intermittent cumulative operating hours) with recording of temperatures at different time. Plot of current density verses current in MI cable and corresponding maximum surface temperature is shown in Fig. 4.10. The maximum surface temperature plotted in Fig 4.10 is not with respect to time but it is plotted with respect to current. It should be noted here that the current through the winding in experiment is maintained constant for specified current density. The experimental observation for current carrying capacity test is given in Table-4.2 & Table-4.3 which is the basis of plot indicated in Fig 4.10. It can be seen from the Table-4.2 & Table-4.3 that the experiment was carried out at different ambient conditions such as air- condition ON, air-

condition OFF, Fan ON, Fan OFF etc. but by maintaining same current value. The maximum temperature reading obtained is during no fan and no air-condition operation. It is observed that MI cable is able to carry currents with current density up to 20 A/mm^2 , which is much higher than conventional motor winding cable capability (2 to 5 A/mm^2).

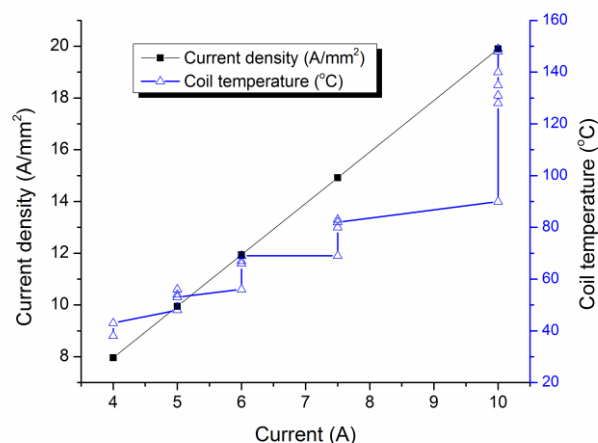


Fig. 4.10 Current carrying capacity of MI cable

Table 4.2 : Tests on 1.5 mm MI cable roll

Sl. No.	Time	Current (Amps)	Current Density (Amp/mm ²)	Temperature (° C)	Ambient Conditions
1	14:25	4	7.96	38	NO FAN NO AC
2	14:40	4	7.96	43	NO FAN NO AC
3	14:50	4	7.96	43	NO FAN NO AC
4	16:20	4	7.96	43	NO FAN NO AC
	Next Day				
5	09:30	5	9.95	39	NO FAN NO AC
6	09:40	5	9.95	53	NO FAN NO AC
7	09:45	5	9.95	56	NO FAN NO AC
8	09:55	5	9.95	54	AC only

9	11:15	5	9.95	53	AC only
10	11:20	6	11.94	56	AC only
11	11:25	6	11.94	66	AC only
12	11:30	6	11.94	67	AC only
13	12:10	6	11.94	66	AC only
14	13:00	6	11.94	69	AC only
15	14:20	6	11.94	69	AC only
16	14:21	7.5	14.92	69	AC only
17	14:25	7.5	14.92	80	AC only
18	14:30	7.5	14.92	83	AC only
19	15:00	7.5	14.92	82	AC only
20	16:10	7.5	14.92	82	AC only
	Next Day				
21	09:55	10	19.9	90	AC only
22	10:00	10	19.9	128	AC only
23	10:05	10	19.9	131	AC only
24	10:10	10	19.9	131	AC only
25	10:20	10	19.9	131	AC only
26	14:30	10	19.9	75	FAN NO AC
27	14:45	10	19.9	140	NO FAN NO AC
28	15:30	10	19.9	149	NO FAN NO AC
29	16:20	10	19.9	148	NO FAN NO AC

Table 4.3 : Tests on 1.5 mm MI cable in wound condition

Sl. No.	Time	Current (Amps)	Current Density (Amp/mm ²)	Temperature (° C)	Ambient Conditions
1	15:10	6	11.94	32	NO FAN NO AC
2	15:35	6	11.94	48	NO FAN NO AC
3	15:45	6	11.94	49	NO FAN NO AC
4	15:46	10	19.9	58	NO FAN NO AC
5	15:55	10	19.9	77	NO FAN NO AC
6	16:25	10	19.9	87	NO FAN NO AC
7	17:00	10	19.9	87	NO FAN NO AC

4.3.2 High temperature induction motor with MI cable

The designed stator frame and rotor was used for high temperature induction motor, except the stator winding, which is now made from MI cable. The stator outer diameter and length was maintained same due to process requirements.

4.3.2.1 Motor design

Apart from stator windings, all other specifications of motor mentioned in Section 4.2 were kept same as given in Table. 4.1. Stator windings were formed with SS sheathed MI cable of 1.0 mm diameter with central copper conductor of 0.35 mm. Photographs of low power motor with MI cable winding are shown in Fig. 4.11, Fig. 4.12 and Fig. 4.13.

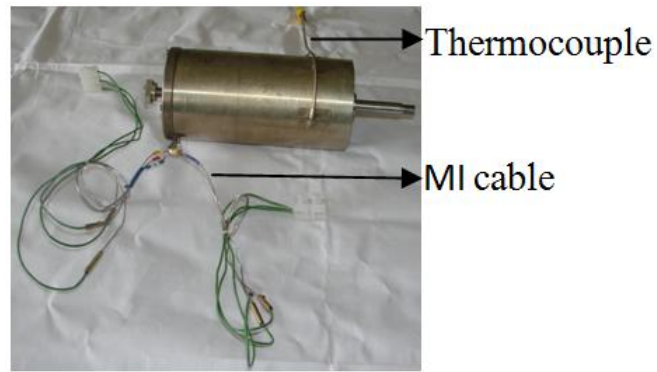


Fig. 4.11 Low power induction motor with MI cable

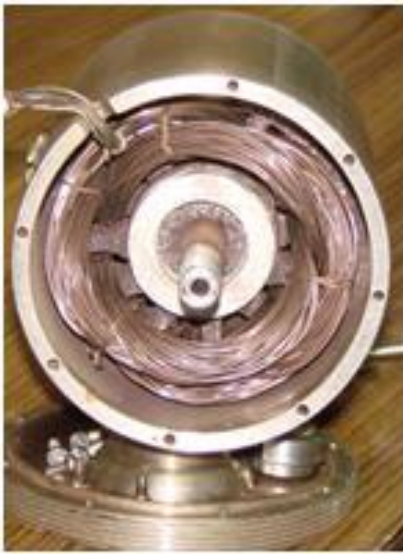


Fig. 4.12 Stator of low power motor with MI cable



Fig. 4.13 Motor in open condition

With reduction in space factor by 50 % because of usage of MI cable in stator windings, only 55 turns per phase were possible. Reduction in number of turns led to increase in air gap flux for a rated voltage. High flux resulted in high magnetizing current, leading to higher copper losses and rise in winding temperature. High temperatures in winding did not affect the reliability of motor due to higher thermal withstand capacity of MI cable stator winding. Stator was designed for star connection and stator flux value was obtained as per following equation.

$$\text{Stator voltage per phase} = E_s = \frac{110}{\sqrt{3}} = 63.5 \text{ V} \quad (4.18)$$

Flux per pole for phase voltage of 63.5 V is

$$\phi_m = \frac{E_s}{4.44 \times f \times T_{ph} \times K_w} \quad (4.19)$$

Where

T_{ph} Turns per phase

K_w Winding factor

$$\phi_m = \frac{63.5}{4.44 \times 65 \times 55 \times 0.955} = 0.004189 \text{ Wb}$$

Magnetic flux density corresponding to the flux per pole given above is 0.6 T.

4.3.3 FEM analysis of high temperature induction motor

FEM analysis of high temperature induction motor was carried out using FEMM code to check the saturation of various parts of the motor and to predict the rotor torque. Two dimensional model of induction motor with MI cable was simulated using non linear ferromagnetic laminated steel BH curves. Magnetic flux density values in various parts of motors with fixed stator current were simulated and used for predicting torque slip characteristics using Maxwell stress tensor method [34,35,36,37,38]. Two dimensional model of high temperature induction motor with dimensions given in Section 2 is shown in Fig. 4.14. Stator and rotor core highlighted in pink color were modeled as silicon steel laminations. Three phase stator windings are placed in stator as shown in Fig 4.14. Constant three-phase currents were applied to the stator windings in model. Stator and rotor core were modeled as silicon steel lamination. The aluminium rotor bars were modeled with a conductivity of 34.45 MS/m [39]. Following approximations were made for two dimensional modeling.

- Increase in rotor resistance due to increase in temperature during long operations was neglected.

- Increase in rotor resistance due to end bars was not considered.
- Flux leakage at rotor ends was not considered.
- Flux leakage at stator end was not considered.

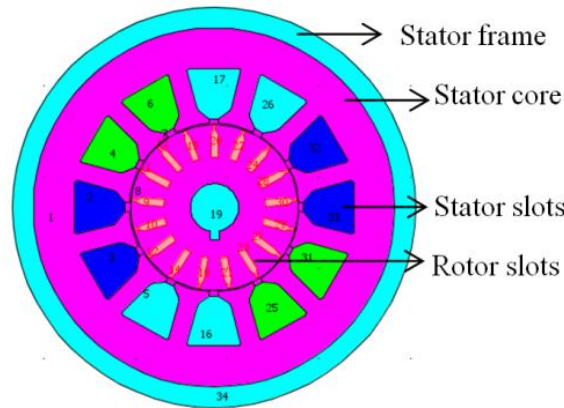


Fig. 4.14 Two dimensional model of induction motor

The analysis was carried out with above mentioned assumptions. Input current density in stator slots and magnetic flux density values in stator and rotor core are shown in Fig. 4.15, Fig. 4.16 & Fig. 4.17 respectively. In modeling constant current of 2 A is given as input in 55 turns of phase A. Input currents of Phase B and Phase C are calculated with incorporation of phase shift of 120 degree each. Magnitude of input current density corresponding to input current of 2 A and 55 turns in stator slots is shown in Fig. 4.15. It can be seen that maximum current density of 1.152×10^6 is observed in phase A. Magnetic flux density values in stator core for input current density shown in Fig. 4.15 is shown in Fig. 4.16. Maximum value of magnetic flux density values in stator core is 0.7 T, which is below the saturation point of silicon steel. The magnetic flux density value in rotor core for input current density is shown in Fig. 4.17. It is observed from Fig. 4.17 that maximum magnetic flux density of 2.28 T is in rotor core portion between rotor bars and air gap.

Electromagnetic torque acting on the rotor is calculated using the Maxwell stress tensor method. Torque verses slip characteristics obtained using FEM analysis for the designed high temperature induction motor is shown in Fig. 4.18. It is observed that trend of the torque characteristics is similar to that of the conventional induction motor. The maximum torque obtained is 0.7 N-m, stable and unstable operating zones are shown in the curve.

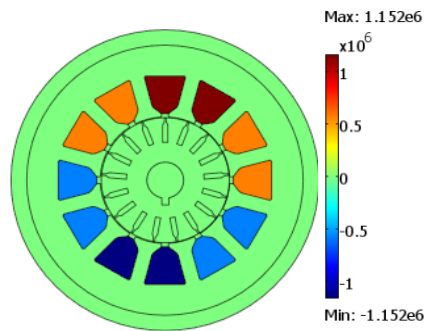


Fig. 4.15 External current density in stator slot (A/mm^2)

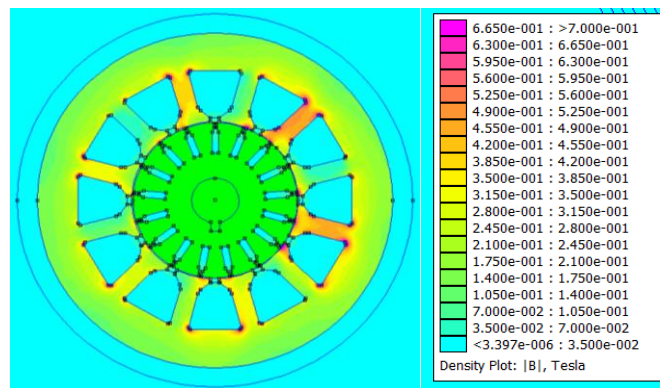


Fig. 4.16 Magnetic flux density plot in stator (T)

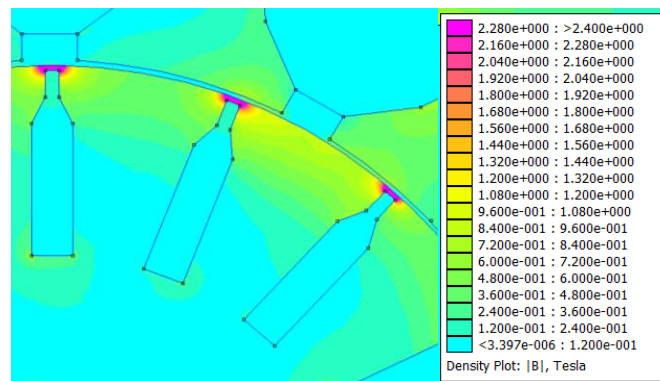


Fig. 4.17 Magnetic flux density plot in rotor (T)

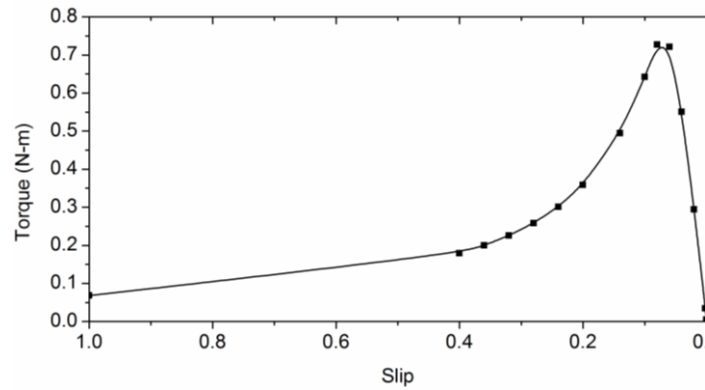


Fig.4.18 Torque - slip characteristics

4.3.4 Test results for high temperature induction motor

The induction motor was tested for its rated current of 2 A at 180 °C. The plot in Fig. 4.19 shows the rise in temperature with respect to time during operation of the motor. The temperature rises initially and then stabilizes at 180 °C. The successful running of motor at 180 °C proved the design intent. Motor testing above 180 °C was not carried out due to the temperature limitations of mechanical bearings used in the motor. The designed motor can be used even for higher temperature operation, if ceramic bearings are used which can withstand higher temperature.

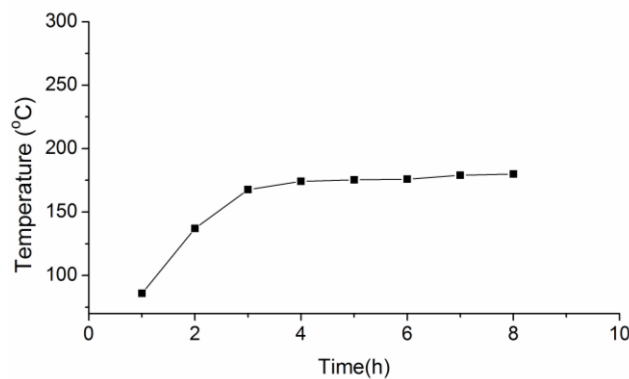


Fig. 4.19 Surface temperature Vs time.

4.4 Demonstration of Use of MI Cable for Rewinding of Conventional Induction Motor

Concept of stator winding made from mineral insulated stainless steel sheathed cable was also proved by rewinding the damaged conventional induction motor using mineral insulated

stainless steel sheathed cable in place of conventional copper cable. The rewound motor shown in Fig. 4.20 worked satisfactorily.



Fig. 4.20 Conventional motor winding replaced with MI cable winding

4.5 Development and Testing of Mineral Insulated Stainless Steel Sheathed Cable for ALIP (Stage II)

Encouraged with the success in development of mineral insulated stainless steel sheathed cable wound compact induction motor, development of mineral insulated stainless steel sheathed cable of 6.0 mm size required for sodium submersible ALIP was initiated. Keeping this in view, specifications were prepared for MI cable to meet the requirement. After few experimental trials, the MI cable was successfully developed.

4.5.1 Construction details of mineral insulated cable

Mineral insulated stainless steel sheathed cable consists of a central copper conductor concentrically placed inside an SS tube. Cross-section of the cable is shown in Fig. 4.21 and its length is 125.0 meters. Figure 4.22 shows the photograph of the developed MI cable.

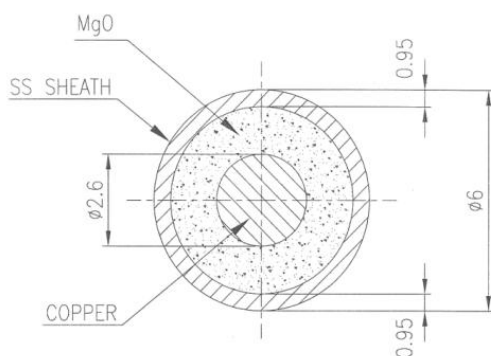


Fig.4.21 Cross-section of MI Cable



Fig.4.22: View of developed MI cable

4.5.2 Tests carried out on MI cable

The following tests were carried out on the MI cable

1. Electrical Resistance Test
2. Cold Insulation Resistance Test
3. Hot Insulation Resistance Test
4. High Voltage Test
5. Radiographic Test
6. Ductility test
7. Cold bend test

The developed MI cable passed all the above tests as per technical specifications.

4.6 Manufacture of Submersible Annular Linear Induction Pump (Stage III)

As part of research work, submersible ALIP was designed and manufactured for sodium draining from reactor pool. The submersible ALIP consists of following important parts/sub-assembly.

- Pump duct
- Lamination and core
- Support flange and cover
- Coil and winding

The above parts are manufactured as per specifications. Material specification and inspections followed during manufacturing are enumerated in Appendix- B.

Conventional electrical insulation can withstand temperatures only upto 200 °C whereas in case of sodium draining from reactor pool, the winding temperature may go as high as 550 °C. Therefore, it was decided to use mineral insulated (MI) stainless steel sheathed cable (with MgO insulation). Manufacturing of submersible ALIP differs from conventional ALIP since a single length of MI cable is needed for making the pump winding. The stainless steel sheathed cable has lower flexibility than the copper cable and hence to gain experience in winding mineral insulated stainless steel sheathed cable, a mockup trial

was carried out. After successful mockup trials, actual winding was performed. The mineral insulated stainless steel sheathed cable winding does not permit any joint unlike in conventional ALIP in which each coil in the slot is joined to other coil in other slot by brazing. Hence, single length of mineral insulated stainless steel sheathed cable was used for winding of each phase. After manufacturing submersible ALIP, helium leak test was carried out. Winding continuity, winding insulation and high voltage tests were carried out successfully. Various stages of manufacturing of ALIP are shown in Fig. 4.23, Fig. 4.24, Fig 4.25 and Fig 4.26.



Fig. 4.23 MI cable winding of submersible ALIP along with fixtures and support



Fig.4.24 Submersible ALIP with MI Cable winding and CRGO laminations



Fig.4.25 Manufactured submersible ALIP with outer stainless steel enclosure



Fig. 4.26 Photograph of manufactured submersible ALIP other view

4.7 Summary

Development of compact sodium submersible ALIP was carried out in three stages. In the first stage, a compact three phase induction motor with mineral insulated stainless steel sheath cable winding was developed to prove the concept of new type of winding. In the second stage, 6.0 mm diameter stainless steel sheathed mineral insulated cable for use in submersible ALIP was developed. In the third stage, sodium submersible ALIP having stator winding made from mineral insulated stainless steel sheathed cable for high temperature application was developed. Helium leak test on pump duct, winding continuity test, insulation test and high voltage test on each phase winding were carried out for the developed ALIP.

Chapter-5

CHAPTER-5

PERFORMANCE EVALUATION OF SODIUM SUBMERSIBLE ALIP

5.1 Introduction

Performance evaluation of the developed pump in sodium is needed to validate the design and qualify it for reactor worthiness. As part of qualification of the pump for reactor operation, its characteristics (Head, Power and Efficiency Vs Flow) and general mechanical/ electrical performances are to be evaluated experimentally in a sodium loop. An experimental facility was designed and erected in existing Bi-Metallic Loop [BIM loop] at IGCAR [46] for testing the sodium submersible ALIP. The details of the test setup in BIM loop along with its mechanical, electrical and instrumentation systems are provided along with operation procedure for testing of the sodium submersible ALIP.

5.2 Description of Sodium Test Facility

The sodium submersible ALIP was installed at cold leg of the Bi-metallic loop in series with the existing 5.0 m³/h pump in the loop. The suction line of the submersible ALIP is connected to the loop return line and the discharge is connected to the existing pump suction through valves. A 1" bypass line was provided for the submersible ALIP test setup so that the main loop alone can be operated after isolating the test setup. The flow sheet of the BIM loop with sodium submersible ALIP is shown in Fig. 5.1. The isometric view of the piping for pump testing setup is shown in Fig. 5.2.

Three manually operated 1" bellow sealed valves were provided in the main flow path viz. pump bypass (VNa11), pump suction (VNa12) and pump discharge (VNa13). Bellow sealed valve VNa12 provided in the pump inlet and bellow sealed valve VNa13 provided in the pump discharge regulate the flow through the pump.

Pressure Pots PP-1 and PP-2 were installed at suitable elevations and connected to the pump suction and discharge lines respectively through ½" Sch. 40 SS pipe lines for

measuring pump developed pressure using pressure balance method. Two ½” bellow sealed valves VNa14 and VNa15 were provided in the pump pressure measuring paths below Pressure pot PP-1 and Pressure pot PP-2 respectively. The pressure pots were provided with four resistance type level probes (RTLTP) corresponding to Low, Operation Low, Operation high and Very high sodium levels. The details of the pressure pots are shown in Fig. 5.3. One permanent magnet type flow meter of range 0-5 m³/h having sensitivity of 1.96 mV/m³/h was installed in the main flow circuit of the BIM loop. The flow through the flow meter is equal to the pump flow when purification circuit of BIM is kept in closed condition.

5.3 Cover Gas System

One argon cover gas system as shown in Fig. 5.4 was provided in the pump test setup. Inlet and outlet lines of ALIP are connected to the Pressure Pots PP-1 and PP-2 through separate lines. The cover gas header is having separate venting and pressurising headers. The pressure pots were individually pressurised and vented during pump testing. Manual and solenoid valves are provided in the cover gas header for pressure regulation in the pressure pots. The solenoid valves are operated from instrumentation control panel.

5.3.1 Inert atmosphere inside submersible ALIP casing

The inert atmosphere inside the submersible ALIP casing is ensured for inhibiting the entry of moisture into the pump and to prevent oxidation of MI cable sheath and magnetic laminations. For maintaining the inert atmosphere, argon line is provided in MI cable entry pipe with provision of argon header with argon cylinder.

5.4 Sodium Pressure Measurement Methodology

To measure the differential pressure across the pump suction and delivery, sodium is allowed to rise in the pressure pots PP-1 and PP-2 when pump under test is in

operation. Sodium levels in pressure pots PP-1 and PP-2 are maintained in between ‘Operation Low’ and ‘Operation High’ by regulating the cover gas pressure. The pressure head developed by the pump is measured through differential pressure at pressure pots PP-1 and PP-2 at the time when sodium levels in both pressure pots are between ‘Operation Low’ and ‘Operation High’ for the applied voltage and flow. The differential pressure gauge reading is noted down along with flow and applied voltage readings for plotting the hydraulic characteristic.

5.5 Power Supply Scheme for Testing of Submersible ALIP

Power supply to submersible annular linear induction pump is arranged through a 200 A, 3-phase motorized auto-transformer and a DOL starter. Input voltage of ALIP is controlled by auto-transformer to vary the pressure head developed. Flow and head variation of pump can be obtained using an auto-transformer or using variable frequency drive (VFD). VFD concept is better than auto-transformer for obtaining variation in pump flow. However in order to demonstrate the proof of concept of Submersible ALIP, auto-transformer readily available was used. Use of VFD has been indicated for future research work for improving efficiency of EM pump. Auto-transformer voltage can be varied remotely from field instrument panel. All control and safety logics are wired to the secondary side contactor. Power wiring diagram for submersible ALIP is shown in Fig. 5.5 and control circuit for ALIP is shown in Fig. 5.6. Auto-transformer secondary voltage, current, pump power and power factor are measured by a digital multifunction meter. Thermal overload relay, HRC fuses and instantaneous over current relay were provided for protection against over load and short circuit.

5.6 Preheating System

Heaters were provided for preheating the sodium pipe lines and for maintaining desired temperature at the surface of submersible ALIP to simulate sodium temperature

when pump is submerged in it.

5.7 Instrumentation and Control

5.7.1 Temperature measurement

Nineteen SS sheathed MgO insulated 3.0 mm dia ungrounded Chromel-Alumel (K type) thermocouples and six SS sheathed MgO insulated 2.0 mm dia ungrounded Chromel-Alumel (K type) thermocouples were used to measure the temperature of ALIP and associated pipe lines. Among them, 23 thermocouples were connected to a temperature indicator through toggle switches in instrumentation panel and remaining two thermocouples (T/C No.8 and T/C No. 8A) were connected to existing Data Acquisition System of BIM Loop.

5.7.2 Level measurement

Pressure pots PP-1 and PP-2 were provided with four resistance type level probes (RTLTP) in each pot to measure the sodium level. Level probes were connected to respective electronic system in the instrumentation panel. Level indications namely Low, Operationn Low, Operation High and High are provided in the instrumentation panel. High levels of sodium in PP-1, PP-2 and appearance /disappearance of level give lamp indication and alarm annunciation in the instrument panel. Details of pressure pot level probes are provided in Table 5.1.

5.7.3 Flow measurement

One permanent magnet type flow meter is provided to measure the sodium flow in submersible ALIP. The flow meter output is connected to a flow indicator mounted in the instrument panel and indication is in engineering units. Flowmeter details are provided in Table 5.2.

5.7.4 Pressure measurement

Two pressure transmitters are provided to measure the cover gas pressure of pressure pot PP-1 and PP-2. One differential pressure transmitter is connected between pressure pot PP-1 and PP-2 to measure the differential pressure. Pressure indicators are provided in the instrument panel with indications in engineering units. Pressure transmitter details are provided in Table 5.3.

A red illuminated push button for pressurization and a green illuminated push button for venting the cover gas for each pressure pots are provided in the instrument panel. DC supply of 24 V is provided to the all the solenoid valves through push buttons.

5.8 Control Logics

Control logics are implemented to ensure the safety and maintaining various parameters for testing and operation of submersible ALIP. Control logics are wired to trip the submersible ALIP for high levels of sodium in pressure pots and low sodium flow. Trip bypass facility is also provided for high sodium levels in pressure pots and low flow. All the control logics are hard wired. Control logic details are provided in Table 5.4.

Table 5.1 Details of Pressure Pot Level Probes

S.No.	Sensor	No. of Probes	Level indication	Remarks
1	RTLTP in PP-1	4	Low Operation low Operation high High	1055.0 mm 550.0 mm 540.0 mm 400.0 mm
2	RTLTP in PP-2	4	Low Operation low Operation high High	1055.0 mm 550.0 mm 540.0 mm 400.0 mm

Table 5.2 Details of Flow Meter

S.No.	Sensor	Range	Sensitivity	Location
1	Permanent magnet flow meter	0-5.0 m ³ /h	1.96 mV/m ³ /h	Submersible ALIP outlet

Table 5.3 Details of Pressure Transmitter

S.No.	Sensor	Range	Location
1	Pressure transmitter	0-10.0 kg/cm ²	PP1
2	Pressure transmitter	0-10.0 kg/cm ²	PP2
3	Differential Pressure transmitter	0-5.0 kg/cm ²	Between PP1 and PP2

Table 5.4 Control Logics

S.No.	Sensor	Measuring parameter	Alarm set point	Indication	Safety action
1	PP-1 RTLP	High level in PP-1	High level appear	Lamp, alarm	Trip SALIP (trip bypass provided)
2	PP-2 RTLP	High level in PP-2	High level appear	Lamp, alarm	Trip SALIP (trip bypass provided)

5.9 Performance Evaluation of Sodium Submersible ALIP

Experimental validation of design and concept was carried out by performing tests on the developed sodium submersible ALIP in sodium loop at conditions similar to reactor conditions except radiation. The pump was tested in sodium loop at sodium temperature of 200 °C to obtain the following characteristics:

- i) Head Vs Flow
- ii) Input power Vs Flow
- iii) Efficiency Vs Flow

The above characteristics cannot be obtained if pump is submerged in sodium because measurement of the developed pressure head is not possible with pressure balance technique. Hence, the pump has to be tested in sodium loop as per the

conventional method at rated sodium temperature. The sodium submergence is simulated by heating the surface of the pump (outer enclosure) upto 200 °C using surface heaters. The pump testing was carried out in Bi-metallic (BIM) loop for obtaining the above mentioned characteristics. Photograph of the pump erected in BIM loop is shown in Fig. 5.7 and photograph of the control and instrument panels is shown in Fig. 5.8. Overstress testing of pump at sodium temperature of 300 °C was also carried out. After obtaining pump characteristics, pump was tested in sodium submerged condition.

5.10 Testing Procedure

Before starting the performance testing of the submersible ALIP, the loop sodium was purified by operating 5.0 m³/h ALIP. During the testing of the sodium submersible ALIP, both purification and carbon meter sections were isolated, so that all the pumped sodium flows through flow meter FM-1. During testing, 5 m³/h ALIP was switched OFF and submersible ALIP was switched ON. The pump was tested as per established procedure [22, 24]. Sodium temperature in the loop was maintained using heaters provided in the test loop at desired temperature for which pump characteristics were to be obtained. For obtaining the head Vs flow characteristics, the pump was energised with three phase power supply at a given voltage by means of an auto-transformer. Sodium flow was measured using permanent magnet flowmeter in BIM loop. Initially, the manually operated sodium valves in both inlet and outlet lines were kept fully opened and a stable flow of sodium was established. Then, the solenoid valves of both pressure pots PP-1 and PP-2 were opened gradually and sodium level was maintained between operation low and operation high levels. The argon cover gas pressures in both pressure pots were recorded. The differential pressure developed by ALIP was read from the differential pressure transmitter across the pressure pot. Input electrical power and other electrical parameters were read from the electrical power supply panel. Thereafter, for

different sodium flow, the outlet sodium valve was throttled and the corresponding pressure head readings were obtained for head Vs flow characteristics. This exercise was repeated at various voltages in the range of 30 V to 120 V.

Experimental readings like pump head developed in kg/cm², flow in m³/h, applied voltage in volts, input current in Amps, pump input electrical power in kW, winding temperature and sodium temperature were recorded. Using experimental data of head and flow, pump hydraulic characteristic of head Vs flow was drawn. Input power Vs flow characteristics was obtained from the experimental readings. Efficiency of the pump was calculated as follows:

$$\text{Efficiency} = \text{Output power} / \text{Input power} \quad (5.1)$$

$$\text{Output power} = 27.25 \times \text{Flow} \times \text{Head} \quad (5.2)$$

where Flow is in m³/h and Head is in kg/cm²

Input power in kW is obtained from the experimental reading while the output power in kW is calculated from the experimental data as per equation 5.2.

5.11 Test Results

Test results on pump characteristics and their comparison with theoretical characteristics are shown in Fig. 5.9 to Fig. 5.14.

Overstress test performed at 300 °C confirmed operation of the pump and its sturdiness at higher temperature. The characteristic of the pump at 300 °C is shown in Fig. 5.15.

After completion of above hydraulic performance testing, endurance testing for 1000 h at 200 °C, 2.0 m³/h and 4.0 kg/cm² of submersible ALIP was carried out. The objective of the endurance testing was to confirm the satisfactory performance of the Submersible ALIP over a long period of operation.

Cavitation test on ALIP was carried to evaluate the limit of inlet pressure in pump which may cause cavitation in the pump. Experiments revealed that the operation of pump at inlet pressure of 0.3 kg/cm^2 (abs) was cavitation free. The low inlet pressure was obtained by throttling the inlet valve. The measurement of inlet pressure was done at constant sodium level in inlet pressure pot using a vacuum pump.

Pressure vs flow characteristic was again obtained after 1000 h of endurance test and the characteristic is shown in Fig. 5.16 (112 V- R curve).

The pump was tested in sodium submerged condition at sodium temperature ranging from 250°C to 500°C for 2000 h. The drawing of facility where sodium submerged test is carried out is shown in Fig. 5.17. Photograph of submerible ALIP along with Integrated Cold Trap (ICT) during erection in the facility for sodium submerged test is shown in Fig. 5.18.

5.12 Discussion on Test Results

Experimental hydraulic characteristic (Head Vs Flow) shown in Fig. 5.9 indicates that pump is capable of developing the required head of 4.0 kg/cm^2 at $2.0 \text{ m}^3/\text{h}$ flow as per design specification at reactor fuel handling temperature of 200°C . The experimental head Vs flow characteristic at 112 Volt is not smooth; this may be due to manual error in measurement of head. Manual measurement of the head by pressure balance technique is a tedious process and human errors are possible. The head Vs flow characteristic has trend of straight line which is attributed to higher resistance value of MI cable winding since the copper conductor used in the MI cable winding is of smaller size. Since the ALIP works on similar principle as of induction motor with exception of field moving linearly instead of rotating, the head Vs flow characteristic of ALIP is similar to torque Vs speed characteristic of induction motor with high resistive winding. The high resistive winding of ALIP makes the head Vs flow characteristic of ALIP as

drooping straight line as obtained in Fig. 5.9. The trend of experimental characteristic (Head Vs Flow) is similar to theoretical characteristic (Fig. 5.10). It is seen that experimental head developed is marginally lower than the theoretical head and this may be attributed to the manufacturing tolerances (slightly higher air gap). During the experiment, flow instability and pump vibrations were not observed which verifies the theoretical calculation in Sec 3.7.

Experimental characteristic (input power Vs flow) at 200 °C is shown in Fig. 5.11. The trend of experimental is similar to theoretical characteristic (Fig. 5.12). The experimental input power is slightly higher than the calculated input power. This may be due to presence of core loss in experiment which is not considered in theoretical calculation.

Experimental efficiency Vs flow at 200 °C is shown in Fig. 5.13. The trend of experimental characteristic is similar to the theoretical characteristic (Fig. 5.14). The efficiency of the developed submersible ALIP (around 1.2%) is found to be less than conventional ALIP (around 5%) of same size. This is due to (i) use of MI cable, which introduces higher resistance in winding hence higher copper loss, (ii) higher eddy current loss in MI cable sheath and winding retainer plate. The higher losses results in lower efficiency.

The overstress test at 300 °C proved robustness of the design and the concept (Fig. 5.15). Experimental characteristic of the pressure head Vs flow obtained after 1000 h endurance test is shown in Fig. 5.16 (112 V- R curve) and the result obtained is nearly same as that of experiments conducted before the endurance test. The repeat test after the endurance test revealed that there is no significant change in the hydraulic characteristic (Head Vs Flow) and the pump continues to develop rated pressure even after considerable duration (1000 h) of operation of the pump at rated operating temperature. Experiments

also revealed that the operation of pump at inlet pressure of 0.3 kg/cm^2 (abs) was cavitation free. Pump testing in sodium submerged condition was also carried out for 2000h.

5.13 Summary

The developed sodium submersible ALIP was tested in a sodium loop that was modified for carrying out the tests. Pressure measurement in sodium loop was carried out by maintaining constant sodium levels in both inlet and outlet pressure pots using argon pressure. The difference in argon pressure to maintain constant sodium levels in both the sodium pots is a measure of the pressure developed by the pump. The experimental characteristics obtained are compared with the theoretical predicted characteristics. The experimental characteristics obtained validated the design and concept of annular linear induction pump having winding made from mineral insulated stainless steel sheathed cable. Tests confirmed the design of ALIP for use in high temperature submerged sodium environment without need of any external cooling. The experimental head developed is slightly less than the theoretical predicted head for given voltage. Similarly, experimental power input is higher than the theoretical power input which results in lower experimental efficiency than the theoretical efficiency. The reasons for above deviation may be attributed to manufacturing tolerance and additional copper loss in pump. Increase in small air gap will cause higher magnetizing current and hence, less pressure head developed. In experiment no flow instability was observed.

In the theoretical model, core loss and duct hydraulic loss are not considered. In the experiments, the input power consists of core as well as hydraulic losses resulting in difference in theoretical and experimental values of various parameters. Eddy current in stainless steel sheathed MI cable and winding retaining steel plate is accounted in the theoretical design calculations with some assumptions and hence there is scope of

difference in theoretical and experimental values. The pressure measurements were carried out manually and level fluctuation in pressure pot may have slight effect on measurements. The overstress test at 300 °C proved robustness of the design and the concept. The pump was operated for 1000 h as endurance test. The pump showed no sign of cavitation during test at below atmospheric pressure in the inlet side. Also testing of pump in fully sodium submerged condition at sodium temperature of 250 °C to 500 °C was carried out for 2000 h operation. The successful performance testing of developed ALIP in sodium has indicated the fulfillment of research objective.

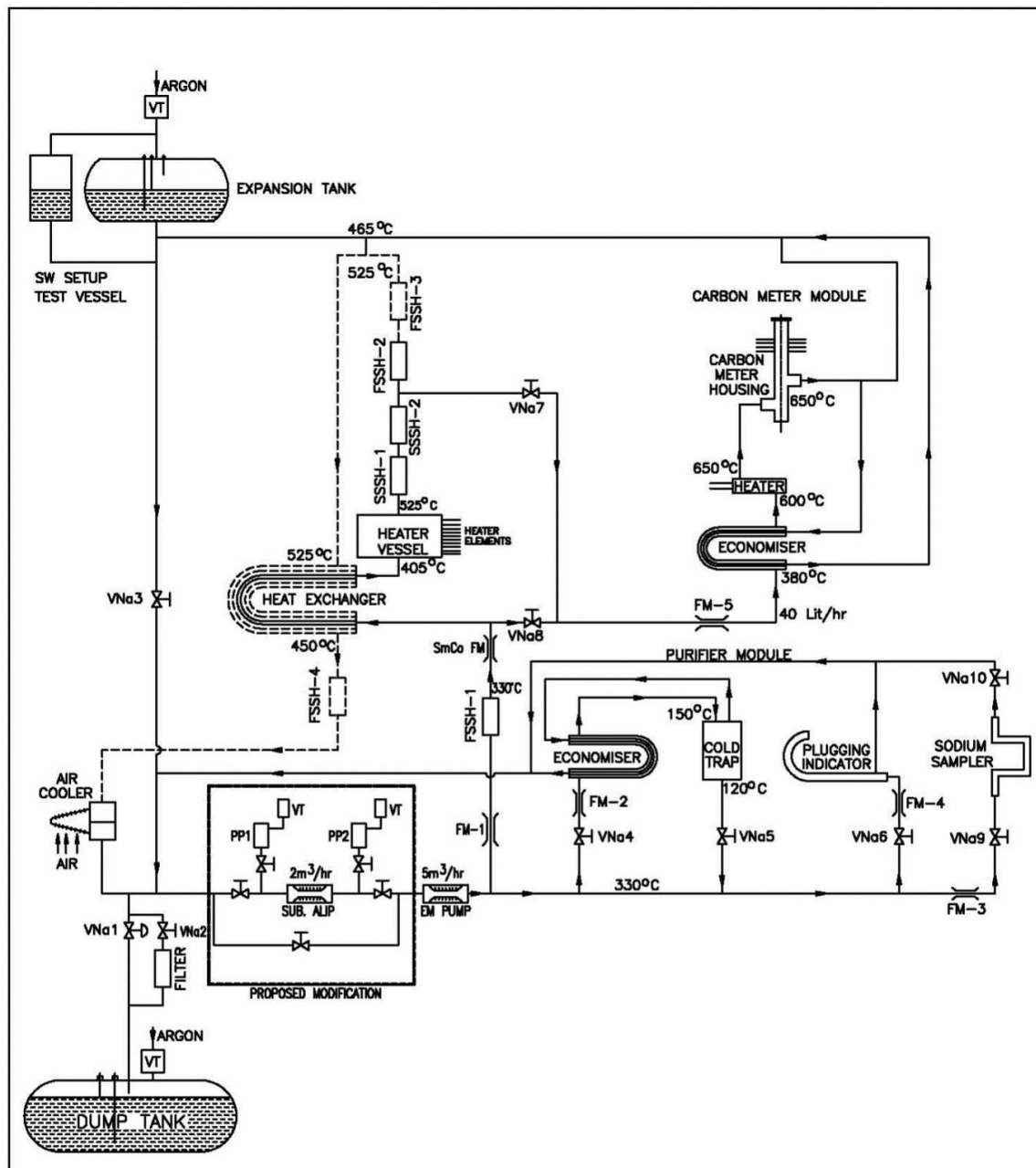


Fig. 5.1 Flow sheet of BIM loop with submersible ALIP

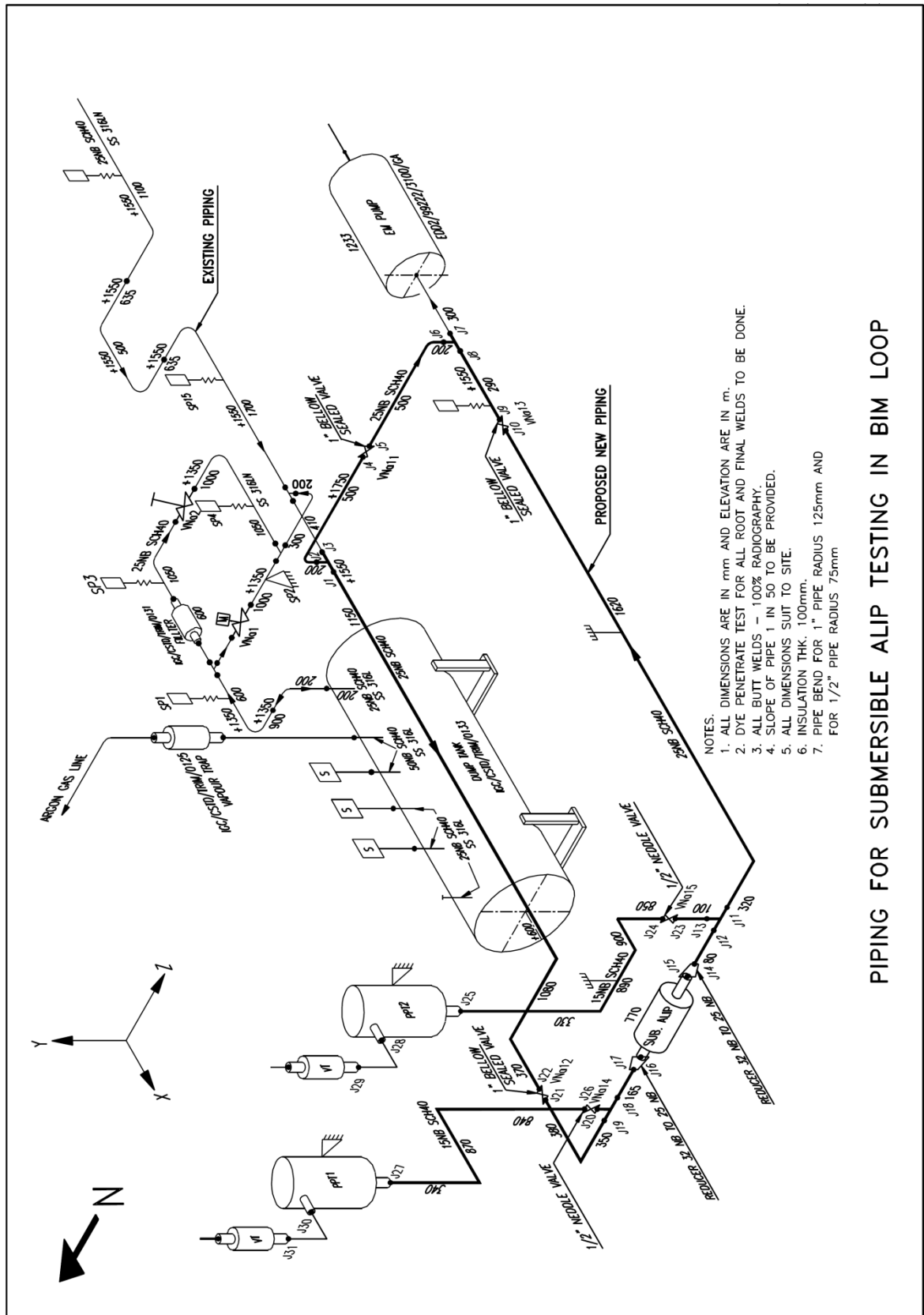


Fig. 5.2 Piping for submersible ALIP testing

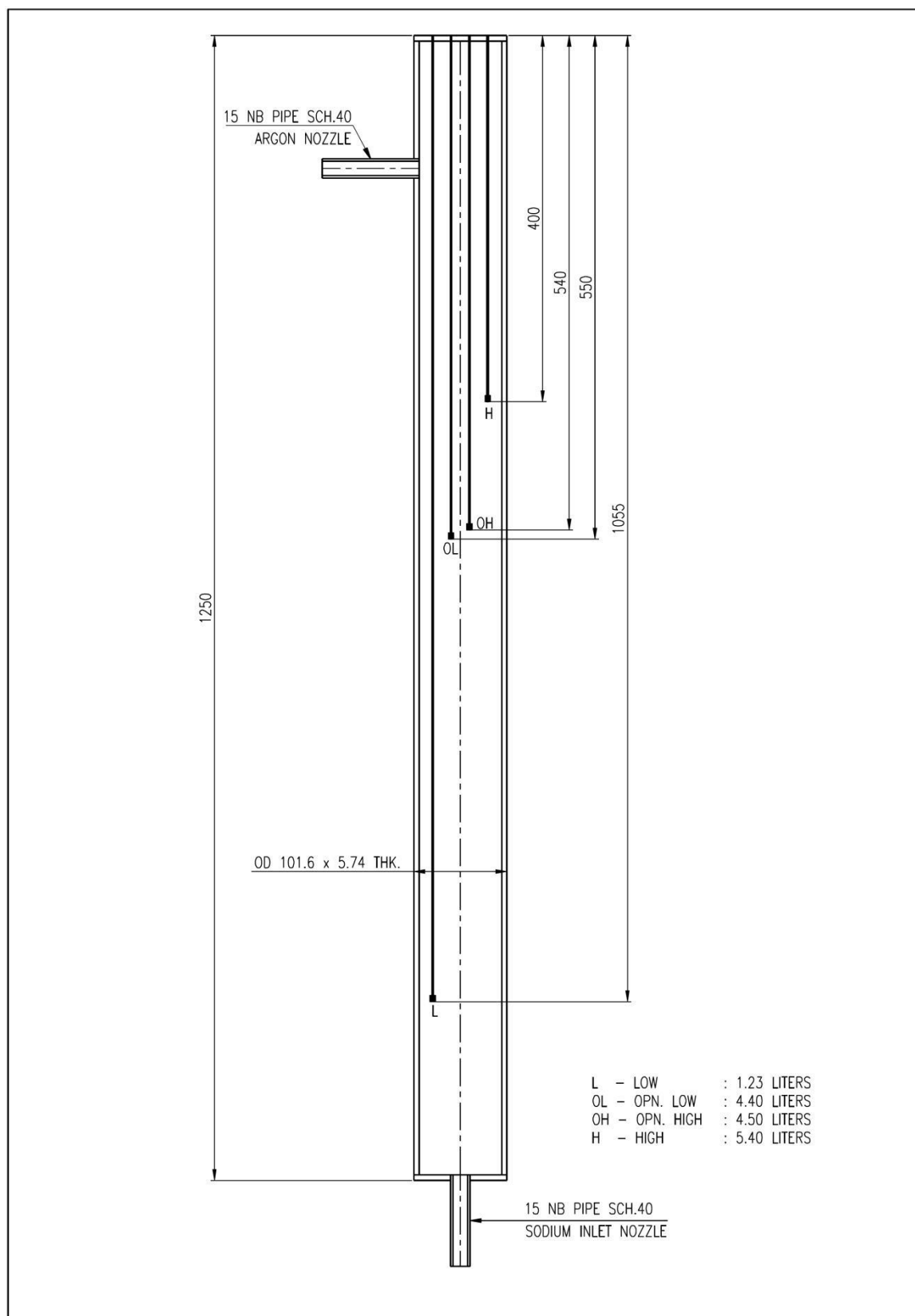


Fig. 5.3 Pressure pot with level probe details

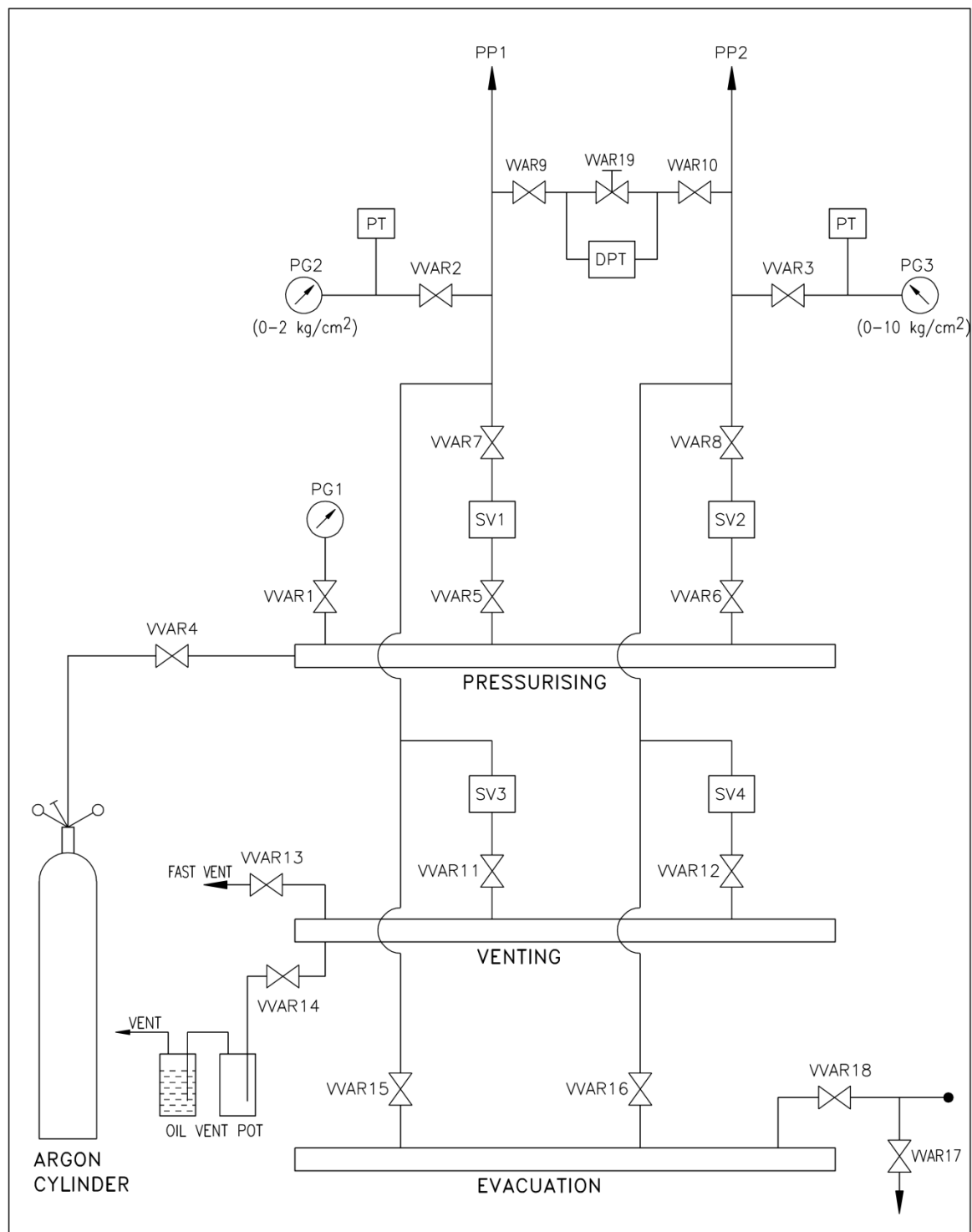


Fig. 5.4 Argon cover gas header for pressure pots of ALIP testing facility

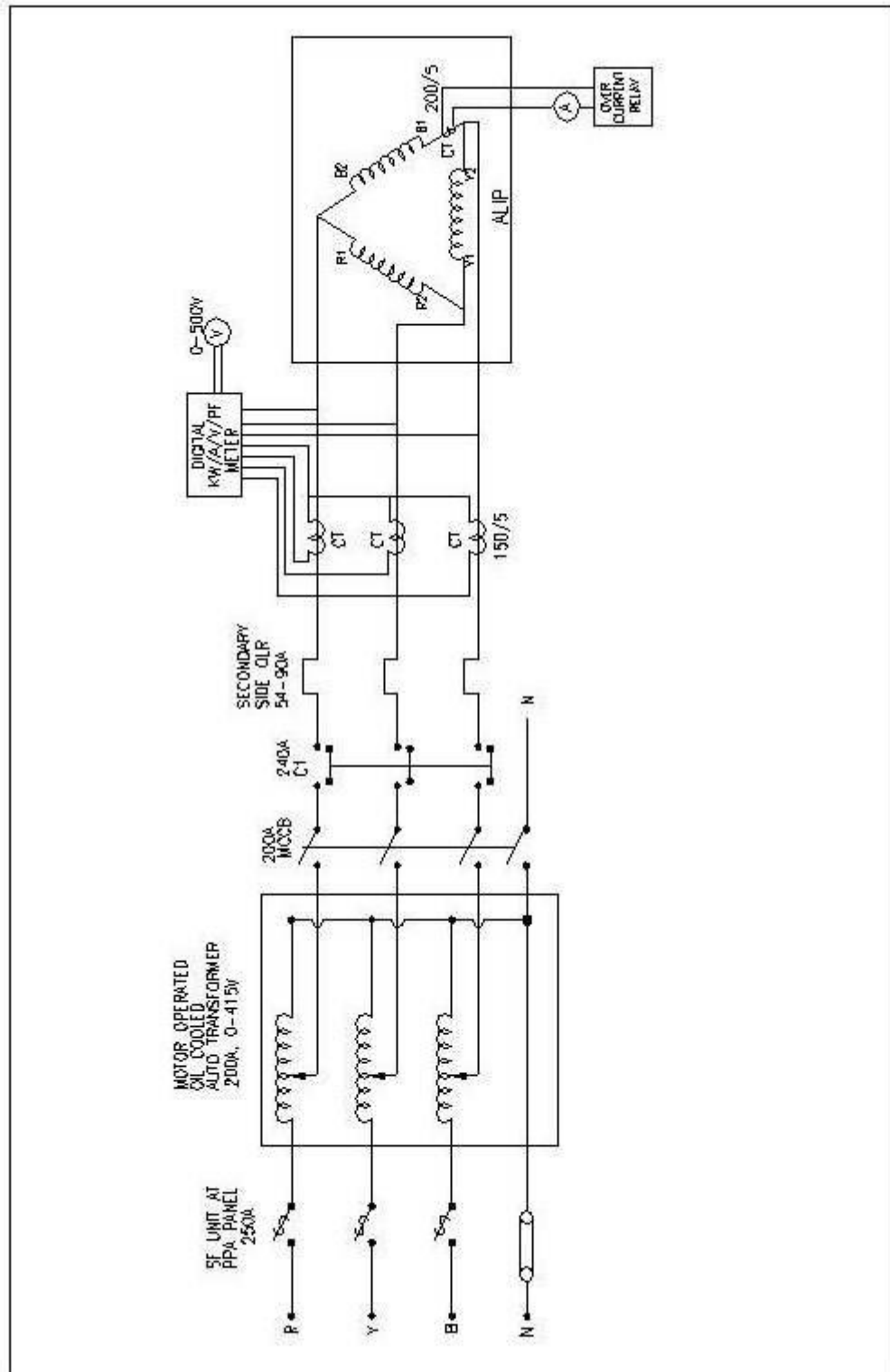


Fig. 5.5 Power supply wiring diagram for submersible ALIP

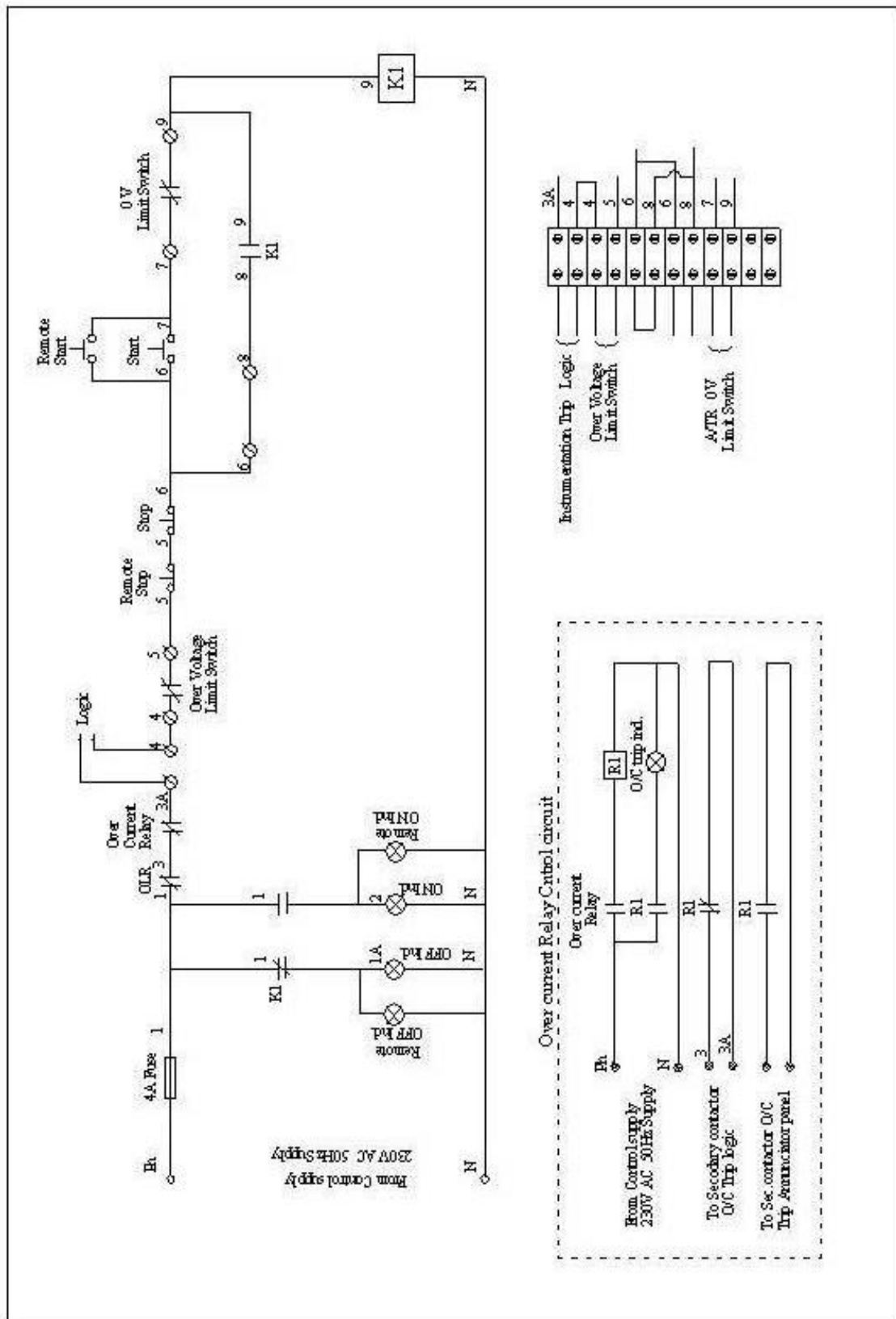


Fig. 5.6 Control circuit wiring diagram for submersible ALIP

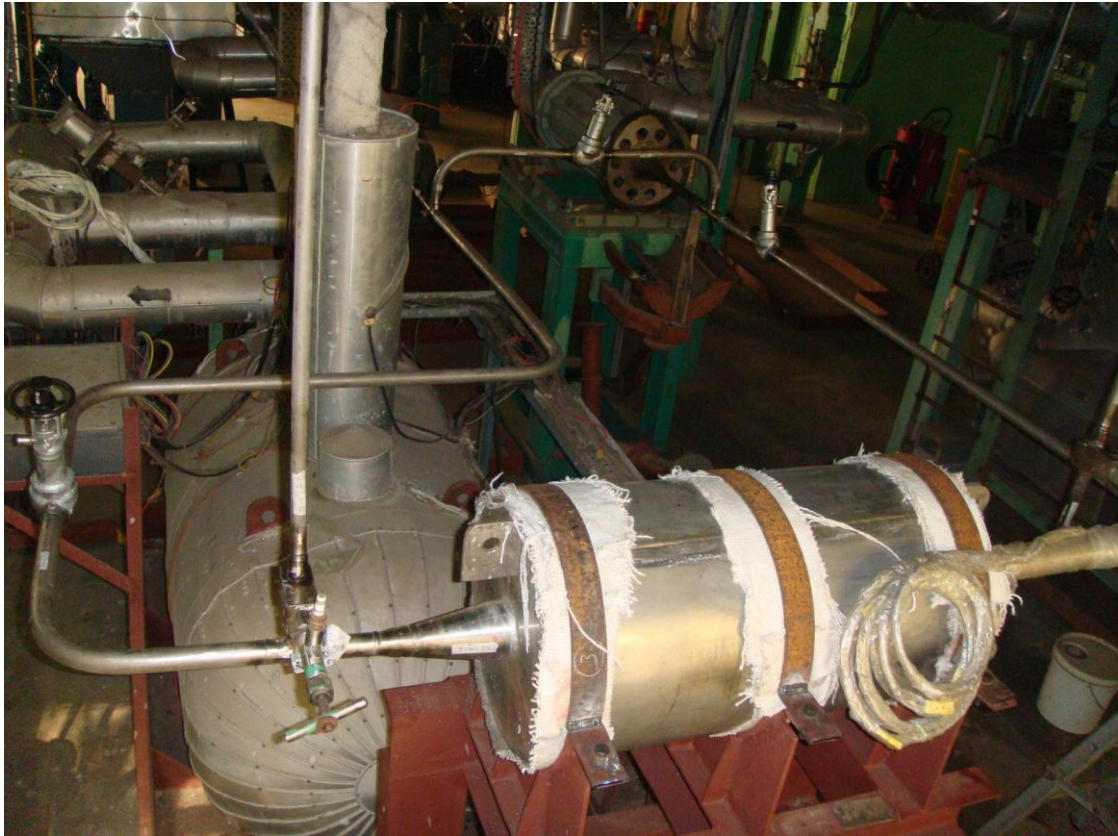


Fig. 5.7 Photograph of pump erected in BIM loop



Fig. 5.8 Photograph of control and instrument panel and other electrical systems

ALIP Test Results

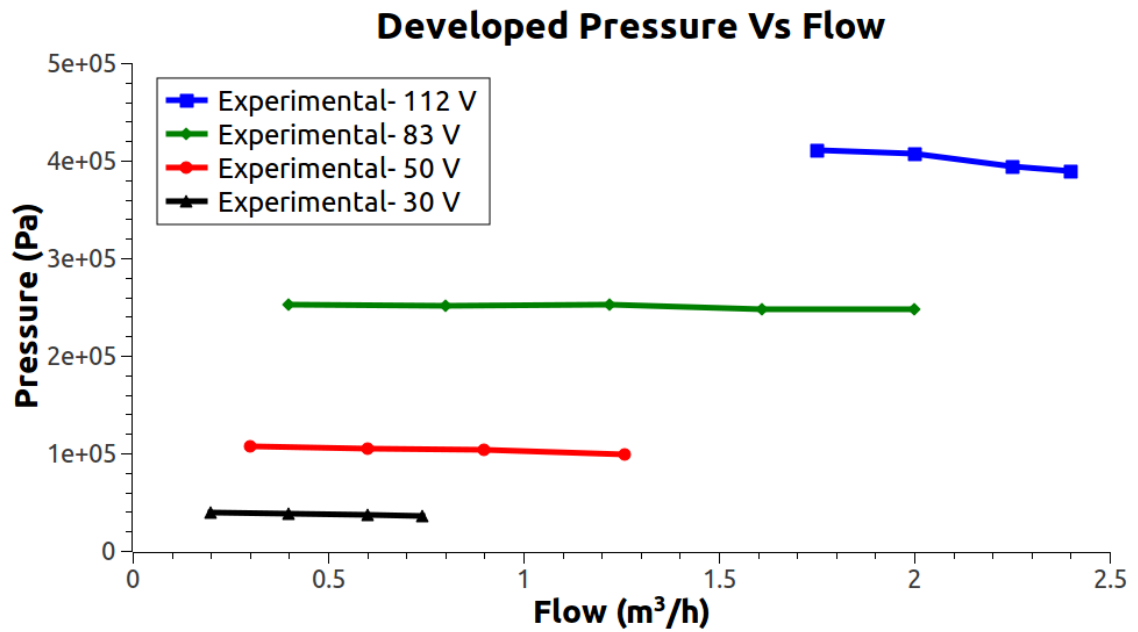


Fig. 5.9 Experimental Pressure Head Vs Flow characteristics at 200 °C

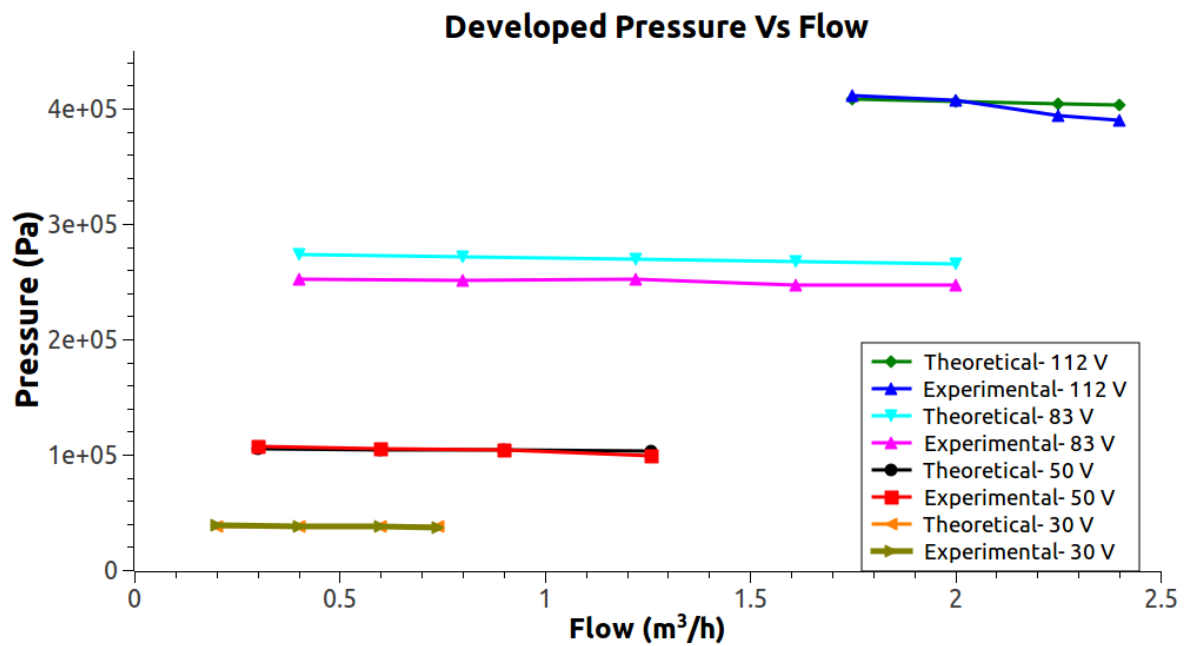


Fig. 5.10 Comparison of experimental and theoretical Pressure Head Vs Flow characteristics at 200 °C

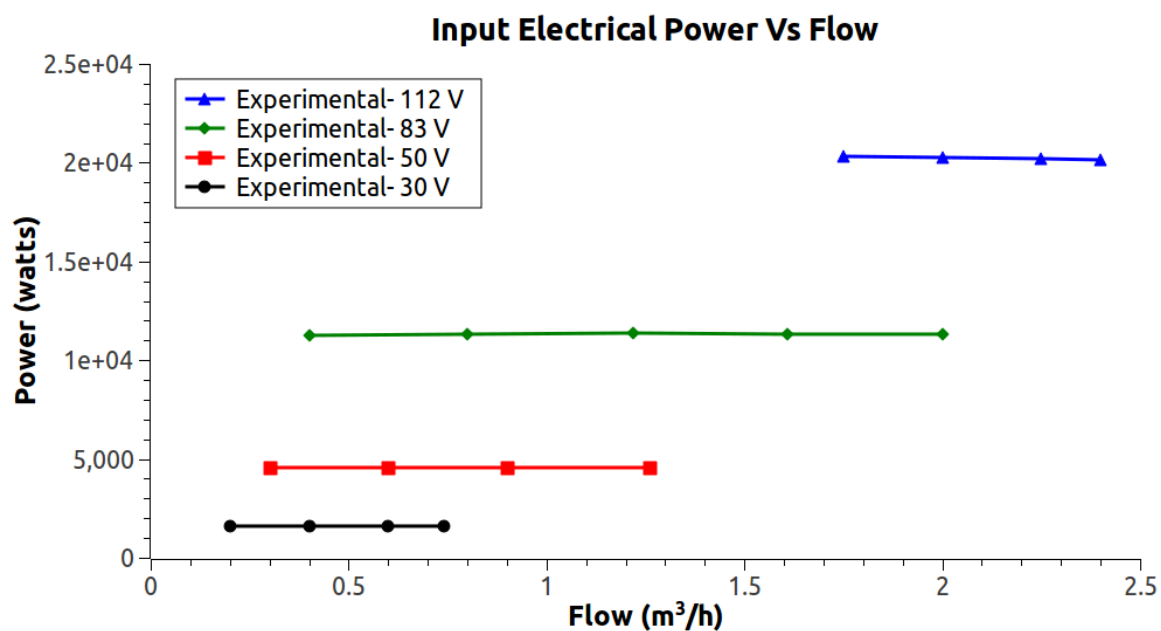


Fig. 5.11 Experimental Input Electrical Power Vs Flow at 200 °C

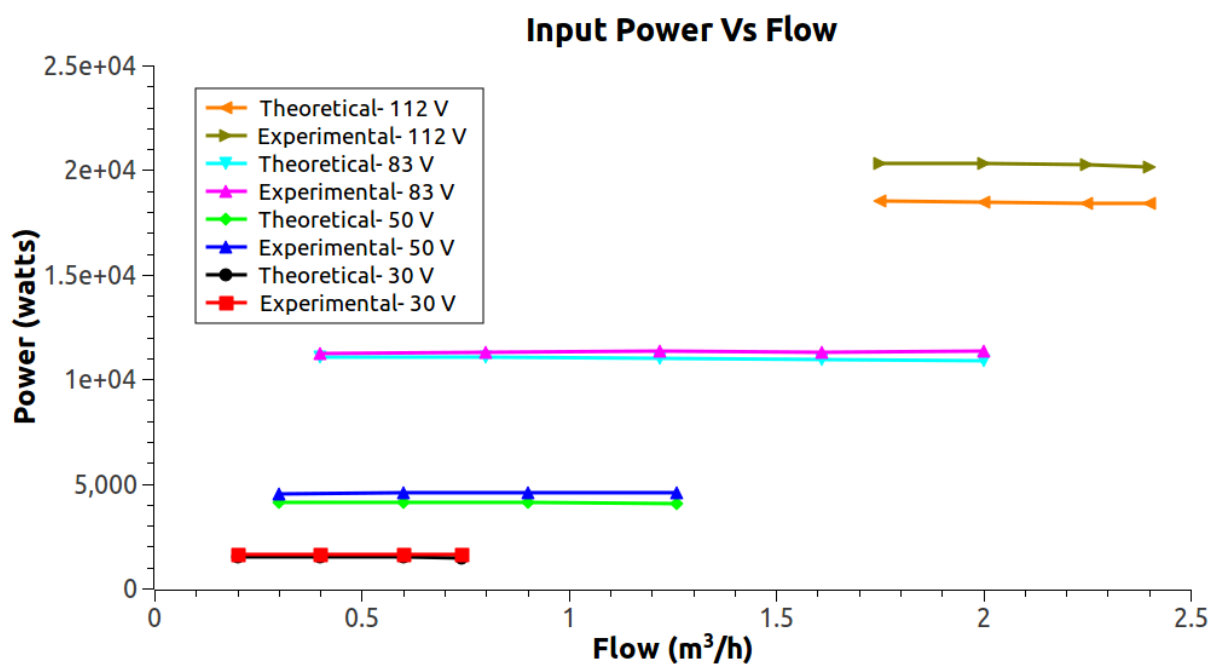


Fig. 5.12 Comparison of Experimental and Theoretical Input Electrical Power Vs Flow at 200 °C

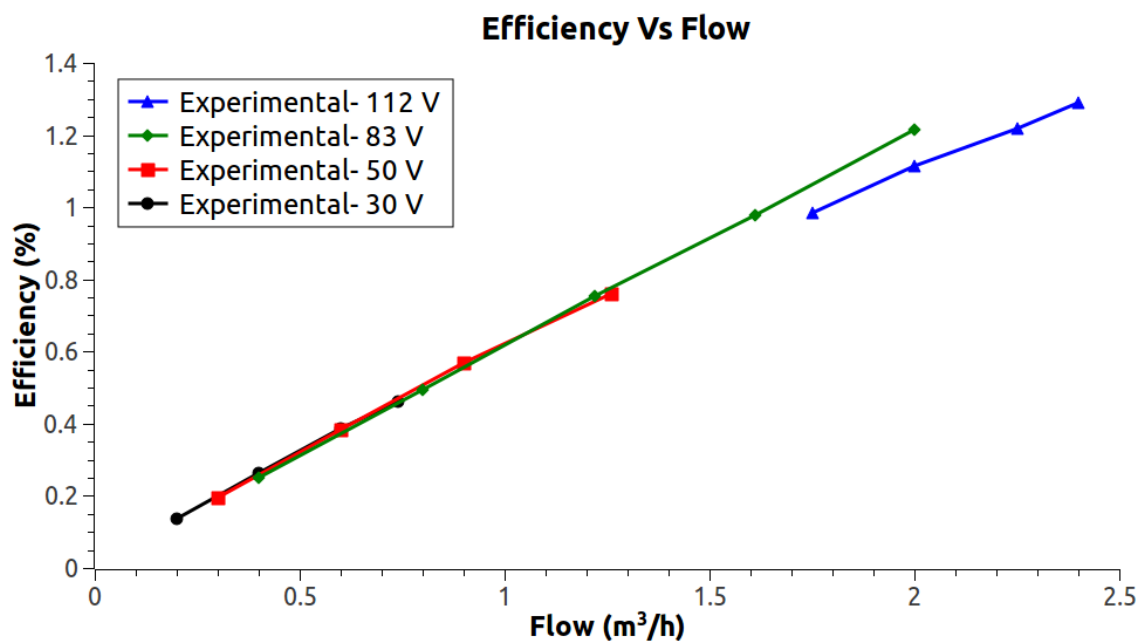


Fig. 5.13 Experimental Efficiency Vs Flow at 200 °C

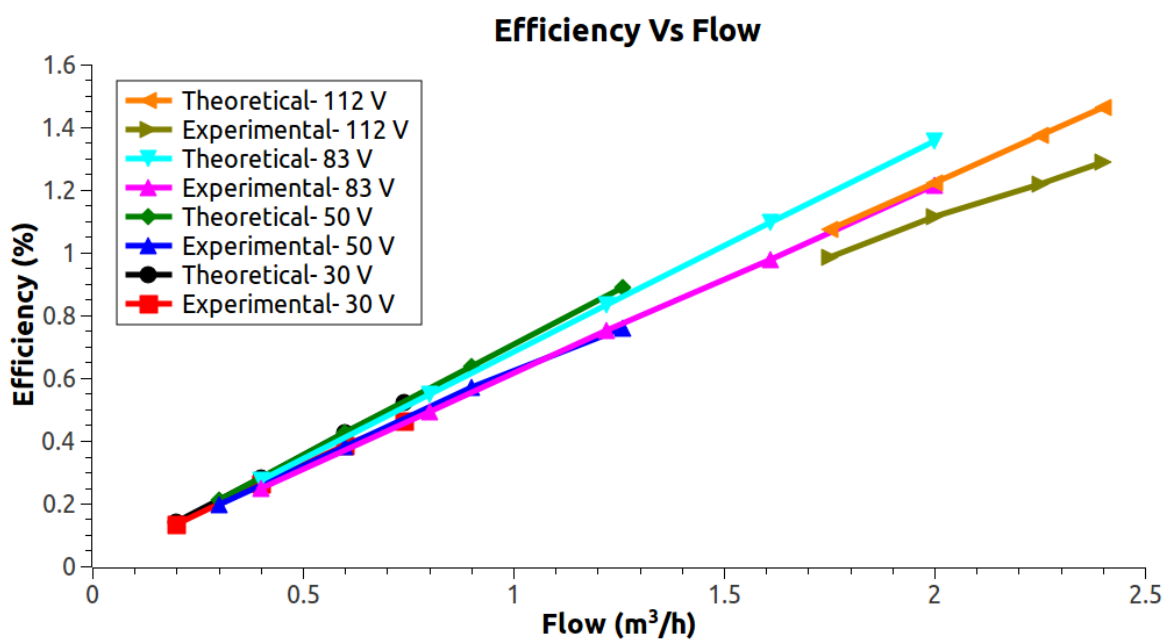


Fig. 5.14 Comparison of Experimental and Theoretical Efficiency Vs Flow at 200 °C

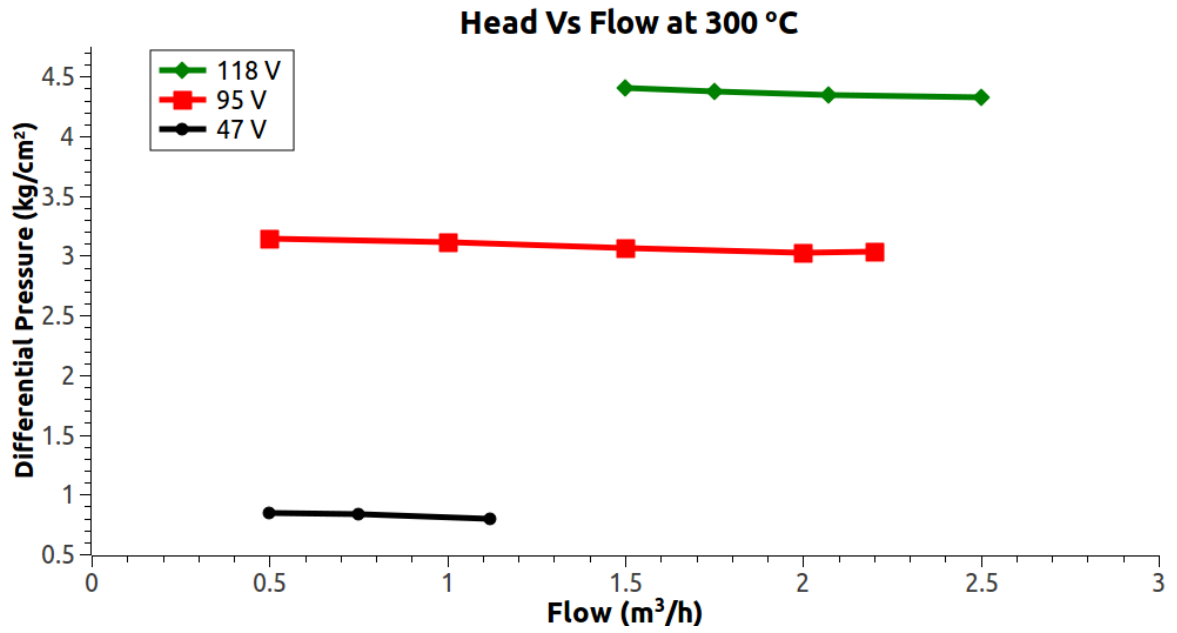


Fig. 5.15 Experimental Pressure Vs Flow at 300 °C (Overstress Test)

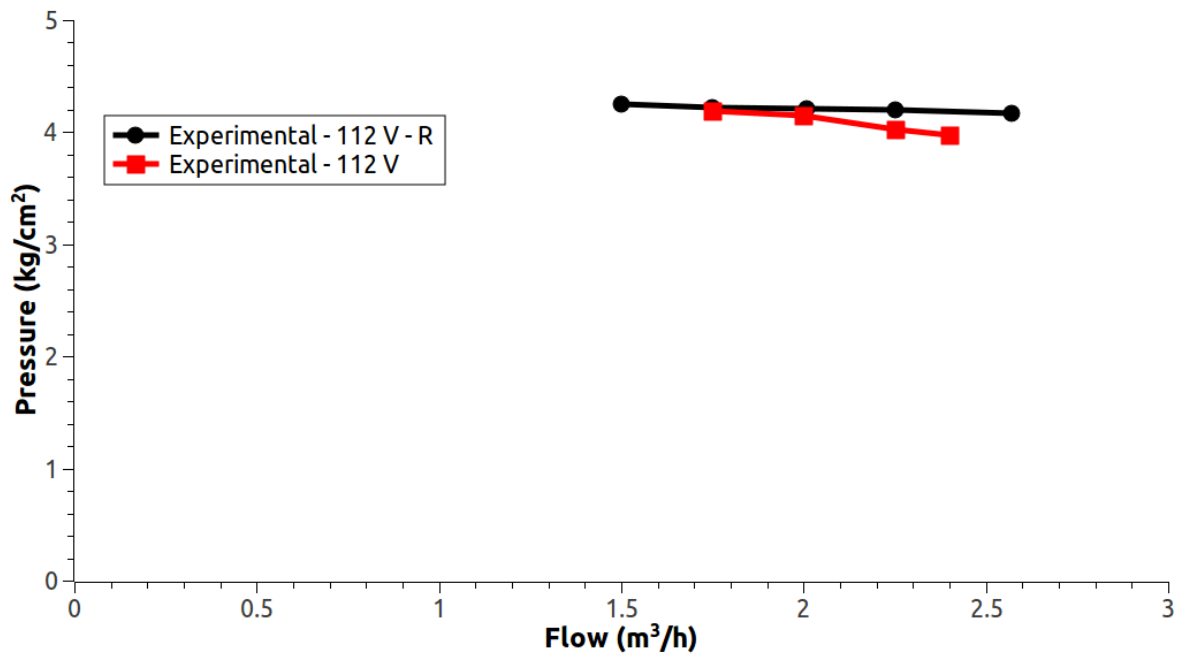


Fig. 5.16 Pressure Vs Flow characteristics after endurance test of 1000 h



Fig. 5.18 Erection of submersible ALIP for testing in ICT

Chapter - 6

CHAPTER 6

SUMMARY AND FUTURE PROSPECTS

6.1 Summary

Research work towards design and development of sodium submersible EM pump for high temperature application was taken up for draining of sodium at 200 °C from the main vessel of PFBR. Sodium draining is envisaged for inspection of sub-assembly during shut down period of reactor operation and during reactor decommissioning. Earlier to this research work, there was no device available which can be used for draining of sodium from main vessel of PFBR. Other countries also had no dedicated device for complete sodium draining, however, electromagnetic pump provided in purification circuit was used for partial draining of sodium during decommissioning stage [44]. Full draining of sodium using purification circuit electromagnetic pump is not possible due to cavitation problem. After studying the constraints, development of device was taken up with the following requirements:

- 1) Operating in sodium submerged condition
- 2) Withstanding sodium temperature of 200 °C
- 3) Operating without any external cooling
- 4) Getting inserted through inspection canal of 450.0 mm diameter and
- 5) Withstanding radiation field present in the reactor.

Various options were studied and based on the literature survey on electromagnetic pumps, it was concluded that annular linear induction pump (ALIP) has the potential to meet the above mentioned requirements. Considering this, research work was carried out to develop an ALIP having stator winding made from mineral insulated stainless steel sheathed cable. This cable had proved its capability for high temperature operation and radiation withstanding capability in various devices such as mutual

inductance type level probe and DSRDM electromagnetic coil [14, 32]. Mathematical modelling and derivation of various ALIP pump parameters were carried out using first principles for better understanding. Design of 2.0 m³/h and 4.0 kg/cm² capacity ALIP was carried out keeping sodium submerged pump hermetically sealed, compact, capable of high temperature operation and radiation withstand capability criteria in mind. Finite Element Method (FEM) analysis was carried out to predict theoretical performance of the designed pump.

In this research work, design of ALIP was initiated with prevailing equivalent circuit approach. This research work resulted in modification of prevailing equivalent circuit to take into account the effect of eddy currents in stainless steel sheathed winding and retainer plates. The modification incorporated in equivalent circuit is new knowledge brought out in the field of ALIP. Design and development of a compact sodium submersible ALIP having mineral insulated stainless steel sheathed winding capable of working in sodium submerged condition at 200 °C without any need of external cooling has demonstrated the fulfilment of research objective.

Manufacturing of ALIP was carried out in three stages. In the first stage, development of 50 W three phase induction motor with 1.5 mm diameter mineral insulated stainless steel sheathed cable was undertaken to prove the concept of mineral insulated cable winding. In the second stage, manufacturing of 6.0 mm diameter mineral insulated cable as per the design requirement of the ALIP was demonstrated. In the third stage, sodium submersible ALIP was fabricated, prior to which, mock up trials for ALIP winding with mineral insulated stainless steel cable were carried out. Stainless steel, mineral insulation and copper conductor (for carrying current) were the materials used in the ALIP. All these materials have proven record of withstanding high temperature and

radiation field. Hence, the designed ALIP can withstand the designated high temperature as well as radiation field making it well suited for reactor operation.

In submersible ALIP winding, copper conductor occupies less area in the stator slot because high percentage of area is being occupied by MgO insulation as well as stainless steel sheath. Less conductor area results in higher current density. The mineral insulated stainless steel sheathed cable can withstand high current density upto 20 A/mm^2 compared to $2 - 5 \text{ A/mm}^2$ in conventional EM pump. However this results in higher copper loss in the winding. The eddy current loss due to stainless steel sheathed winding, retainer plate and higher copper loss in winding has reduced the efficiency of the designed ALIP considerably low (around 1.5 %) compared to conventional ALIP of same capacity which may have efficiency around 5.0 %. The designed ALIP is capable of developing required pumping pressure of 4.0 kg/cm^2 at $2.0 \text{ m}^3/\text{h}$ flow. The designed pump has 400.0 mm diameter lateral dimension which can be easily inserted through available inspection canal of PFBR.

The concept of ALIP, having stator winding made from mineral insulated stainless steel sheath cable which can withstand temperature up to 550°C is new and it is not reported in open literature. ALIP design was carried out as per lump parameter model and the design was analysed using a commercial FEM software.

The manufactured ALIP was tested in sodium loop under similar condition to reactor (except radiation). The sodium testing at 200°C without any external cooling of ALIP has validated the design and the new concept. The stator winding withstood temperature of 550°C during endurance testing of 1000 h. During testing, no flow instability was observed. Pump characteristics such as Pressure Head V/s Flow, Input Power Vs Flow, Efficiency Vs Flow at 200°C were obtained from experiments. Overstress test at 300°C and endurance testing for 1000 h proves robustness of the

design and the concept. The pump has operated without cavitation at low inlet pressure at rated flow. The pump has been also operated in sodium submerged condition for 2000 h at temperature varying from 250 °C to 500 °C which is much above the rated operating condition.

Application of this research work is not limited to above mentioned application but it can be used in many other applications in sodium cooled fast reactors and sodium experimental facilities such as integrated cold trap system and in-core material testing.

6.2 Future Research Prospects

The completed research work has opened new avenues of research. Research work can be initiated for development of fire survival induction motor based on stator winding made from mineral insulated stainless steel sheath cable. The fire survival induction motor can be used for pumping fire extinguisher even they themselves are engulfed in fire.

The present bearing used in the motor can not work at high temperature ($>150\text{ }^{\circ}\text{C}$) because of evaporation of lubricant. This opens an avenue for development of high temperature bearings made of ceramic, which does not require the use of any lubricant. Ceramics are also suggested because they can withstand high temperature due to lower coefficient of thermal expansion compared to metal.

In the present design, considerable slot space is used by non-current carrying materials like steel and MgO, resulting in higher resistance of winding due to lower area available for copper, leading to higher loss and lower efficiency of ALIP. In future, research work may be extended to develop winding insulation using Mica and other ceramic powder with suitable adhesive for high temperature operation in radiation field. This research will lead to better slot utilization by copper winding, resulting in better efficiency of ALIP.

In future, research work can be initiated for precise calculation of eddy current loss in mineral insulated stainless steel sheath cable of ALIP and its effect on ALIP performance. Further research in the domain of use of variable frequency power supply for improving the efficiency of ALIP may be carried out. FEM modelling may be efficient tool for carrying out further research towards analysis of pump magnetic field and performance evaluation. In the modelling, it is essential to take account of stainless steel sheath over the copper core and azimuthal irregularity of positioning of stator core for accurate theoretical performance evaluation. This can also be taken up as future research work. Research can be extended towards optimization of pump performance as well as in the field of understanding pump instability criteria.

Appendix - A

APPENDIX-A

CALCULATIONS FOR 2.0 m³/h, 4.0 kg/cm² SUBMERSIBLE ANNULAR LINEAR INDUCTION PUMP (ALIP)

Various parameters of the pump were designed as per the mathematical model developed in chapter 2 and as per electromagnetic hand book [12]. In design, some of the input parameters are chosen as per requirement and based on earlier experience and other are computed as per the developed model.

$$\text{Flow} = 2.0 \text{ m}^3/\text{hr}$$

$$E_b = \text{Input Voltage} = 150 \text{ V}$$

$$T_{Cu} = \text{Temperature of the Copper/ MI Winding} = 600^\circ\text{C}.$$

$$T_1 = \text{Specified Liquid Metal Temperature} = 600^\circ \text{ C}$$

$$D_1 = \text{Annular passage} = 2.09 \text{ mm}$$

$$D_2 = \text{Thickness of the outer duct wall} = 3 \text{ mm}$$

$$D_3 = \text{Clearance between Outer duct wall and the stator bore surface} = 2 \text{ mm}$$

$$D_4 = \text{Thickness of SS jacket surrounding the core} = 1.65 \text{ mm}$$

$$D_9 = \text{Diameter of centre core} = 45 \text{ mm}$$

$$D_{12} = \text{Clearance between bottom of coil side and bottom of slot} = 0 \text{ mm}$$

$$D_{13} = \text{Depth of coil side} = 11 \text{ layers of Dia } 6.05 \text{ mm MI Cable} = 11 \times 7 = 77 \text{ mm}$$

(Taking coil expansion during winding into account since winding may not remain very tight during winding process.)

$$D_{10} = \text{Width of Stator Tooth} = 10 \text{ mm}$$

$$D_{11} = \text{Width of Stator Slot} = 16 \text{ mm}$$

$$N_1 = \text{Number of Poles} = 4$$

$$N_2 = \text{Number of Phases} = 3$$

$$N_3 = \text{Number of slots per pole per phase} = 2$$

$$N_7 = \text{Number of turns per coil} = 22$$

$K_p = \text{Pitch factor} = 1$

$$Q_{\text{spec}} = \frac{2}{3600} \text{ m}^3 / \text{sec} = 5.555 \times 10^{-4} \text{ m}^3 / \text{sec} \quad (\text{A-1})$$

$P_1 = \text{specified Pressure Rise} = 4 \text{ kg/cm}^2$

(Requirement is 4 kg/cm^2 but pump has to be designed for 1.375 times requirement to take care of inlet pressure drop and other uncertainties as per previous experience)

$P_2 = \text{Internal Developed pumping pressure} = 1.375 \times P_1 = 1.375 \times 4 \times 9.81 \times 10^4 \text{ N/m}^2 = 539550 \text{ Pa}$

$V_{\text{fmax}} = \text{Maximum allowable liquid metal velocity} = 9.14 \text{ m/sec}$

$f = \text{frequency of the applied voltage} = 50 \text{ Hz}$

The inner duct pipe has OD 48.3 mm and thickness of 1.65 mm (40 NB Sch-5). The outer duct pipe is having OD of 58.48 mm and thickness 3mm (50 NB sch-40, OD is to machined to get 58.48mm OD)

$D_1 = 2.09 \text{ mm}$ (Annular gap for Sodium flow)

$D_2 = 3.0 \text{ mm}$ (Thickness of outer duct wall)

$D_3 = 2.0 \text{ mm}$ (Gap between outer duct wall and Stator bore Surface)

$D_4 = 1.65 \text{ mm}$ (Thickness of SS jacket surrounding the core)

$D_5 = \text{Total radial distance from the surface of stator bore to the surface of centre core}$

$$D_5 = D_1 + D_2 + D_3 + D_4 \quad (\text{A-2})$$

$$D_5 = 2.09 + 3.0 + 2.0 + 1.65$$

$$= 8.74 \text{ mm}$$

$$\approx 8.8 \text{ mm}$$

The inner duct pipe is of 48.3 mm OD & thickness 1.65 mm

$$D_9 = 48.3 - 2 \times 1.65 = 45.0 \text{ mm} \quad (\text{A-3})$$

So, 40NB Sch-5 pipe should be used for Inner Duct.

Selection of outer Pipe

The required size of outer pipe can be obtained from a 50NB Sch-40 (OD = 60.3 mm, thickness = 3.91 mm & ID = 52.48 mm by machining the OD to 58.48 mm which is the required OD.

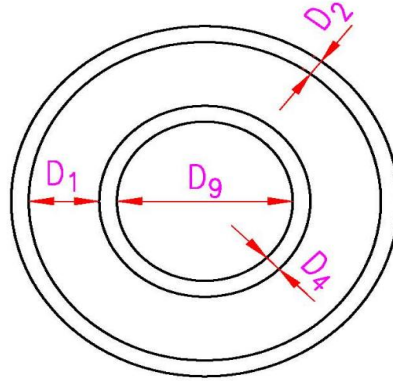


Fig. 3.1 : Duct dimension

$$\text{Area of Annular Gap} = \frac{\pi}{4} (52.48^2 - 48.3^2) = 330.86 \text{ mm}^2 \quad (\text{A-4})$$

$$\text{Computed velocity of sodium in Annulus } V_f = \frac{Q_{\text{spec}}}{\text{Annulus Area}} \quad (\text{A-5})$$

$$V_f = \frac{5.555 \times 10^{-4} \text{ m}^3 / \text{sec}}{330.86 \times 10^{-6} \text{ m}^2} = 1.697 \text{ m/sec}$$

$$V_f = 1.68 \text{ m/sec}$$

D₇ = Mean Diameter of Annulus

$$D_7 = D_9 + 2 \times D_4 + D_1 \quad (\text{A-6})$$

$$D_7 = 45.0 + 2 \times 1.65 + 2.09 = 50.39 \text{ mm}$$

D₈ = Bore Diameter of Stator Surface

= OD of outer Stator Surface

$$= \text{OD of outer pipe} + 2 \times \text{Clearance (D}_3) \quad (\text{A-7})$$

$$= 58.48 + 2 \times 2$$

$$D_8 = 62.48 \text{ mm}$$

$$D_9 = 45 \text{ mm}$$

$$D_6 = \text{Pole-Pitch} = \text{slot per pole per phase} \times \text{No. of phases} \times \text{Slot pitch}$$

$$D_6 = N_3 N_2 (D_{10} + D_{11}) \quad (A-8)$$

$$D_6 = 2 \times 3 \times (10 + 16)$$

$$D_6 = 156 \text{ mm}$$

$$D_{12} = \text{Clearance between bottom of coil side and bottom of slot} = 0 \text{ mm}$$

$$D_{13} = \text{Depth of coil side} = 11 \times 7 = 77 \text{ mm}$$

$$D_{14} = \text{Depth of slot} = 90 \text{ mm}$$

(Depth of the slot has been provided somewhat extra to take care of the compressibility of MI cable in the slot)

$$D_{15} = \text{Mean length of coil turn} = \pi \times \text{Mean diameter of coil} \quad (A-9)$$

$$= \pi \times (\text{Bore dia} + \text{Slot Depth})$$

$$= \pi \times (62.48 + 90)$$

$$D_{15} = 479.03 \text{ mm}$$

$$N_1 = \text{No. of Poles produced by stator} = 4$$

$$N_2 = \text{No. of Phases} = 3$$

$$N_3 = \text{No. of slots per pole per phase} = 2$$

$$N_4 = \text{No. of slots in the stator} = N_1 \times N_2 \times N_3 = 24$$

$$N_5 = \text{No. of teeth in the stator} = N_4 + 1 = 25$$

$$N_6 = \text{No. of Stator coils} = N_4 = \text{No. of Slots} = 24$$

$$N_7 = \text{No. of Turns per coil} = 22$$

$$D_{17} = \text{Depth of back iron (yoke)} = 29 \text{ mm}$$

$$D_{18} = \text{Overall Diameter of pump}$$

$$D_{18} = D_8 + 2 \times D_{14} + 2 \times D_{17} \quad (A-10)$$

$$D_{18} = 62.48 + 2 \times 90 + 2 \times 29 = 300.48 \text{ mm}$$

$$D_{19} = \text{Pump Length} = N_4 (D_{10} + D_{11}) + D_{10} \quad (A-11)$$

$$D_{19} = 24 \times (10 + 18) + 10 = 634 \text{ mm}$$

$$N_{sc} = \text{Effective Number of turns in series per phase}$$

$$= \frac{N_7 N_6}{N_2} = \frac{22 \times 24}{3} = 176 \text{ turns} \quad (A-12)$$

K_p = pitch factor = 1

K_d = Winding Distribution Factor

$$K_d = \frac{\sin\left(\frac{\pi}{2N_2}\right)}{N_3 \sin\left(\frac{\pi}{2N_2N_3}\right)} = \frac{\sin\left(\frac{180}{2 \times 3}\right)}{2 \sin\left(\frac{180}{2 \times 3 \times 2}\right)} = \frac{\sin 30^\circ}{2 \sin 15^\circ} = 0.9659 \quad (A-13)$$

N_8 = Carter Co-efficient

$$= \frac{2}{\pi} \left[\tan^{-1} \left(\frac{D_{11}}{2D_5} \right) - \frac{D_5}{D_{11}} \ln \left(1 + \left(\frac{D_{11}}{D_5 \times 2} \right)^2 \right) \right] \quad (A-14)$$

$$= \frac{2}{\pi} \left[\tan^{-1} \left(\frac{16}{2 \times 8.8} \right) - \frac{8.8}{16} \ln \left(1 + \left(\frac{16}{8.8 \times 2} \right)^2 \right) \right]$$

$$N_8 = 0.26024$$

N_9 = Multiplier for D_5 to account for apparent increase in D_5 due to slot

$$= \frac{D_{10} + D_{11}}{D_{10} + D_{11}(1 - N_8)} = \frac{10 + 16}{10 + 16 \times (1 - 0.26024)} \quad (A-15)$$

$$N_9 = 1.1906$$

$$Q_{syn} = 2\pi f D_7 D_1 D_6 \quad (A-16)$$

$$= 2\pi \times 50 \times 50.39 \times 2.09 \times 156 \times 10^{-9} \text{ m}^3/\text{sec}$$

$$Q_{syn} = 5.1612 \times 10^{-3} \text{ m}^3/\text{sec}$$

$$Q_{spec} = \text{flow/sec} = 2.0/3600 = 5.55555 \times 10^{-4} \text{ m}^3/\text{sec}$$

Sodium velocity in Annulus = 1.68 m/sec

$$\text{Slip} = \frac{Q_{syn} - Q_{spec}}{Q_{syn}} = \frac{5.1612 \times 10^{-3} - 5.5555 \times 10^{-4}}{5.1612 \times 10^{-3}} \quad (A-17)$$

$$\text{Slip} = 0.8923$$

Resistivity of Copper at 600 °C

$$\rho_{Cu} = [148.54 + 0.2748(1.8 \times T_{Cu} + 32) + 0.000058 (1.8T_{Cu} + 32)^2] \times 10^{-10} \quad (A-18)$$

$$\rho_{Cu} = [148.54 + 0.2748(1.8 \times 600 + 32) + 0.000058 (1.8 \times 600 + 32)^2] \times 10^{-10}$$

$$\rho_{Cu} = [148.54 + 311.1376 + 71.7195] \times 10^{-10}$$

$$\rho_{Cu} = 531.397 \times 10^{-10} \Omega \text{ m}$$

Resistivity of Stainless Steel at 600 °C

$$\rho_{SS} = [6.96 \times 10^{-7} + 8.78 \times 10^{-10} \times T_{SS} - 3.01 \times 10^{-13} T_{SS}^2] \quad (A-19)$$

Temperature of Stainless Steel T_{SS} = Temperature of Liquid Metal = T_1 = 600 °C

$$\rho_{SS} = [6.96 \times 10^{-7} + 8.78 \times 10^{-10} \times 600 - 3.01 \times 10^{-13} 600^2]$$

$$\rho_{SS} = [6.96 \times 10^{-7} + 5.268 \times 10^{-7} - 1.0836 \times 10^{-7}]$$

$$\rho_{SS} = 1.11444 \times 10^{-6} \Omega \text{ m}$$

Resistivity of Sodium at 600°C

$$\rho_{Na} = 8.14 \times 10^{-8} + 2.27 \times 10^{-10} \times T_1 + 2.99 \times 10^{-13} T_1^2 \quad (A-20)$$

$$\rho_{Na} = 8.14 \times 10^{-8} + 2.27 \times 10^{-10} \times 600 + 2.99 \times 10^{-13} \times 600^2$$

$$\rho_{Na} = 8.14 \times 10^{-8} + 1.362 \times 10^{-7} + 1.0764 \times 10^{-7}$$

$$\rho_{Na} = 3.2524 \times 10^{-7} \Omega \text{ m}$$

R_1 , Resistance of Stator Copper Winding

Length of Cu-winding = Length of mean turn x Total no. of turns per phase

$$= D_{15} \times N_{sc} \quad (A-21)$$

$$= 479.03 \times 176 = 84.309 \text{ metres}$$

Taking into account the compressibility of MI Cable and the extra length required for making the terminations, the length of the MI winding can be taken as 130 metres.

Therefore, Resistance of Stator MI winding per phase

$$= \frac{\text{resistivity of Copper at } 600^\circ\text{C} \times \text{Length of Copper winding}}{\text{Area of Copper conductor}} \quad (A-22)$$

For the chosen MI Cable, the conductor diameter is 2.6mm

$$\text{Therefore, area of copper conductor} = (\pi/4) \times (2.6 \times 10^{-3})^2 = 5.26837 \times 10^{-6} \text{ m}^2$$

$$\text{Resistance } R_1 = \frac{130 \times 531.397 \times 10^{-10}}{5.26837 \times 10^{-6}} = 1.3112 \Omega \text{ per phase}$$

X_1 – Stator winding Leakage Reactance

$$X_1 = \frac{4.96 \times 10^{-5} f N_1 N_3 N_7^2 \left[\frac{D_8 D_{13}}{6} + \frac{D_8 D_{12}}{2} \right]}{D_{11}} \quad (A-23)$$

$$= \frac{4.96 \times 10^{-5} \times 50 \times 4 \times 2 \times 22^2}{16 \times 10^{-3}} \left[\frac{62.48 \times 10^{-3} \times 77 \times 10^{-3}}{6} + \frac{62.48 \times 10^{-3} \times 0}{2} \right]$$

$X_1 = 0.4812 \Omega$ per phase

X_m – Magnetising Reactance

$$X_m = \frac{2.5 \times 10^{-6} \times f \times f_b \times f_d \times N_2 D_6 D_7 (N_{sc} K_p K_d)^2}{N_1 N_9 D_5} \quad (A-24)$$

f_d = Flux distribution factor – the ratio of the average value of flux wave to the maximum value of the flux wave. For sinusoidal flux distribution, $f_d = 0.637$ (or, $(2/\pi)$).

f_b = Form factor of flux wave; represents the ration of the peak value to the rms value. For a sinusoidal flux wave, $f_b = 1.11$

$$X_m = \frac{2.5 \times 10^{-6} \times 50 \times 1.11 \times 0.637 \times 3 \times 156 \times 10^{-3} \times 50.39 \times 10^{-3} (176 \times 1 \times 0.9659)^2}{4 \times 1.1906 \times 8.8 \times 10^{-3}}$$

$X_m = 1.4502 \Omega$ per phase

R_w – Equivalent Resistance of the outer annulus Wall

$$R_w = \frac{\pi \rho_{ss} N_2 (D_1 + D_2 + D_7) (N_{sc} K_p K_d)^2}{D_2 (N_4 D_{11} + N_5 D_{10})} \quad (A-25)$$

$$= \frac{\pi \times 1.11444 \times 10^{-6} \times 3 \times (2.09 + 3.0 + 50.39) \times 10^{-3} \times (176 \times 1 \times 0.9659)^2}{3 \times 10^{-3} \times (24 \times 16 + 25 \times 10) \times 10^{-3}}$$

$R_w = 8.8538 \Omega$ per phase

R_j – Equivalent Resistance of jacket around Centre Core

$$R_j = \frac{\pi \rho_{ss} N_2 (D_4 + D_9) (N_{sc} K_p K_d)^2}{D_4 (N_4 D_{11} + N_5 D_{10})} \quad (A-26)$$

$$= \frac{\pi \times 1.1144 \times 10^{-6} \times 3 \times (1.65 + 45) \times 10^{-3} \times (176 \times 1 \times 0.9659)^2}{1.65 \times 10^{-3} (24 \times 16 + 25 \times 10) \times 10^{-3}}$$

$R_j = 13.5357 \Omega$ per phase

R_c – Equivalent Resistance of R_w and R_j in parallel

$$R_c = \frac{R_j R_w}{R_j + R_w} = \frac{13.5357 \times 8.8538}{13.5357 + 8.8538} \quad (\text{A-27})$$

$R_c = 5.3526 \, \Omega$ per phase

R_f – Equivalent Resistance of Sodium

$$R_f = \frac{\rho_{Na} \pi D_7 N_2 (N_{sc} k_p k_d)^2}{D_1 (N_4 D_{11} + N_5 D_{10})} \quad (\text{A-28})$$

$$= \frac{\pi \times 3.2524 \times 10^{-7} \times 3 \times 50.39 \times 10^{-3} \times (176 \times 1 \times 0.9659)^2}{2.09 \times 10^{-3} \times (24 \times 16 + 25 \times 10) \times 10^{-3}}$$

$R_f = 3.36868 \, \Omega$ per phase

R_{cf} – Equivalent Resistance of R_c & Sodium Resistance R_f/s in parallel

$$R_{cf} = \frac{R_c \times \frac{R_f}{s}}{R_c + \frac{R_f}{s}} = \frac{R_c \times R_f}{(s \times R_c + R_f)} \quad (\text{A-29})$$

$$R_{cf} = \frac{5.3526 \times 3.36868}{(0.8923 \times 5.3526 + 3.36868)} = 2.2137 \, \Omega \text{ per phase}$$

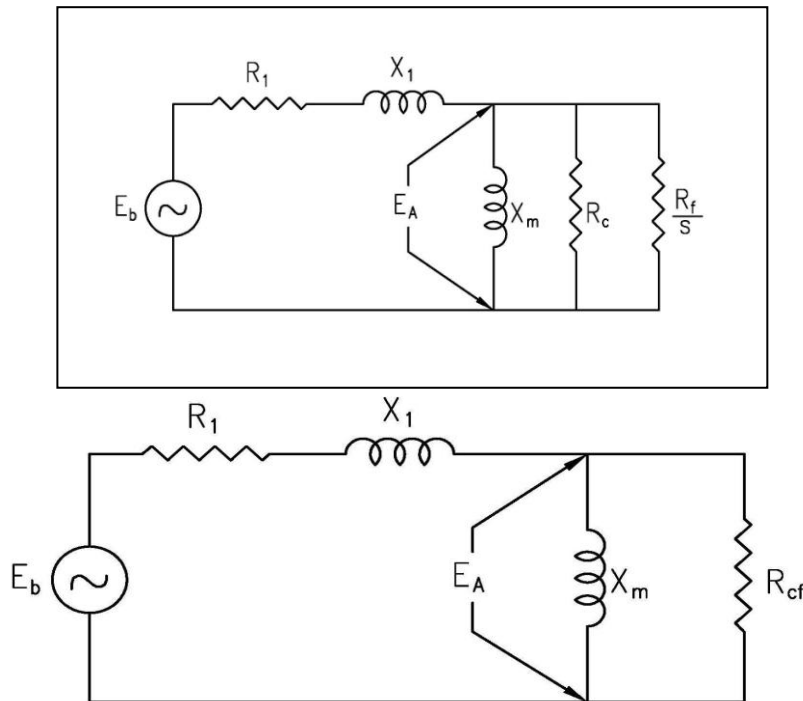


Fig. 3.2 Equivalent circuit of ALIP after R_c & R_f/s in parallel

When X_m and R_{cf} in parallel is solved, impedance having real part and imaginary part is obtained. Let the real part of this parallel combination be Z_{a1} & imaginary part be Z_{a2} .

Then,

$$Z_{a1} = \frac{R_{cf} \times X_m^2}{R_{cf}^2 + X_m^2} = \frac{2.2137 \times 1.4502^2}{2.2137^2 + 1.4502^2} = 0.6647 \Omega \text{ per phase} \quad (A-30)$$

$$Z_{a2} = \frac{R_{cf}^2 \times X_m}{R_{cf}^2 + X_m^2} = \frac{2.2137^2 \times 1.4502}{2.2137^2 + 1.4502^2} = 1.0147 \Omega \text{ per phase} \quad (A-31)$$

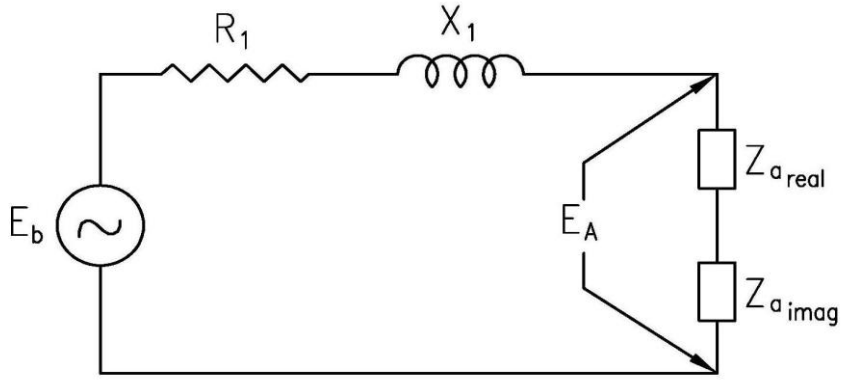


Fig. 3.3 Equivalent circuit of ALIP with Z_a real and imaginary part

Z_c – Total Equivalent Impedance

$$\begin{aligned} Z_c &= \sqrt{(R_1 + Z_{a1})^2 + (X_1 + Z_{a2})^2} = \sqrt{(R_1 + Z_{a1})^2 + (X_1 + Z_{a2})^2} \\ &= \sqrt{(1.3112 + 0.6647)^2 + (0.4812 + 1.0147)^2} \end{aligned} \quad (A-32)$$

$$Z_c = 2.4784 \Omega \text{ per phase}$$

$$\text{Power Factor} = \cos \left[\tan^{-1} \left(\frac{X_1 + Z_{a2}}{R_1 + Z_{a1}} \right) \right] = \cos \left[\tan^{-1} \left(\frac{1.4959}{1.9759} \right) \right] = 0.7972 \quad (A-33)$$

Input Current at 150 V

$$I_b = \text{Input current (in phase winding)} = \frac{E_b}{Z_c} = \frac{150}{2.4784} = 60.522 \text{ Amp} \quad (A-34)$$

$$\text{Input Power} = 3 E_b I_b \cos \phi \quad (A-35)$$

$$= 3 \times 150 \times 60.522 \times 0.7972 = 21714.34 \text{ Watts}$$

Input Power = 21.71 kW

E_A – Voltage induced in X_m

$$E_A = E_b \angle 0 - (R_1 + jX_1) \times I_b \angle \theta \quad (A-36)$$

$$= 69.146 + j 24.681$$

$$E_A = 73.419 \text{ Volts}$$

$$\text{Phase angle of } E_A \text{ with respect to } E_b = \tan^{-1} \left(\frac{24.681}{69.146} \right) = 19.64^\circ \quad (A-37)$$

P_o – Pressure rise across the pump

$$P_o = \left(\frac{N_1 - 1}{N_1 + 1} \right) \left(\frac{N_2 s E_A^2}{R_f Q_{\text{syn}}} \right) - k_1 Q_{\text{spec}}^2 \quad (A-38)$$

Neglecting Hydraulic losses

$$P_o = \left(\frac{N_1 - 1}{N_1 + 1} \right) \left(\frac{N_2 s E_A^2}{R_f Q_{\text{syn}}} \right) \quad (A-39)$$

$$= \left(\frac{4 - 1}{4 + 1} \right) \left(\frac{3 \times 0.8923 \times 73.419^2}{3.36868 \times 5.1612 \times 10^{-3}} \right)$$

$$P_o = 497993.4345 \text{ Pascal}$$

$$P_o = \frac{497993.4345}{9.81 \times 10^4} = 5.076 \text{ kg/cm}^2 \quad (A-40)$$

Taking conservative approach, therefore, the head developed by pump at rated flow and

at 150 V = 4 kg/cm². This is meeting the requirement.

$$\text{Output of Pump} = P_o \times Q_{\text{spec}} \quad (A-41)$$

$$= 497993.4345 \times 5.55 \times 10^{-4}$$

$$= 276.66 \text{ Watts}$$

$$\text{Efficiency of Pump} = \frac{\text{Pump output (mech) Power}}{\text{Pump Input (Electrical) Power}} \times 100 \% \quad (A-42)$$

$$= \frac{276.66}{21714.34} \times 100$$

$$\text{Efficiency of Pump} = 1.274 \%$$

$$\text{Total Flux } \phi_t = \frac{N_1 E_A}{2 f f_b k_p k_d N_{sc}} \quad (\text{A-43})$$

$$= \frac{4 \times 73.419}{2 \times 50 \times 1.11 \times 1 \times 0.9659 \times 176}$$

$$\phi_t = 0.015663394 \text{ wb}$$

B_j - Jacket Flux Density

$$B_j = \frac{0.637 \phi_t}{N_1 D_9^2} = \frac{0.637 \times 0.015663394}{4 \times (45 \times 10^{-3})^2} \quad (\text{A-44})$$

$$B_j = 1.2239 \text{ Wb/m}^2$$

B_t – Tooth Flux Density

$$B_t = \frac{\phi_t}{\pi N_5 D_8 D_{10} \times 0.9 \times f_d} \quad (\text{A-45})$$

$$B_t = \frac{0.015663394}{\pi \times 25 \times 62.48 \times 10^{-3} \times 10 \times 10^{-3} \times 0.9 \times 0.637}$$

$$B_t = 0.5532 \text{ Wb/m}^2$$

Wall Losses

$$\text{Loss in Wall } L_w = \frac{N_2 E_A^2}{R_c} = \frac{3 \times 73.419^2}{5.3526} = 3021.18 \text{ Watts} \quad (\text{A-46})$$

$$L_w = 3021.18 \text{ kW}$$

$$\text{Losses in Sodium, } L_{sod} = \frac{N_2 s^2 E_A^2}{R_f} = \frac{3 \times (0.8923 \times 73.419)^2}{3.3686} \quad (\text{A-47})$$

$$L_{sod} = 3822.65 \text{ Watts}$$

Cu-loss in Stator (L_{Cu})

$$L_{Cu} = N_2 I^2 R_1, \quad L_{Cu} = 3 \times 60.90^2 \times 1.3112 \quad (\text{A-48})$$

$$L_{Cu} = 14409.402 \text{ Watts.} \quad L_{Cu} = 14.409 \text{ kW}$$

I_m Magnetising Current

$$I_m = \frac{E_A}{X_m} = \frac{73.419}{1.4502} = 50.62 \text{ Amp} \quad (\text{A-49})$$

Appendix - B

APPENDIX – B

Material specification and inspections followed during manufacturing

B.1 Specification of cold rolled grain oriented steel (CRGO – 41) for lamination

- a) Applicable Standard : IS 3024 (Wherever applicable)
- b) Nominal Thickness : 0.28mm
- c) Insulation : Both surface of lamination are insulated with inorganic insulation coating capable of withstanding stress relief annealing.
- d) Annealing : Punched and sheared laminations were annealed at 1033 K – 1063K by Conveyor Annealing process and IR was checked at regular interval to ensure no appreciable drop in IR as per standard.
- e) Lamination :
 - i) Grain orientation for stator is along the tooth length. The laminations were free from burrs and irregularities to enable proper stacking. Minimum oil was used during punching and all traces of oil were removed before taking up annealing.
 - ii) For centre core, direction of grain orientation was along the length of the lamination. No oil was used while shearing.
- f) Guaranteed maximum iron loss: 0.9 W/kg at 1.5T and 50 Hz. In the direction of grain orientation.
- g) Inspection of CRGO 41:
 - i) Chemical analysis of CRGO-41 material
(Minimum content of Silicon shall be 3%)
 - ii) Test certificate from a mutually accepted agency for maximum iron loss value was checked to confirm that the material corresponds to CRGO-41
 - iii) Dimensions of the punched and sheared laminations, insulation resistance of inorganic coating by 50V megger, watt loss and grain orientation were inspected.
 - iv) Stress relief annealing was carried out and watt loss and IR were checked again.

B.2 ALIP Assembly

First coils were wound on the outer duct assembly as shown in the drawings and checks mentioned were carried out. The inner duct assembly was manufactured and inserted inside the outer duct assembly and tack welded. Both the support flanges were inserted from both the ends of duct assembly. All the stator core assembly were fixed between support flange one by one. Support flanges and outer duct were welded. MI cable leads were brought out suitably from the top/right flange through cylindrical pipe of suitable length. Then the outer cylindrical enclosure was inserted over two support flanges and welded to both the support flanges. Suitable sealing arrangement for the MI cable leads to come out from the ALIP was made.

B.3 Inspection and Tests

B.3.1 Dimensional inspection

Dimensional check for the individual components and the completed pump were carried out as per the approved procedures.

B.3.2 Non-destructive examinations

B.3.2.1 Liquid penetrant examination of weld edge preparation, root pass & final pass for all butt welds and root pass & final pass for all fillet welds was carried out as per specification. No indication was acceptance criteria for weld edge preparation.

B.3.2.2 Radiographic examination was carried out for 100% weld length on all the finish butt welds as per specification. The acceptance criteria for radiographic examination was as per class-1. In case of full penetration weld joints where radiographic examination cannot be performed satisfactorily, ultrasonic examination for 100% weld length as per was carried out.

B.3.2.3 Leak detection of completed / finished component was done under vacuum with helium. Wherever weld joints were not accessible for repair after global leak

testing, that individual component was helium leak tested stage wise before final assembly. Whenever leak detection under vacuum was not feasible, leak detection using helium under pressure was done.

B.3.3 Inspection on assembly of stainless steel sodium duct

- a) Dimension check : On all individual machined/fabricated parts and assemblies.
- b) Measurement of weight of centre core assembly and ring flux test on centre core assembly was done before welding of centre core.
- c) Welding inspection:
 - i) Dimensional check on edge preparation
 - ii) Liquid penetration (LP) check on edge preparation
 - iii) LP check on each weld pass.
- d) Radiography: All the butt weld joints of stainless steel are 100% radiographed after final pass.
- e) Pneumatic test and Helium leak test:
 - i) Pneumatic and Helium test on outer duct assembly before fabrication of winding on duct:

After completing the duct assembly (outer duct with fins welded), pneumatic test (on duct assembly) was carried out with 2.0 MPa (g) and the test procedure and acceptance criteria was as per ASME Section III sub-section NB. Pneumatic test was followed by Helium leak test by evacuating the outer duct.

- ii) Pneumatic and Helium test on complete duct assembly with fabricated winding on duct:

After completing the duct assembly (outer and inner duct welded), pneumatic test (on duct assembly) was carried out with 2.0 MPa (g) and the test procedure and acceptance criteria was as per ASME Section III sub-section NB. Pneumatic test

was followed by Helium leak test by evacuating the duct.

iii) Pneumatic & Helium leak test on inner duct assembly:

After completion of lamination filling in the inner core and after welding the diffuser cone, the entire inner duct assembly underwent pneumatic pressure test (external) as per ASME section III, sub-section NB. The test pressure was 2.0 MPa (g) external to the inner duct assembly. A separate container of carbon steel was made to keep the inner duct assembly for pressure testing.

Helium leak test for inner duct under vacuum was carried out after the completion of pneumatic test. A hole drilled for helium leak test was plugged and welded after the test and DP check was carried out as per specification.

iv) Pneumatic & Helium leak test on Duct assembly:

After completing the duct assembly (outer duct with fins welded and central core assembled), pneumatic test (on duct assembly) was carried out with 2.0 MPa (g) and test procedure and acceptance criteria were as per ASME Section III sub-section NB. Pneumatic test was followed by Helium leak test by evacuating the outer duct and it was carried out as per specification.

B.3.4 Inspection on coil/winding during manufacture

a) Winding inspection during coil fabrication

- i. Proper laying of coil and checking of proper direction of coil
 - ii. Insulation resistance between coil conductor and the ground. IR value was greater than 100000 Mega ohms (measurement as per IS 7816).
 - iii HV test at 2.5 kV r.m.s for one minute between Phase to earth and between phase to phase. It withstood the HV test.
- iv) Vibrations and current balance checked at 60 to 80 V in the final assembly for short time not exceeding 3 minutes.

References

REFERENCES

- 1 Anil Kakodkar, “Evolution of nuclear reactor containments in India: Addressing the present day challenges”, Nuclear Engineering and Design 269 (2014) 3–22.
- 2 Chetal, S.C., Balasubramanian, V., Chellapandi, P., Mohanakrishnan, P., Puthiyavinayagam, P., Pillai, C.P., Raghupathy, S., Shanmugham, T.K., Pillai, C.S., The design of the prototype fast breeder reactor. Nuclear Engineering and Design 236, 852–860, 2006.
- 3 Kazumi Aoto, Philippe Dufour, Yang Hongyi, Jean Paul Glatz, Yeong-il Kim, Yury Ashurko, Robert Hill, Nariaki Uto, “A summary of sodium-cooled fast reactor development”, Progress in Nuclear Energy, 2014, <http://dx.doi.org/10.1016/j.pnucene.2014.05.008>
- 4 R.K. Sinha, A. Kakodkar, “Design and development of the AHWR—the Indian thorium fuelled innovative nuclear reactor”, Nuclear Engineering and Design 236 (2006) 683–700.
- 5 Jagdish Tyagi, Mithilesh Kumar, H.G. Lele, P. Munshi, “Thermal hydraulic analysis of the AHWR—The Indian thorium fuelled innovative nuclear reactor”, Nuclear Engineering and Design 262 (2013) 21–28.
- 6 G. Srinivasan, K.V. Suresh Kumar, B. Rajendran, P.V. Ramalingam, “The Fast Breeder Test Reactor—Design and operating experiences”, Nuclear Engineering and Design 236 (2006) 796–811.
- 7 J.I. Sylvia, M.R. Jeyan, M. Anbucheliyan, C. Asokane, V. Rajan Babu, B. Babu, K.K. Rajan, K. Velusamy, T. Jayakumar, “Ultrasonic imaging of projected components of PFBR”, Nuclear Engineering and Design 258 (2013) 266–274.
- 8 B K Nashine, S K Dash, K Gurumurthy, U Kale, V D Sharma, R Prabhakar, M Rajan & G. Vaidyanathan, “Performance testing of indigenously developed DC conduction pump for sodium cooled fast reactor”, Indian Journal of Engineering & Materials Sciences Vol. 14, June 2007, pp. 209-214
- 9 Aizawa Kosuke, Chikazawa Yoshitaka, Kotake Shoji, Ara Kuniaki, Aizawa Rie and Ota Hiroyuki, Electromagnetic Pumps for main cooling Systems of Commercialized sodium-cooled fast reactor, Journal of Nuclear Science and Technology, Vol. 48, No.3, p. 344-352, 2011.

- 10 Andreev, A. M. , Danilin, V. G. , Karasev B. G. , Kirillov, I.R. , Choice of constructional schemes of electromagnetic pumps for atomic energy stations with fast reactors, *Magnitnaya Gidrodinamika*, No. 1, pp- 101-105, January-March, 1982.
- 11 Anisimov, A. M. , Vitkovsky, I.V., Golovanov, M. M. , Kirillov, I. R., Krizhanovsky, S. A. , Preslitsky, G. V. , Chaika, P. Yu., Zotov, V. G. , and Sedakov, V. Yu., *Electromagnetic Pumps for BN-800*, *Atomic Energy*, Vol. 112, No. 6, October 2012.
- 12 Baker, R.S. and Tessier, M.J., "Handbook of Electromagnetic Pump Technology", Elsevier Publications, 1987.
- 13 Blake, L.R. , Conduction and induction pumps for liquid metals, *Proceedings of the IEE - Part A: Power Engineering*, Volume 104, Issue 13, p. 49 – 67, February 1957.
- 14 J.I. Sylvia , P. Vijayamohana Rao, B. Babu, K. Madhusoodanan, "Development of mutual inductance type sodium level detectors for PFBR", *Nuclear Engineering and Design* 262 (2013) 219–227.
- 15 Kirillov, I.R., *Electromagnetic Pumps for nuclear power*, *Magnitnaya Gidrodinamika*, No.3, pp. 87-97, July-September, 1982.
- 16 Hee Reyoung Kim, Yong Bum Lee, A design and characteristic experiment of the small annular linear induction electromagnetic pump, *Annals of Nuclear Energy* 38 , 1046-1052, 2011.
- 17 Say, M.G., *The Performance and Design of Alternating Current Machines*, Third Edition, CBS Publishers, 2000
- 18 Kirillov, I.R., Obukhov, D.M., "Two Dimensional model for analysis of cylindrical linear induction pump characteristics: model description and numerical analysis", *Energy Conversion and Management* 44 (2003).
- 19 Sharma Prashant, Sivakumar L.S. Rajendra Prasad, R., Saxena D.K., Suresh Kumar V.A., Nashine B. K., Noushad I.B., Rajan, K.K., Kalyanasundaram, P., "Design, Development and Testing of A Large Capacity Annular Linear Induction Pump", *Journal Of Energy Procedia*, Vol.7, pp.622-629, 2011.
- 20 Watt, D. A. "The design of electromagnetic Pumps for Liquid metals", *The Institution of Electrical Engineers*, Paper No. 2763 U, Dec. 1958.
- 21 Werkoff, F., "Finite-Length Effects and Stability of Electromagnetic Pumps", *Experimental Thermal and Fluid Science* 1991.
- 22 Masayoshi Nakazaki, et al, Performance evaluation of the Sodium Immersed Self Cooled Electromagnetic Pump, *Proceeding of ICONE 5*, May 26-30,1997, Nice, France

- 23 H.V. Khang, A. Arkkio, “Eddy-Current Loss Modelling for Form- Wound Induction Motor Using Circuit Model”, IEEE Transaction on Magnetics, Vol.48, No 2, Feb 2012.
- 24 Hee Reyoung KIM, Sang Hee HONG, Design and Experimental Characterization of an EM Pump, Journal of Korean Physical Society, Vol 35, No 4, Oct 1999, pp 309-314
- 25 M Nakazaki, et al Development of Sodium Immersed Self Cooled Electromagnetic Pump, FR91, Tokyo 1991, P2.16-1 to P2. 16-7
- 26 Hiroyuki OTA, et al, Development of 160 m³/h Large Capacity Sodium Immersed Self Cooled Electromagnetic Pump, Journal of Nuclear Science and Technology, Vol 41, No4, p 511-523, April 2004
- 27 W. Kwant, A. W. Fanning, Y. Dayal, H. Ikeda, J. Taguchi, M. Nakazaki, J. M. Boggio, In –Sodium Testing and Performance of A 43.5 m³/min Electromagnetic Pump for LMR Application, Proceeding of ICONE 5, May 26-30,1997, Nice, France
- 28 Hideo Araseki, Igor Kirillov, Anatoly Ogorodnikov, Gennady Preslitsky, Pulsations of Parameters in Annular Linear Electromagnetic Pumps for Fast Breeder Reactors, 11th International Conference On Nuclear Engineering, Tokyo, Japan, April 20-23, 2003
- 29 A.W.Fanning, W.Kwant, M.Patel, Double Stator Electromagnetic Pump for the ALMR Primary System”, International Conference on design and Safety of Advance NPPS, Tokyo October 92.
- 30 P. Del Vecchio, A. Geri and G.M.Vecca,Superconducting Magnet for Electromagnetic D.C.Pumps”, IEEE Trans. on Magnetics, VOL. MAG-21, NO.2, MARCH 1985.
- 31 Vitkovskii, I.V., Kirillov, I.R. , Chaika. P. Yu., Kryuchkov, E. A. , Poplavskii, V. M., Nosov, Yu. V., and Oshkanov, N. N., Performance-based reliability assessment of electromagnetic pumps, Atomic Energy, vol. 102, 2007.
- 32 H. Bock and M. Suleiman, Investigations of mineral insulated cables exposed to high temperature and intense gamma radiation, Nuclear Instruments and Methods- 148- (1978) 43-50; North-Holland Publishing Co.
- 33 Prashant Sharma, R.Vijayashree, B.K. Nashine, S.K. Dash, G. Vijayakumar, K.A.Gopal, S. Sosamma, C. Babu Rao, K.K. Rajan, Sensor development for position detection of diverse safety rod of fast reactor, Annals of Nuclear Energy, Volume 46, August 2012, Pages 189–196.
- 34 D. C. Meeker, Finite Element Method, Magnetics, Version 4.2.
- 35 J. Pedra, I. Candela, A.Barrera, Saturation model for squirrel-cage induction motors, Electric Power Systems Research 79 (2009) 1054–1061.

- 36 B. Laporte, G. Vinsard, J.C. Mercier, A computation method for induction motors in steady-state, *Mathematics and Computers in Simulation* 38 (1995) 369-376.
- 37 Y.S. Chen, Y.D. Cheng, J.J. Liao, C.C. Chiou, Development of a finite element solution module for the analysis of the dynamic behaviour and balancing effects of an induction motor system, *Finite Elements in Analysis and Design* 44 (2008) 483 – 492.
- 38 D. Sarkar, A.K. Naskar, Computation of thermal condition in an induction motor during reactor starting, *Electrical Power and Energy Systems* 44 (2013) 938–948.
- 39 Ying Xie, Yunyang Wang, 3D temperature field analysis of the induction motors with broken bar fault, *Applied Thermal Engineering* 66 (2014) 25-34.
- 40 http://www.niiefa.spb.su/site/right/energy/mgd/electromagnetic_pumps_for_liquid_metals/?lang=en
- 41 S. Poinso, J.Rapin, Construction and tests In Sodium of A 600m³/hour Annular Linear Induction Pump Computation / Experience and Comparison, 4th International Conference Liquid Metal Engineering and Technology, Avignon, France, October 1988, Vol-1..
- 42 C.Deverge, J.P.Lefrere, P.Peturaud, M.Sauvage, The use of electromagnetic pumps in large LMFBR plants, *Proc. of the 3rd International Conference on Liquid Engineering and Technology*, Vol. 3, 245, April 1984, Oxford.
- 43 Electromagnetic Induction Pump for Liquid Metal, Types: 100m³/h and 50 m³/h, Interatom Manual, 1988.
- 44 Decommissioning of Fast Reactors after Sodium Draining, IAEA- Techdoc-1633.
- 45 Annular Induction Pumps, IA-21 – IA -81, Novatome Manual, May 1982.
- 46 N. Sivai bharasi, K. Thyagarajan, H. Shaikh, M. Radhika, A.K. balamurugan, S. Venugopal, A. Moitra, S. Kalavathy, S. Chandramouli, A.K. Tyagi, R.K. Dayal, and K.K. Rajan, Evaluation of Microstructural, Mechanical Properties and Corrosion Behavior of AISI Type 316LN Stainless Steel and Modified 9Cr-1Mo Steel Exposed in a Dynamic Bimetallic Sodium Loop at 798 K (525 °C) for 16,000 Hours, *Metallurgical and Materials Transactions A*, Volume 43A, February 2012.
- 47 A. Gailitis, O. Lielausis, Instability of homogeneous velocity distribution in an induction type MHD machine, *Magetohydrodynamics*, (1975), No 1, pp 87-101.
- 48 H. Araseki, I. R. Kirillov, G.V. Preslitsky, A.P. Ogorodnikov, Magetohydrodynamic instability in annular linear induction pump, Part I. Experiment and numerical analysis, *Nuclear Engineering and Design* (2004), pp 29-55

PUBLICATIONS

Publications

(a) Published:

1. Design, in-sodium testing and performance evaluation of annular linear induction pump for a sodium cooled fast reactor

B.K. Nashine and B.Purna Chandra Rao

Journal of Annals of Nuclear Energy, 73, 2014, 527-536.

2. Design of high temperature induction motor for application in sodium cooled fast reactor control system

B.K. Nashine, Vijay Sharma and B. Purna Chandra Rao

The Journal of CPRI, Vol. 11, No. 2, June 2015

.